Karlsruhe Institute of Technology

Local Hadley and Walker Circulations over Africa and Their Influence on Precipitation

Master's Thesis by

Alexander Gerco Jong

At the KIT Department of Physics
Institute for Meteorology and Climate Research
Troposphere Research (IMKTRO)

Advisor:	Prof. Dr. Peter Knippertz
Co-advisor:	Dr. Juliane Schwendike (University of Leeds, UK)
Supervisor:	Prof. Dr. Andreas Fink

December 2024 – December 2025

Karlsruhe Institute of Technology
Department of Physics
76131 Karlsruhe
Germany

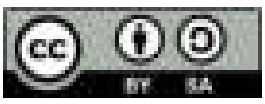

Local Hadley and Walker Circulations over Africa and Their Influence on Precipitation (Master's Thesis)

Ich versichere wahrheitsgemäß, die Arbeit selbständig verfasst, alle benutzten Quellen und Hilfsmittel vollständig und genau angegeben und alles kenntlich gemacht zu haben, was aus Arbeiten anderer unverändert oder mit Abänderungen entnommen wurde sowie die Satzung des KIT zur Sicherung guter wissenschaftlicher Praxis in der jeweils gültigen Fassung beachtet zu haben.

Karlsruhe, December 2025

. . . . . .

(Alexander Gerco Jong)

Abstract

Rainfall is of vital importance to livelihoods in Africa, yet progress in its forecasting remains relatively slow. The Hadley and Walker circulations strongly influence mean precipitation patterns and variability. These circulations are far from spatially symmetric, motivating a local perspective. Here, the ψ-vector method is applied to reanalysis-derived vertical velocity (1960–2022) to decompose the three-dimensional circulation into meridional and zonal components and to examine their relationship with observed rainfall variability, including influences from the Indian Ocean Dipole (IOD) and equatorial Kelvin waves.

The reanalysis-derived ascending total mass flux reproduces observed mean precipitation patterns well, with the meridional component (local Hadley circulation) generally showing higher correlations with rainfall variability than the zonal component (local Walker circulation). Recent rainfall trends (2000–2020) exhibit pronounced seasonal and regional differences. Decreased December–February (DJF) and March–May (MAM) rainfall over Madagascar is linked to weaker meridional flux in the south and weaker zonal flux along the coasts. Increased rainfall over East Africa during MAM results from a more northward-focused ascending branch of the local Hadley circulation, whereas the observed increase in September–November (SON) rainfall is driven by a positive trend in zonal mass flux. Over the western Sahel, increased June–August (JJA) rainfall is associated with comparable changes in both circulation components. Finally, decreased SON rainfall over Southern Africa is related to reduced zonal mass flux in the northern part of the region and reduced meridional mass flux in the south.

The local Hadley circulation responds as strongly, or more strongly, than the local Walker circulation to the IOD. During positive events, the ascending branch shifts northward over the eastern Indian Ocean, with anomalously high meridional mass flux over the western basin, whereas during negative events, anomalously high meridional mass flux is confined to the Java–Sumatra region, with anomalously low flux elsewhere across the Indian Ocean.

Equatorial Kelvin waves induce meridional and zonal mass flux anomalies comparable in magnitude to the mean strength of the local Hadley and Walker circulations, acting through both their zonal wind component and convective coupling. Kelvin wave–related meridional mass flux anomalies are confined to regions of mean ascent, while the East African highlands block much of the overall wave signal, especially the zonal component, although weakened meridional anomalies persist aloft

Together, these findings highlight the spatially asymmetric and transient nature of the large-scale tropical circulations. They provide the first quantitative insight into the response of the local Hadley circulation to the IOD and further support the emerging view that synoptic variability plays a key role in modulating the large-scale tropical circulations.

Zusammenfassung

Niederschlag ist für die Lebensgrundlagen in Afrika von zentraler Bedeutung, doch die Fortschritte bei dessen Vorhersage erfolgen nur langsam. Die großräumige tropische Zirkulation, in Form der Hadley und Walker Zirkulationen, beeinflusst die mittlere Niederschlagsverteilung und deren Variabilität stark. Da diese Zirkulationen nicht räumlich symmetrisch sind, ist eine regionale Betrachtung erforderlich. Die ψ-Vektor-Methode wurde auf ERA5-Vertikalgeschwindigkeiten (1960–2022) angewendet, um die dreidimensionale Zirkulation in meridionale und zonale Komponenten zu zerlegen und deren Zusammenhang mit beobachteter Niederschlagsvariabilität zu untersuchen, einschließlich Einflüssen durch den Indischen Ozean-Dipol (IOD) und äquatoriale Kelvin-Wellen.

Der aus Reanalyse-Daten berechnete Gesamtmassenstrom spiegelt die beobachtete mittlere Niederschlagsverteilung gut wider. Dabei korreliert der meridionale Massenfluss (lokale Hadley Zirkulation) im Allgemeinen stärker mit dem Niederschlag als der zonale Massenfluss (lokale Walker Zirkulation). Trends der letzte zwei Jahrzehnten (2000–2020) zeigen ausgeprägte saisonale und regionale Unterschiede: Rückgänge des Niederschlags im Dezember–Februar (DJF) und März–Mai (MAM) über Madagaskar stehen im Zusammenhang mit einem general abgeschwächten meridionalen Massenfluss und abgeschwächten zonalem Massenfluss an der Küstse; Der verstärkte Niederschlag über Ostafrika während MAM resultiert aus einem nach Norden verschobenen aufsteigenden Ast der lokalen Hadley-Zirkulation, während der beobachtete Anstieg des Niederschlags in September–November (SON) durch einen positiven Trend im zonalen Massenfluss verursacht wird; Niederschlagsanstiege im Juni–August (JJA) über Teilen des westlichen Sahel resultieren aus etwa gleich starken Änderungen im zonalen und meridionalen Massenfluss; SON–Trockenheit im südlichen Afrika ist auf reduzierten zonalen Massenfluss im Norden und meridionalen Massenfluss im Süden zurückzuführen.

Die lokale Hadley Zirkulation reagiert auf den IOD ebenso stark oder sogar stärker als die lokale Walker Zirkulation, wobei sie während positiver Ereignisse einen nach Norden verschobenen aufsteigenden Ast über dem östlichen Indischen Ozean zeigt und über dem westlichen Indischen Ozean verstärkt wird. Während negativer Ereignisse verstärkt sich der meridionale Massenfluss in der Region Java–Sumatra, während er über weite Teile des Indischen Ozeans zunimmt.

Kelvinwellen induzieren meridionale und zonale Massenflussanomalien, die in ihrer Stärke mit der mittleren Stärke der lokalen Hadley und Walker Zirkulation vergleichbar sind, sowohl über ihre zonale Windkomponente als auch über konvektive Kopplung. Die meridionalen Massenflussanomalien im Zusammenhang mit Kelvinwellen sind auf Regionen mit mittlerem Aufstieg beschränkt. Das ostafrikanische Hochland blockiert einen Großteil des

Gesamtsignals der Wellen, insbesondere der zonalen Komponente, obwohl abgeschwächte meridionale Anomalien in höheren Atmosphärenschichten bestehen bleiben.

Zusammen verdeutlichen diese Ergebnisse die räumlich asymmetrische und transiente Natur der großskaligen tropischen Zirkulationen. Sie liefern den ersten quantitativen Einblick in die Reaktion der lokalen Hadley Zirkulation auf den IOD und stützen zudem die zunehmende Auffassung, dass synoptische Variabilität eine zentrale Rolle bei der Modulation der großskaligen tropischen Zirkulation spielt.

Contents

Abbreviations

AMO	Atlantic Multidecadal Oscillation
ARC	African Rainfall Climatology Version 2
CA	Central Africa
CHIRPS	Climate Hazards Infrared Precipitation with Stations
CRU	Climatic Research Unit
DJF	December–February
DMI	Dipole Mode Index
EA	East Africa
EIO	eastern Indian Ocean
ENSO	El Niño–Southern Oscillation
ERA5	fifth-generation European Centre for Medium-Range Weather Forecasts Reanalysis
FROGS	Frequent Rainfall Observations on GridS
GPCC	Global Precipitation Climatology Centre
GPCP	Global Precipitation Climatology Project
IMERG	Integrated Multi-satellitE Retrievals for GPM
IOD	Indian Ocean Dipole
ITCZ	Intertropical Convergence Zone
JJA	June–August
JJAS	June–September
MAM	March–May
MCS	mesoscale convective system
MJO	Madden-Julian Oscillation
MRG	mixed Rossby-Gravity wave
nIOD	negative Indian Ocean Dipole
NWP	numerical weather prediction
OLR	outgoing longwave radiation
OND	October–December
pIOD	positive Indian Ocean Dipole
SAM	Southern Annular Mode
SON	September–November
SST	sea surface temperature
TAMSAT	Tropical Applications of Meteorology using SATellite
WA	West Africa
WIO	western Indian Ocean

1. Introduction

1.1. Motivation

The African continent is currently home to over 1.5 billion people, and, as the fastest-growing continent, it could reach up to 2.8 billion inhabitants by 2050 (Simane et al., 2025). This expected growth will further strain water resources that are already stressed. Nearly 93% of Sub-Saharan Africa's agricultural land is rain-fed (UNDPAfrica, 2012) and roughly 60% of Africans are employed in the agriculture sector (Simane et al., 2025), making their livelihoods acutely vulnerable to precipitation changes.

Rainfall variability is a systemic threat with far-reaching consequences that extend beyond food production. Extreme hydrometeorological events such as droughts and heavy precipitation are becoming increasingly frequent (Intergovernmental Panel On Climate Change (IPCC), 2023). Moreover, the spread of diseases such as malaria, dengue, cholera, and meningitis is closely linked to precipitation patterns and is sensitive to their variability (Kurane, 2010; Ahmed et al., 2018; Mafwele and Lee, 2022; Cliff et al., 2025). Even the transition to cleaner energy is vulnerable, as hydropower, which supplies an average of 17% of Africa's electricity (exceeding 80% in some countries), faces growing climate risks due to the long operational lifespan of infrastructure being exposed to decades of climatic fluctuations (IEA, 2020).

The physical mechanisms driving rainfall itself are complex and controlled by multi-scale processes from large-scale global modes of climate variability to small-scale local convective dynamics. This complexity is also partly reflected by the slow progress in weather and seasonal forecasting in Africa, which is critically hampered by persistent gaps in scientific understanding, observational data, and numerical model capability (Lamptey et al., 2024).

1.2. Connection between Tropical Large-Scale Circulation and Rainfall

Large-scale circulation in the tropics is strongly characterized by vertical overturning (Hartmann, 1994). Two of the most prominent large-scale circulations are the Hadley and Walker circulations. They can be understood as the meridional response of the wind field to the zonally averaged net heating in the tropics and the zonal response of the wind field to the zonal asymmetries in the meridionally averaged net tropical heating, respectively.

These thermally driven circulations, in turn, strongly influence precipitation patterns in the tropics (Ma et al., 2018).

1.2.1. Rainfall and the Hadley Circulation

For the Hadley circulation, several studies have shown that changes in both its strength and meridional position shape precipitation patterns across the tropics and subtropics (Schwendike et al., 2015; Lau and Kim, 2015; Burls et al., 2019; Joseph et al., 2024). Schwendike et al. (2015) show a systematic southward displacement of the local Hadley circulation from Africa to the Pacific and a strengthening over parts of the Americas and the Atlantic from 1979 to 2009, with precipitation trends closely following these changes. Lau and Kim (2015) corroborate these findings by demonstrating that poleward shifts of the Hadley circulation edges are associated with enhanced subsidence and reduced precipitation on the poleward flanks of the circulation. Such an expansion of the Hadley circulation has been linked both to multidecadal declines in rainfall days in South Africa (Burls et al., 2019) and to increased precipitation in regions such as Northwest India (Joseph et al., 2024). Moreover, rainfall in the Sahel has long been understood to follow shifts in the interhemispheric temperature gradient, which displace the ascending branch of the Hadley circulation and change monsoon rainfall (Schneider et al., 2014).

1.2.2. Rainfall and the Walker Circulation

Similarly, numerous studies have highlighted that changes in the Walker circulation are closely tied to shifts in tropical precipitation patterns. Schwendike et al. (2015) show that relative changes in the local Walker circulation are larger than those in the local Hadley circulation, with significant regional weakening over the Indian and Atlantic Oceans and enhanced zonal overturning over Africa, the Maritime Continent, and South America. Over the Indo-Pacific sector, sustained warming of the Indian Ocean has driven a westward extension of the Walker circulation's Indo-Pacific ascending branch, suppressing convection over East Africa and contributing to the post-1980 decline in March–May (MAM) rainfall (Williams and Funk, 2011). Furthermore, intensification of the Indian Ocean Walker cell has been repeatedly linked with drought in the region (Funk et al., 2023). This relationship might be subject to change, as projected weakening of the Indian Ocean Walker cell under positive Indian Ocean Dipole (pIOD)-like warming is expected to enhance rainfall over East Africa while reducing it over the Maritime Continent (Sharma et al., 2022). Beyond Africa, strong Atlantic-Pacific sea surface temperature (SST) gradients have been associated with a strengthened ascending branch of the Walker cell over Amazonia and increased flooding across the Amazon Basin (Barichivich et al., 2018). In the Pacific, the Walker circulation is projected to weaken under global warming (Deser et al., 2010; Tokinaga et al., 2012; Bellomo and Clement, 2015; Watanabe et al., 2023), yet it has intensified in recent decades (Watanabe et al., 2023). These circulation changes are expected to reshape regional precipitation accordingly.

1.3. Methods for Studying Hadley and Walker Circulations

The Hadley and Walker circulations are often calculated based on zonal and meridional averages (Hartmann, 1994; Oort and Yienger, 1996; Williams and Funk, 2011; Stachnik and Schumacher, 2011; Mathew and Kumar, 2019; Yu and Zwiers, 2010; Yu et al., 2012; Bayr et al., 2014; Wang et al., 2021; Sharma et al., 2022). However, significant regional differences in these circulations are obscured when they are averaged over a limited area. This motivates the need for methods that can locally split the circulation into zonal and meridional parts. One such approach is the ψ-vector method (Schwendike et al., 2014, 2015, 2021), which, through Helmholtz decomposition, unambiguously separates the three-dimensional circulation into two-dimensional components that each independently satisfy continuity. A more complex three-dimensional decomposition has been developed by Hu et al. (2017) and accounts for the vorticity contributed by the three-dimensional divergent motions, which traditional two-dimensional methods attribute wholly to the rotational wind. However, the results remain similar to the two-dimensional decomposition in the tropics, particularly at 500 hPa (Hu et al., 2017).

Studies specifically focusing on Africa have applied a wide range of methods to investigate the Hadley and Walker circulations. These include the zonal-mean meridional mass stream function (Mahlobo et al., 2019; Longandjo and Rouault, 2024; Mahlobo et al., 2024; Ramotubei et al., 2025), the meridional-mean zonal mass stream function (Longandjo and Rouault, 2020), the meridional-mean vertical velocity (Hua et al., 2016) alongside the meridional-mean zonal wind (Munday and Washington, 2018; King et al., 2021) or the divergent zonal wind (Cook and Vizy, 2016), as well as the ψ-vector method (de Oliveira et al., 2018; Mahlobo et al., 2019; Zhao and Cook, 2021). Overall, although the ψ-vector method allows for a more unambiguous local perspective, averaging-based approaches remain common in recent studies focusing on Africa, highlighting a continued reliance on traditional methods

The same is true for the previously mentioned studies discussing trends, which mainly use proxies for changes in the Hadley or Walker circulation such as: mean sea level pressure (Burls et al., 2019; Joseph et al., 2024), atmospheric heating (Funk et al., 2023), or mean-meridional vertical and zonal winds (Williams and Funk, 2011). In contrast, using the ψ-vector method, Schwendike et al. (2015) examined circulation trends directly, revealing significant long-term zonally and meridionally asymmetrical trends in the local Hadley and Walker circulations. However, their study did not examine the potential drivers of these trends, and it relied on older reanalysis products. Applying their framework to the newer fifth-generation European Centre for Medium-Range Weather Forecasts Reanalysis (ERA5) (Hersbach et al., 2020) provides an opportunity to reassess these circulation changes with higher-quality data and to take the next step by speculating about potential drivers. Moreover, through a comprehensive comparison with multiple rainfall datasets, uncertainties in the observed reanalysis trends can be better constrained.

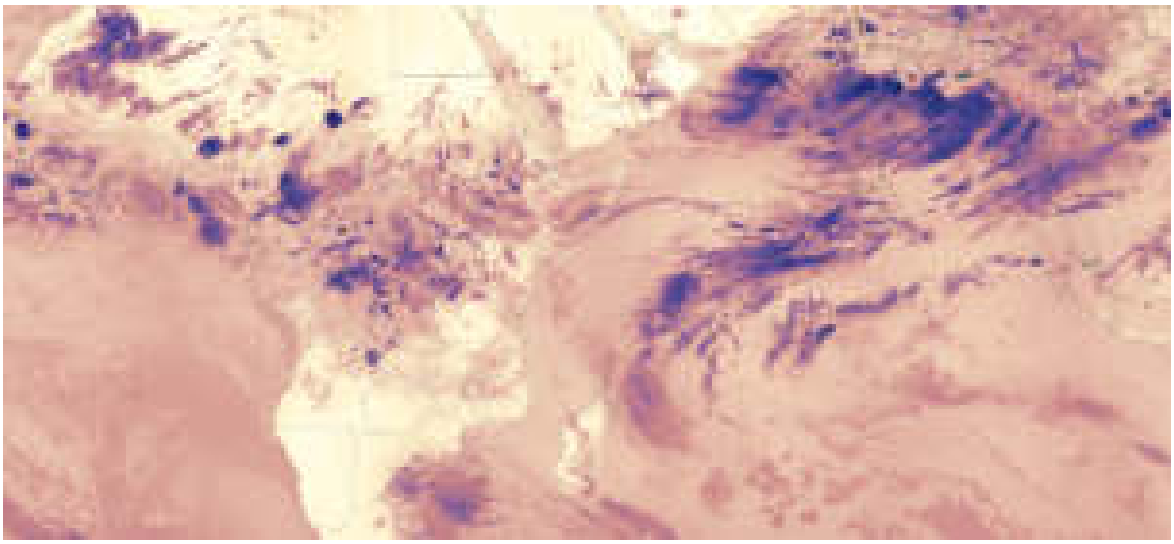

Figure 1.1.: Brightness Temperature (Band I5, Day) from the Visible Infrared Imaging Radiometer Suite (VIIRS) onboard the NOAA-20 satellite, obtained from NASA Worldview (`https://go.nasa.gov/48JD2ps`), for 6 September 2019. This date falls within an extreme positive Indian Ocean Dipole event; on the same day, a Kelvin wave was observed over Ethiopia (see Fig. A.1).

1.4. The Indian Ocean Dipole

Using the ψ-vector method, Schwendike et al. (2014) found that, while the classical focus had been on the response of the Pacific Walker cell to the El Niño–Southern Oscillation (ENSO), the local Hadley circulation in the Pacific has a stronger response, indicating that ENSO cannot be viewed solely as a zonal phenomenon. A related mode of variability in the Indian Ocean is the Indian Ocean Dipole (IOD), which is characterized by a zonal pattern of SST anomalies, with cooler (warmer) SSTs near the coast of Sumatra and warmer (cooler) SSTs in the western Indian Ocean during the positive (negative) phase (Saji et al., 1999). These SST changes subsequently alter convection and precipitation across the Indian Ocean (evidenced by the cloud-free conditions over Sumatra and Java in Fig. 1.1). During a pIOD event, warmer SSTs in the western Indian Ocean enhance convection over East Africa, whereas during a negative Indian Ocean Dipole (nIOD), cooler SSTs suppress it. As a result, the IOD plays a major role in regulating variability in the short rainy season (September–November (SON)) (Black et al., 2003; Behera et al., 2005; Bahaga et al., 2019). Yet, both the modeling and the physical understanding of IOD events remain less well developed than for ENSO events (Wang et al., 2024a).

Many studies have identified changes in the Indian Ocean Walker cell as a key feature of IOD events, and there is broad agreement that zonal overturning changes drive IOD-associated rainfall variability (Saji et al., 1999; Webster et al., 1999; Hameed and Yamagata, 2003; Cai et al., 2013; Mohtadi et al., 2017; Lu et al., 2018). However, not only zonal but also meridional changes play an important role in IOD dynamics. Since the IOD was first identified, changes in the southeasterly trade winds linked to monsoon variability have been recognized as a key process in its development and evolution (Saji et al., 1999). Despite this

early insight, the exact nature of the IOD-monsoon interaction remains poorly understood. Subsequent studies consistently emphasized that, during an IOD event, variations in the southerlies modulate coastal upwelling and evaporative cooling, thereby affecting SSTs in the eastern Indian Ocean (EIO) (Vinayachandran et al., 1999; Saji et al., 1999; Spencer et al., 2005; Cai et al., 2013; Zhang et al., 2020; Wang et al., 2020). Building on this mechanism, it has been proposed that an anomalously northward-displaced Hadley circulation can help trigger a pIOD event (Kajikawa et al., 2003; Fischer et al., 2005; Rao et al., 2009), and that further intensification of pIOD events may arise from IOD-monsoon interactions during strong monsoon years (Swapna and Krishnan, 2008). This connection appears robust across timescales: proxy evidence also links more pIOD-like conditions in the past to a northward-shifted Intertropical Convergence Zone (ITCZ) (Griffiths et al., 2010). Extreme pIOD events (such as the 2019 one) are also associated with unusually strong monsoon rainfall over India (Ratna et al., 2021), which is evident in the satellite image shown in Figure 1.1.

In addition to the well-known zonal SST gradient, the IOD is also linked to a meridional SST gradient of comparable magnitude in the EIO, which has been suggested to induce meridional circulation anomalies (Weller and Cai, 2014). Notably, this meridional gradient exhibits a relationship with EIO precipitation that is as strong as that of the zonal gradient (Weller and Cai, 2014). However, more work is still needed to improve our understanding of the IOD-Hadley-monsoon connection (Wang et al., 2024a). Since the studies cited above rely primarily on proxies for Hadley circulation changes, such as pressure, rainfall, and wind, applying the ψ-vector method will provide the first quantitative assessment of IOD-related Hadley circulation changes.

1.5. Kelvin Wave Impacts on the Local Hadley and Walker Circulations

While the traditional, zonally symmetric view of the Hadley circulation has been useful, recent work has highlighted the importance of zonal asymmetries and transient fluctuations on time scales from days to months in shaping its dynamics (Horinouchi, 2012; Hoskins et al., 2020; Hoskins and Yang, 2021; Tomassini and Yang, 2022; Thakur et al., 2024). The Walker circulation also exhibits a transient nature (Yano et al., 2002) and can be interpreted as the combined response of stationary Kelvin and Rossby waves to diabatic heating (Stechmann and Ogrosky, 2014). Temporal variability on synoptic timescales and zonal asymmetries in the Hadley and Walker circulations are a necessary precondition for organized convection to actively modulate, rather than passively respond to, large-scale overturning motions (Tomassini, 2020). Taken together, the view of the large-scale tropical circulation that emerges is not a steady, axisymmetric feature but rather a dynamically varying system whose strength and structure are closely tied to tropical convection. Daily snapshots of brightness temperature (Fig. 1.1) illustrate that what emerges as "circulation" is the cumulative effect of constantly evolving convective activity.

Equatorial waves constitute a major component of this synoptic variability in the tropics, and indeed, mixed Rossby-Gravity wave (MRG) activity has been shown to play a significant role in modulating the strength of the local Hadley circulation over the Atlantic and Eastern Pacific Ocean (Tomassini and Yang, 2022; Baruah et al., 2025). Similarly, the Madden-Julian Oscillation (MJO) has also been shown to strongly modulate both local Hadley and Walker circulations (Schwendike et al., 2021). These findings confirm that synoptic variability plays a central yet underexplored role in governing the transient variability of the large-scale overturning circulations. Equatorial waves are both a product of latent heat release by moist convection and, in turn, modulators of tropical convection itself (Kiladis et al., 2009). By coupling with convection through regions of convergence and divergence, they can enhance or suppress rainfall depending on their phase.

Among the equatorial waves, Kelvin waves (such as the one over Ethiopia in Fig. 1.1) account for a large fraction of the wave-related rainfall variability across Africa (Lubis and Jacobi, 2015; Schlueter et al., 2019). While their effects on rainfall are well documented, their dynamical implications for the large-scale circulation are less well studied. What is known, is that through the two-way coupling with convection, equatorial waves can influence the local Hadley circulation both directly, by their meridional flow component, and indirectly, through interactions with moist convection that enhance upper-level outflow (Tomassini and Yang, 2022, and references therein). Given their potential zonal component and close coupling with convection, equatorial waves likely exert a similar influence on the Walker circulation, although this relationship remains less well established in the literature. Therefore, by applying the ψ-vector, the present work aims to contribute to the understanding of how equatorial waves modulate Local Hadley and Walker circulations over Africa.

1.6. Research Questions

This study addresses the overarching question of how local Hadley and Walker circulations influence observed rainfall variability over Africa, including trends, and influences of the IOD and equatorial Kelvin waves.

The main questions each section tries to answer are as follows:

- **Section 4.1**: How do the mean local and regional Hadley and Walker circulations vary across Africa, and how are these variations linked to observed rainfall?
- **Section 4.2**: How well does ERA5 data correlate with observed precipitation, and to what extent can rainfall variability be attributed to local circulation components?
- **Section 4.3**: How have precipitation and local circulation patterns changed over the past two decades, and what physical mechanisms drive these trends?
- **Section 4.4**: How does the IOD influence local Hadley and Walker circulations and the associated rainfall response over Africa and the Indian Ocean?

- **Section 4.5**: How do Kelvin waves influence the local Hadley and Walker circulations over Africa?

Overall, the present work provides several novel contributions: the first qualitative comparison between local circulation (trends) and rainfall (trends) from many observed precipitation datasets; the first quantitative assessment of the local Hadley circulation response to IOD events; and the first study to show the effects of Kelvin waves on the local Hadley and Walker circulations.

2. Theoretical Background

2.1. The Hadley Circulation

The Hadley circulation is traditionally known as a large-scale overturning circulation that extends roughly between the Tropics of Cancer and Capricorn, covering about half the globe (Fig. 2.1). It plays a central role in Earth's energy balance by redistributing heat from the equator to higher latitudes and can be thought of as the meridional response of the wind field to the zonally averaged net heating in the tropics.

Precipitation, rather than temperature, defines the seasonal cycle over most of Africa, with regional climates shaped by the alternation between rainy and dry periods. These precipitation patterns are largely governed by the seasonal progression of the ascending branch of the Hadley circulation, which influences the meridional position, intensity, and timing of the tropical rain belt (Lim Kam Sian et al., 2023). It thereby determines the modality of rainy seasons across the continent; in West Africa, the rainy season occurs once per year when the tropical rain belt reaches its maximum poleward extent, whereas equatorial regions experience two rainy seasons as the rain belt passes over them twice. In contrast, the strength and location of the subsiding branches influences the location of arid regions and deserts. This is true around, not only in Africa, but around the globe and combined the Hadley Circulation influences the climate experienced by most of the world's population, both by shaping habitable regions over the long term and by affecting shorter-term climate events such as ENSO (Diaz et al., 2004).

The scientific foundations of what is now known as the Hadley circulation were laid in the late seventeenth and early eighteenth centuries, when British scientists such as Sir Edmund Halley and Sir George Hadley sought to explain the persistent trade winds reported by sailors (Halley, 1686; Hadley, 1735). Halley assembled one of the earliest near-global climatologies of surface winds, producing maps that captured tropical wind patterns with remarkable accuracy and that remain broadly valid even to today. In the same work, he already proposed that the observed winds were linked with a vertically overturning circulation driven by differential solar heating, featuring poleward flow aloft and a compensating equatorward return flow near the surface. However, Halley could not account for the easterly direction of the trades. Hadley resolved this by incorporating the effect of Earth's rotation and angular momentum conservation, providing the first correct physical mechanism for the trade winds and the conceptual basis of the modern Hadley circulation.

Hadley's theory, which proposed a single, thermally driven overturning cell from the equator to the poles, was ultimately too simple to capture the full complexity of Earth's atmosphere

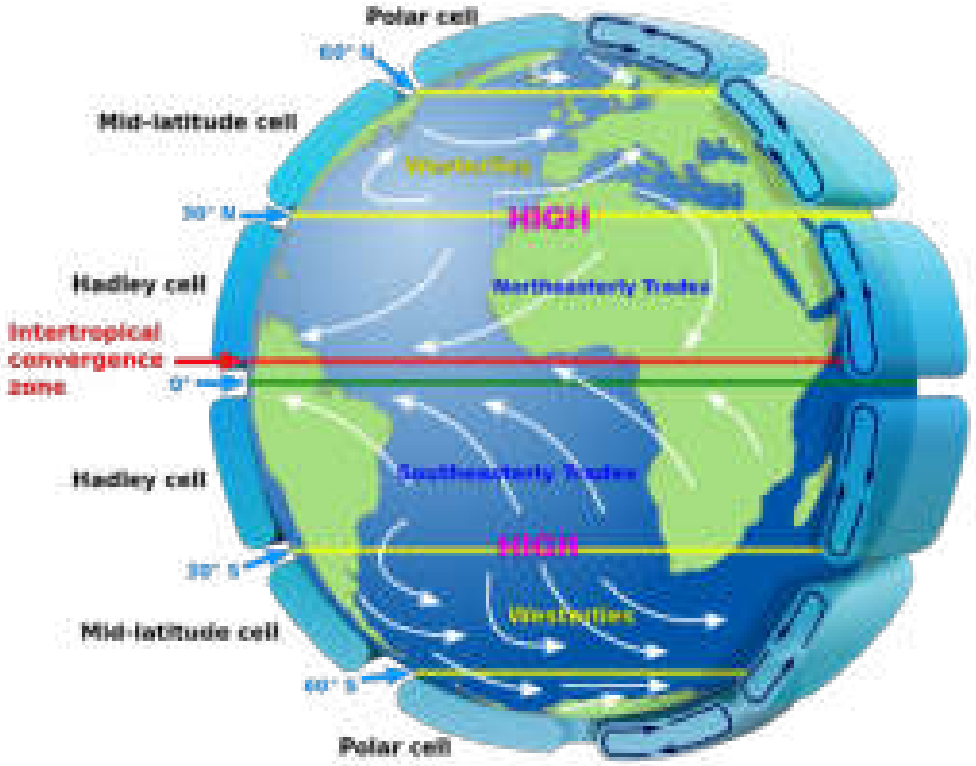

Figure 2.1.: Idealized representation of Earth's major atmospheric circulation cells (Hadley, Ferrel, and Polar) under equinox conditions. Source: Kaidor, CC BY-SA 3.0 `https://creativecommons.org/licenses/by-sa/3.0`, via Wikimedia Commons.

(Fig. 2.1). In the nineteenth century, new observations revealed that midlatitude surface westerlies had a mean poleward component, contradicting the equatorward return flow predicted by a single Hadley cell (Lorenz, 1983). To reconcile theory with observations, Thomson (1892) and Ferrel (1860) introduced a secondary, shallow, thermally indirect meridional circulation cell beneath the Hadley circulation. They made use of a "new" force, the one that we now know as the Coriolis force, and noted that the flow in higher latitudes should be deflected towards the east. Furthermore, they proposed that due to friction, these near-surface westerlies should be significantly weaker than the upper-level flow, while the strength of the pressure gradient decreases more slowly, creating a force imbalance that drives air poleward. In this arrangement, the Coriolis force on the surface poleward wind approximately balances surface drag. They still believed the upper branch of the large Hadley cell extended from equator to pole, to transport angular momentum.

With further advances in upper-air measurements in the early twentieth century, it became clear that this poleward upper-level flow assumed by Hadley and Ferrel did not extend to the poles and instead terminates in the subtropics (Lorenz, 1983) (Fig. 2.1). The theory then shifted to incorporate the critical role of atmospheric macroturbulence and eddies (large-scale transient weather systems) in the mid-latitudes (e.g., Defant, 1921). These eddies

were understood to be the new primary mechanism for transporting heat and angular momentum poleward outside of the tropics.

A natural question then emerged: if midlatitude eddies play such a dominant role in transporting heat and momentum poleward, to what extent can the Hadley circulation be understood using axisymmetric theory at all? Beginning in the late 1970s, two complementary theoretical frameworks developed in parallel. One was the axisymmetric limit, used in studies such as Schneider (1977) and Held and Hou (1980), which examined the Hadley circulation in the absence of eddies and derived analytical predictions for its strength and latitudinal extent. Although highly idealized, these models proved influential; they showed that the width of the tropical overturning circulation could be predicted from planetary parameters, and this framework became foundational to many later studies of tropical expansion.

In contrast, the second approach emphasized the eddy-driven, small-Rossby-number limit, in which the strength of the Hadley circulation is linearly related to the eddy momentum flux divergence in the subtropics, and changes in its extent are related to baroclinic instability (Walker and Schneider, 2006). In a sense, the observed contraction of the Hadley circulation during an El Niño event (Levine and Schneider, 2015) can be seen as a direct consequence of this dependence on baroclinicity. During such an event, the tropics warm relatively compared to the subtropics, the meridional temperature gradient increases, and the Hadley circulation contracts (Levine and Schneider, 2015).

Both theories remain relevant, but in different dynamical regimes. Axisymmetric theory best describes situations where eddy influence is weak, such as in the solstitial winter cell, whereas the small-Rossby-number limit is more appropriate near equinox, when eddy momentum fluxes strongly influence the circulation (Lionello et al., 2024). However, both frameworks are fundamentally dry and omitting water in the form of ocean heat transport and moist atmospheric convection leaves out processes that are central to the real circulation. This omission is notable, given that in the tropics, the ocean transports as much or more energy poleward than the atmosphere (Fasullo and Trenberth, 2008), and that the ascending branch of the Hadley circulation near the ITCZ is dominated by deep moist convection. Therefore, a complete understanding of the Hadley circulation requires considering the coupled ocean–atmosphere energy balance and the moist convection driving the ascent.

The ocean plays a fundamental role in shaping the Hadley circulation because it determines the spatial distribution of heat across both hemispheres. SST patterns set the hemispheric energy balance, and the atmosphere adjusts its circulation to compensate. A well-known example is the mean position of the ITCZ, which lies north of the equator because the Atlantic Meridional Overturning Circulation transports heat into the Northern Hemisphere, requiring the atmosphere to transport energy southward (Schneider et al., 2014).

Moreover, shifts in the ITCZ are also closely tied to oceanic changes. Kang et al. (2009) showed that when ocean heat is redistributed southward, the ITCZ shifts southward and the Northern Hemisphere Hadley cell strengthens to supply the required compensating northward atmospheric heat transport. Chemke (2021) further demonstrated that changes in ocean heat uptake substantially reduce the projected weakening and widening of the

Hadley circulation, offsetting nearly two-thirds of the weakening and about one-third of the hemispheric widening. These results make it clear that the ocean actively modulates Hadley cell strength and structure, rather than simply providing a boundary condition.

Both meridional and zonal SST gradients help explain how this oceanic influence operates. Meridional SST gradients redistribute heating between hemispheres and therefore modify the overturning circulation, while zonal gradients can couple variability across basins. An example of both these processes working in tandem is presented by Zaplotnik et al. (2022), for the Atlantic Multidecadal Oscillation (AMO). During a positive AMO phase, anomalously warm tropical Atlantic SSTs increase the meridional gradient, strengthening the regional Atlantic Hadley circulation. The enhanced Atlantic–Pacific SST contrast intensifies easterlies over the western Pacific, cools the eastern Pacific through the Bjerknes feedback, and strengthens the Walker circulation, which in turn locally strengthens the Hadley circulation in the Indo-Pacific. This sequence shows how basin-scale SST anomalies can propagate through the coupled system and influence overturning circulations far beyond their region of origin.

Examples like these highlight an important point: there may be no meaningful sense in which a single, global Hadley circulation exists; basin-wide circulations have their own local response. As emphasized by Lionello et al. (2024), the idealized global cell masks the strong zonal asymmetries in both ascent and descent, as well as in the climate responses across basins. Furthermore, just as the Hadley circulation is not zonally uniform, it is also not temporally uniform. Its variability on seasonal to interannual timescales is shaped not only by midlatitude eddies but also by tropical transient disturbances. Indeed, Tomassini (2020) argues that zonal and temporal variations in the Hadley–Walker system are a prerequisite for organized convection to actively influence, rather than merely respond to, the large-scale overturning. This perspective suggests that moving forward, the Hadley circulation should be assessed regionally and with explicit attention to the role of transient eddies and coupled variability.

2.2. The Walker Circulation

The zonal counterpart to the Hadley circulation was recognized much later, with early hints appearing in the work of Sir Gilbert Walker, who investigated pressure anomalies associated with what he termed the Southern Oscillation (Walker, 1925). However, it was Bjerknes (1969) who first clearly postulated a zonal overturning circulation along the equatorial Pacific and coined the term Walker Circulation. Bjerknes interpreted this Pacific east–west cell as a thermally direct atmospheric circulation driven by the longitudinal SST gradient and strongly coupled to ocean–atmosphere feedbacks in the equatorial Pacific.

In its classical form, the Pacific Walker cell consists of low-level easterly winds across the tropical Pacific, rising motion over the warm western Pacific, an upper-tropospheric return flow to the east, and subsidence over the cooler eastern Pacific. The circulation is associated with relatively low sea level pressure and warm lower-tropospheric temperatures in the west,

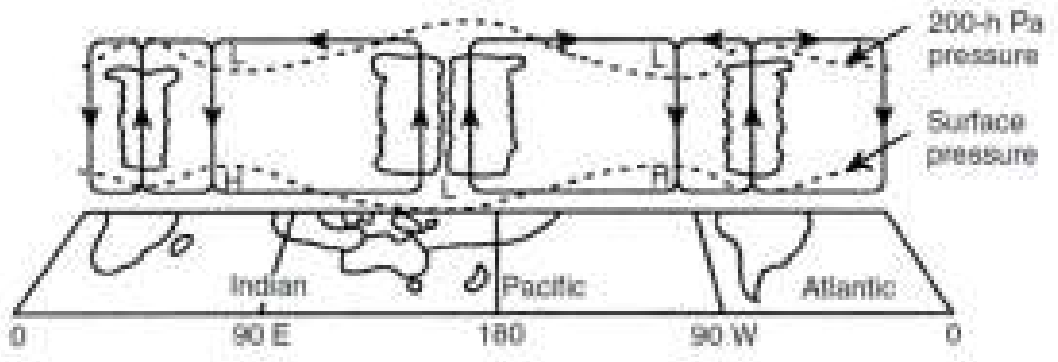

Figure 2.2.: Schematic representation of the Walker circulation and its cells, along the longitude-height plane. Reprinted from Encyclopedia of Atmospheric Sciences, K-M Lau, S. Yang, Walker Circulation, Pages 2505-2510, Copyright (2003), with permission from Elsevier.

and higher pressure and colder conditions in the east. The resulting basin-wide pressure gradient drives the surface easterlies and maintains a state of strong zonal asymmetry in both the tropical ocean and atmosphere.

Although originally identified only in the Pacific, subsequent observations and theoretical work have shown that similar zonal overturning cells exist across the other tropical basins (Lau and Yang, 2003). Today, the term Walker circulation is used more broadly to denote the family of zonal overturning circulation cells along the equatorial belt (see Fig. 2.2). In addition to the dominant Pacific branch, interconnected Walker cells occur over the Indian and Atlantic Oceans. Over the Indian Ocean, rising motion is centered over the Maritime Continent, and subsidence occurs over the western Indian Ocean, producing lower-tropospheric westerlies. Across the Atlantic, ascent is found over Africa and South America, while subsidence dominates over the Atlantic.

The formation and maintenance of Walker circulations arise from the strong zonal asymmetry of tropical SST, which is itself shaped by the coupling between surface winds, ocean currents, upwelling processes, and the atmospheric response to convection. This configuration converts available potential energy into kinetic energy through a thermally direct circulation, maintaining the pattern of rising warm air, upper-level return flow, and subsidence in cooler regions.

A defining characteristic of the Walker circulations is their strong sensitivity to interannual SST variations. Bjerknes's original hypothesis, that variability in the Walker circulation is tightly linked to ENSO, has since been confirmed by decades of observational and modeling work. During El Niño events, the weakening of the Pacific easterlies leads to reduced upwelling and a more zonally uniform thermocline and SST distribution, weakening the Pacific Walker circulation. In contrast, La Niña conditions strengthen the surface easterlies, enhance the zonal thermal gradient, deepen the thermocline in the west, and reinforce the zonal overturning. And as mentioned in section 1, a similar coupled mode of variability

exists in the Indian Ocean, where changes in SST associated with different phases of the IOD are closely linked to fluctuations in the Indian Ocean Walker cell.

Recent work has shown that, much like the Hadley circulation, the Walker cells are highly regional in character, with their position and intensity varying markedly from season to season (Schwendike et al., 2014, 2015). Instead of representing a steady, quasi-permanent overturning structure, they exhibit substantial transient variability on short timescales. As mentioned before, the passage of a Madden–Julian Oscillation event can temporarily double the strength of a regional Walker cell or cause it to collapse entirely (Schwendike et al., 2021). Thus, as with the Hadley circulation, the Walker circulations are best examined from a regional perspective and with explicit attention to their transient variability.

3. Data and Method

3.1. The ψ-Vector Method

The ψ-Vector Method, originally developed by Keyser et al. (1989) and later adapted by Schwendike et al. (2014), enables the decomposition of the irrotational winds into two independent, orthogonal overturning circulations, each satisfying continuity in a Cartesian framework formulated in spherical pressure coordinates.

Starting with the continuity equation in pressure coordinates:

$$\nabla_p \cdot v + \frac{\partial \omega}{\partial p} = 0, \tag{3.1}$$

where ∇_p is the horizontal gradient operator in isobaric coordinates, v is the horizontal wind field, ω is the vertical pressure velocity and p is the pressure.

According to Helmholtz's theorem, the horizontal wind field (u) can be split into two components

$$u = u_{div} + u_{rot}, \tag{3.2}$$

where u_div corresponds to the divergent part of the flow (curl-free) and u_rot to the rotational part of the flow (divergence-free). The divergent part can furthermore be related to a velocity potential (χ) by

$$u_{div} = \nabla \chi. \tag{3.3}$$

Keeping in mind that the divergence of the rotational part of the horizontal wind field is zero, the new continuity equation is then

$$\nabla_p^2 \cdot \chi + \frac{\partial \omega}{\partial p} = 0. \tag{3.4}$$

A potential function μ is introduced so that the velocity potential can be expressed as

$$\chi = \frac{\partial \mu}{\partial p}. \tag{3.5}$$

This substitution removes the vertical derivative in the continuity equation and reduces it to a horizontal Poisson equation. The resulting expression

$$\nabla_p^2 \mu = -\omega, \tag{3.6}$$

can then be inverted and solved with spherical harmonics to obtain μ.

Introducing the vector stream function

$$\psi = -\nabla_p \mu \tag{3.7}$$

allows equation 3.7 to be written as

$$\nabla_p \cdot \psi = \omega, \tag{3.8}$$

where ψ points towards regions of upward motion and away from regions of downward motion.

Combining equations 3.1, 3.5 and 3.7, the divergent wind can be decomposed into zonal and meridional components by writing it in terms of the stream function as

$$u_{div} = (u_\psi, u_\lambda) = -\frac{\partial \psi}{\partial p} = -(\frac{\partial \psi_\phi}{\partial p}, \frac{\partial \psi_\lambda}{\partial p}), \tag{3.9}$$

where u_ψ and u_λ denote the meridional and zonal components of the divergent part of the horizontal wind and ψ_ϕ and ψ_λ represent the corresponding meridional and zonal stream functions. This relationship makes intuitive sense: if the maximum vertical velocity is assumed to be located at mid-levels, then the low-level flow is parallel and the upper-level flow antiparallel to the ψ-vector. This means that ascent is accompanied by low-level convergence and upper-level divergence, consistent with divergent motion.

The vertical velocity can then be partitioned into meridional and zonal components according to

$$\omega_\phi \cos\phi = \frac{1}{a}\frac{\partial}{\partial \phi}(\psi_\phi \cos\phi) = \frac{1}{a^2}\frac{\partial}{\partial \phi}\left(\cos\phi \frac{\partial \mu}{\partial \phi}\right), \tag{3.10}$$

$$\omega_\lambda \cos\phi = \frac{1}{a}\frac{\partial \psi_\lambda}{\partial \lambda} = \frac{1}{a^2 \cos\phi}\frac{\partial^2 \mu}{\partial \lambda^2}, \tag{3.11}$$

where ω_ϕ and ω_λ denote the vertical velocity associated with the meridional and zonal direction, and a is the Earth's radius. The mass fluxes associated with the meridional and zonal directions are then

$$m_\phi = \omega_\phi \cos\phi / g \quad \text{and} \quad m_\lambda = \omega_\lambda \cos\phi / g, \tag{3.12}$$

where g is the gravitational acceleration.

The result is a decomposition of the vertical motion, on a point basis, into meridional and zonal components, which are referred to as the local Hadley and local Walker circulations in the tropics, respectively. By taking the zonal or meridional average of the local Hadley or Walker circulation over a restricted latitude/longitude belt, a latitude/longitude height cross-section of the overturning circulation is obtained. The averaging operators are

$$[A]_{\lambda_1}^{\lambda_2} = \frac{1}{\Delta\lambda} \int_{\lambda_1}^{\lambda_2} A \mathrm{d}\lambda \text{ and } < A >_{\phi_1}^{\phi_2} = \frac{1}{\Delta\phi} \int_{\phi_1}^{\phi_2} A \mathrm{d}\phi, \tag{3.13}$$

where A is any given variable, the integral boundaries are the initial and final longitudes/latitudes, and $\Delta\lambda/\Delta\phi$ is the difference between the integral boundaries. This average over a restricted area is referred to as the regional Hadley circulation ($[m_\phi]_{\lambda_1}^{\lambda 2}$) and the regional Walker circulation ($< m_\lambda >_{\phi_1}^{\phi_2}$). One must be careful choosing the averaging interval, especially for the local Walker circulation, as the contribution of the meridional component cannot be ignored, especially over thin latitude belts. The same averaging can be done for the decomposed horizontal and vertical wind fields and allows the wind to be represented in the plane of the cross-section used for the regional circulations.

3.2. The ERA5 Global Reanalysis

In this study, the ψ-vector method is applied to the ERA5 dataset (Hersbach et al., 2020), at 0.25° × 0.25° horizontal grid spacing, with 27 pressure levels from 1000 hPa to 100 hPa, on a daily time scale, covering the period 1960-2022 as made available by the WeatherBench 2 project (`https://weatherbench2.readthedocs.io/en/latest/data-guide.html`) (Rasp et al., 2024).

Reanalysis products have become indispensable in climate research because they provide a continuous, physically consistent representation of the historical atmosphere. By combining data assimilation techniques with short-term numerical forecasts, reanalyses transform diverse past observations into a unified global dataset. ERA5 employs four-dimensional variational assimilation (4D-Var; Dimet and Talagrand, 1986), which ensures temporal consistency by assimilating observations over a finite time window rather than treating each measurement independently. This approach allows the resulting fields to evolve smoothly in time while remaining closely constrained by available observations.

The expansion of meteorological satellite monitoring has dramatically improved global observational coverage and, with it, numerical weather prediction (NWP) skill (Bauer et al., 2015). Satellites can deliver accurate retrievals for several key variables, such as outgoing longwave radiation (OLR), total column water vapor, (sea) surface temperature, and precipitation. Nevertheless, satellite systems also exhibit important limitations. Cloudy regions often produce incomplete or uncertain measurements; precipitation retrievals remain highly uncertain over land and areas with complex topography; and many dynamical variables, such as vertical velocity, are currently not available from large-scale retrievals. As a result, satellites alone cannot provide the temporally and spatially consistent global fields required for all climate applications. In situ and ground-based observations, in turn, are spatially inhomogeneous, being concentrated mainly in wealthier populated regions and largely absent over remote areas.

For these reasons, reanalysis is particularly well-suited for the objectives of the present work. Reanalysis data provides a homogeneous, continuous, physically constrained, global representation of the large-scale circulation, making them the most reliable and complete datasets available for obtaining vertical velocity. However, reanalyses are not perfect depictions of historical weather: inaccurate, sparse, or evolving observing systems introduce uncertainties, and the underlying NWP models inevitably carry structural assumptions and biases. Ideally, the method would be applied to multiple reanalysis products to capture model uncertainty. Due to time constraints, this was not done, which represents a limitation of the present work. Schwendike et al. (2015) showed that, while the general pattern of mass flux is consistent across four different reanalyses, there are notable differences in magnitude and trend, which would not be captured in the present work. Even tough, as mentioned, observational precipitation datasets have their own uncertainties, examining both reanalysis and observational data in tandem allows uncertainties in both precipitation estimates and reanalysis products to be better understood.

3.3. Observational Precipitation Datasets

Multiple (quasi-) observational precipitation data sources were used to investigate the relationship between precipitation mass flux and precipitation. Specifically, ERA5 precipitation, the Global Precipitation Climatology Project (GPCP) version 2.3 (Adler et al., 2018) (available at: `https://cds.climate.copernicus.eu/datasets/satellite-precipitation`), and the Integrated Multi-satellitE Retrievals for GPM (IMERG) version 7.0 Final Run (Huffman et al., 2023) were used. The GPCP dataset provides monthly precipitation estimates at a spatial grid spacing of 2.5° × 2.5° from 1979 onward, offering a long-term record that enables the construction of a robust climatology, while also encompassing many positive and negative IOD events for the analysis of associated anomalies. In contrast, IMERG offers higher spatial grid spacing (0.1° × 0.1°), but its data record begins in 2000 onward, allowing for more detailed spatial analyses over a shorter period. Due to its finer spatial grid spacing, IMERG is employed for comparison with regional circulation features, as the coarser GPCP grid would yield only a few bars in the bar plot (e.g., Fig. 4.2). For the Kelvin wave anomaly analysis, the

daily GPCP product was used. IMERG data are available over a comparable time period and offer finer spatial resolution. However, using IMERG would have substantially increased the computational cost of generating the 1000 random anomalies required for the significance estimation (see Sec. 3.6). Given that Kelvin wave anomalies are large-scale features, the finer grid spacing was not considered essential. Therefore, the coarser-resolution GPCP data were chosen as a practical trade-off to reduce computational expense.

Additionally, the Frequent Rainfall Observations on GridS (FROGS) database (Roca et al., 2019) (available from: `https://ipsl.pages.in2p3.fr/espri/espri-obs/distribution/doc-pages/How_to_download_frogs/`) was used to analyze the consistency of rainfall trends between different observational sources and to assess the degree of correlation between precipitation and meridional/zonal mass flux. The FROGS database includes several gridded daily precipitation datasets at a $1^\circ \times 1^\circ$ spatial grid spacing, thereby providing a straightforward means to compare multiple datasets. The datasets that are compared in the present work are: ERA5, IMERG v07b Final Run, GPCP v3.2, African Rainfall Climatology Version 2 (ARC) (Novella and Thiaw, 2013), Global Precipitation Climatology Centre (GPCC) Full Data Daily V2022 (Schneider et al., 2022), Climate Hazards Infrared Precipitation with Stations (CHIRPS) version 2.0 (Funk et al., 2015b), and Tropical Applications of Meteorology using SATellite (TAMSAT) version 3.1 (Maidment et al., 2017). GPCP and GPCC are only availible until 2020 and thus for the trend calculation all datasets have been limited to this year. For the correlation and trend comparison, the ERA5, GPCP and IMERG used are those derived from the FROGS dataset. For the decomposition of the correlation, native ERA5 is used.

3.4. Identification of IOD Events

For the identification of positive and negative phases of the IOD, the monthly Dipole Mode Index (DMI) (Saji et al., 1999), based on the HadISST1.1 sea surface temperature dataset (Rayner et al., 2003) and provided by the National Oceanic and Atmospheric Administration Physical Sciences Laboratory, was used (available at `https://psl.noaa.gov/data/timeseries/month/DMI/`). The DMI was calculated as the difference between SST anomalies averaged over the western tropical Indian Ocean (50°E–70°E, 10°S–10°N) and the southeastern tropical Indian Ocean (90°E–110°E, 10°S–0°). A positive (negative) IOD event was defined as a period comprising at least three consecutive months with DMI values exceeding 0.4°C (falling below -0.4°C) (Jain et al., 2025).

3.5. Identification of Kelvin Waves

Kelvin waves were identified by applying wavenumber-frequency filtering to daily ERA5 OLR data over the 1960–2022 period and the 5°N–5°S band, following the method of Wheeler and Kiladis (1999). First, deseasonalized OLR anomalies were calculated by constructing a daily climatology, smoothing it by removing the first three harmonics, and subtracting the result from the original data. The anomalies were then detrended and transformed into the

wavenumber-frequency domain using a two-dimensional fast Fourier transform. Kelvin wave signals were isolated by retaining only spectral components within the Kelvin-wave ranges defined by Wheeler and Kiladis (1999): periods of 2.5–20 days, zonal wavenumbers 1–14, and equivalent depths of 8–90 m. Finally, an inverse Fourier transform was applied to reconstruct the filtered Kelvin-wave variability in longitude-time space. Following (Riley et al., 2011), the filtered signal (W1) and its time derivative (W2) were standardized by their standard deviation. The local wave amplitude was then calculated as $A = \sqrt{W_1^2 + W_2^2}$, and a wave was considered active if $A \geq 1$. The local wave phase is given by $\theta = \arctan(W_1/W_2)$. The 360° phase cycle was divided into eight phases: phase 1 ($157.5° < \theta < 202.5°$) corresponds to the local dry phase, phase 5 ($337.5° < \theta < 22.5°$) to the local wet phase, and phases 3 ($67.5° < \theta < 112.5°$) and 7 ($247.5° < \theta < 292.5°$) represent neutral phases.

Besides the frequency-wavenumber filtering method used in the present work, another major approach for identifying equatorial waves is the two-dimensional spatial projection technique based on parabolic cylinder functions (Yang et al., 2003). In this method, wind and geopotential fields are projected onto the theoretical meridional structures of equatorial wave modes, and the resulting projection amplitudes provide a measure of how closely the observed or simulated fields resemble these idealized wave patterns. Typically, a time-space filter is still applied beforehand to separate eastward- and westward-propagating components.

The non-dispersive nature of Kelvin waves generally leads to good agreement between different identification techniques (Knippertz et al., 2022). Nevertheless, the narrow filter windows used in the frequency-wavenumber filtering method have been shown to occasionally extract coherent-looking patterns from random data (Knippertz et al., 2022). Therefore, it is recommended to use another identification method, such as the spatial projection method, alongside the frequency-wavenumber filtering. This issue is partly mitigated in the present work, as only waves with a relatively high amplitude are considered. In short, since the present work focuses exclusively on Kelvin waves, the limitations associated with relying on a single identification technique are reduced, though they cannot be eliminated.

Another shortcoming of OLR-based wave detection methods is that they miss the dry waves. However, since the present work is primarily concerned with precipitation variability and therefore with convectively coupled waves, it is not problematic. Moreover, the present work adopts a climatological perspective, analyzing more than 60 years of data. The long time series ensures that the frequency-wavenumber filtering method, which requires a relatively wide temporal window, can be applied without limitation.

3.6. Composite Anomalies

Dates corresponding to the phenomenon of interest (IOD or Kelvin wave phases) were first identified by the methods mentioned above. A composite was then calculated by averaging the variable over the selected dates, and then the anomaly was obtained by subtracting the 1960–2022 climatology. Statistical significance was assessed using a bootstrap resampling

approach (Hesterberg, 2011). For each anomaly, the same number of dates (as the identified event) was randomly selected from the same season of the full dataset 1,000 times without replacement, and the corresponding random composites were computed and compared to the climatology. At each grid point, the 2.5th and 97.5th percentiles of the resulting distribution of random anomalies defined a 95% confidence interval. Observed anomalies falling outside this interval were considered statistically significant at the 0.05 level.

4. Results

4.1. Local to Regional Mean Hadley and Walker Circulations and Associated Precipitation

To establish a baseline for subsequent analysis, this section presents the mean local and regional Hadley and Walker circulations and discusses their connection to the observed precipitation patterns.

4.1.1. Local Hadley and Walker Circulations

Figure 4.1 shows the mean 1960–2022 daily mass flux at 500 hPa with the mean daily precipitation rate from GPCP overlaid as contours. The panels are arranged with columns representing the total (first column), meridional (second column), and zonal (third column) mass fluxes, and rows representing the seasons December–February (DJF), MAM, June–August (JJA), and SON. Because this study covers the entire African continent, the division into the four classical seasons was chosen as a reasonable way to separate thermal and pluvial regimes, although it may not be perfectly representative for all regions of Africa. The black boxes drawn in the last two columns indicate the regions over which the mass flux will later be averaged to construct the regional Hadley and Walker circulations. The three regions marked by the black boxes in the second column of Figure 4.1 are hereafter referred to as West Africa (WA), Central Africa (CA), and East Africa (EA).

The total mass flux is the sum of the meridional mass flux and the zonal mass flux. The main regions of ascent are Central tropical Africa (DJF, MAM & SON), the Guinea Coast (MAM, JJA & SON), the East African highlands (MAM, JJA & SON), and Madagascar (DJF). The main regions of descent are the Sahara, the Subtropical Atlantic Ocean, and the Horn of Africa. From Figure 1a, d, g, and j, it can be seen that there is a strong link between total mass flux and precipitation, as the distribution of areas with positive total mass flux (ascent) matches the mean observed precipitation distribution from GPCP.

The local Hadley circulation is characterized by zonally stretching bands of ascent and descent that migrate meridionally over the continent throughout the year. The ascending branch reaches its southernmost position around 20°S in DJF and then progresses north until its maximum northward position at around 15°N in JJA. The ascent/descent is strongest in the summer/winter hemisphere, and both are most prominent in JJA. The local Hadley circulation shows distinct regional differences. In WA, there is only one main region of

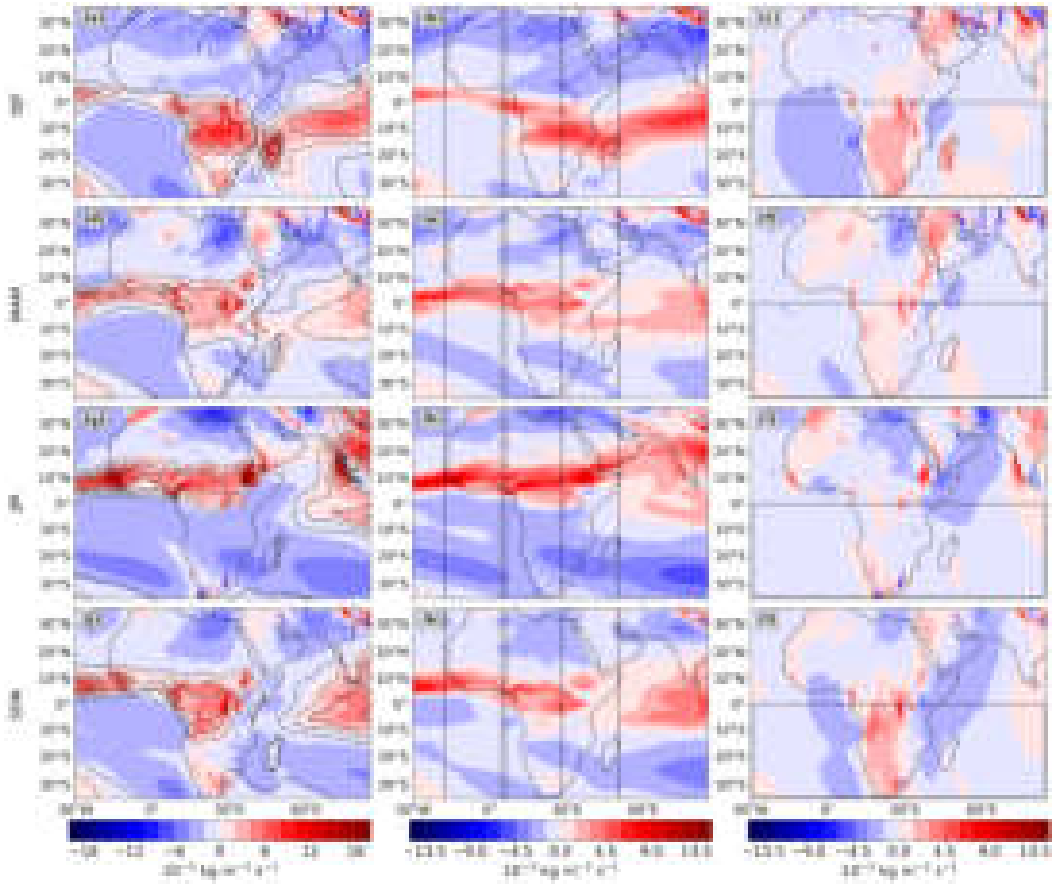

Figure 4.1.: The total mass flux (first column), meridional mass flux (second column), and zonal mass flux (third column) (kg m^{-2} s^{-1}) at 500 hPa calculated from the ERA5 (1960–2022) for the seasons December–February (DJF) (a-c), MAM (d-f), June–August (JJA) (g-i), and SON (j-l). Mass fluxes are shown as shaded colors, with red indicating ascent and blue indicating descent. Dotted black contours show mean GPCP precipitation (1979–2022), with contour levels from 2 to 12 mm day^{-1} in steps of 2 mm day^{-1}. Solid black lines mark the areas defining the regions used for calculating the regional Hadley and Walker circulations.

ascent, which is most prominent in JJA and overall tends to stay at or north of the equator. In CA, there is one main region of ascent in MAM, JJA & SON, and two main regions of ascent in DJF. Ascent in CA is most prominent in SON. In EA, there is one main region of ascent in DJF and JJA, two main regions in SON, and three regions in MAM. The local Hadley circulations shown in Figure 4.1 closely resemble those reported by Schwendike et al. (2015), for other reanalysis datasets.

The local Walker circulation is characterized by meridionally stretched areas of ascent and descent. The main region of ascent are Africa south of the equator (DJF, MAM & SON) and the East African Highlands (year-round). Unlike the local Hadley circulation, the positions of the regions of descent and ascent in the local Walker circulation are relatively stable, and changes in strength mostly dominate the seasonal variability. The local Walker circulation is most prominent in DJF and SON, both marked by strong ascent over the

continent and descent over the Atlantic and Indian Ocean. In DJF there is also strong zonal ascent over Madagascar. In MAM, the circulation weakens, with significant ascent remaining only over the East African Highlands. By JJA, the pattern is dominated by widespread descent, and ascent is confined to the East African Highlands and the Upper Guinea Coast. The DJF patterns in ERA5 agree well with those reported for other reanalysis datasets by Schwendike et al. (2015), whereas the JJA patterns show larger differences. This is consistent with their finding that over Africa, agreement among reanalysis datasets for the local Walker circulation is generally higher in DJF and weaker in JJA.

4.1.2. Regional Hadley Circulations

The previous section showed that the local Hadley and Walker circulations over Africa exhibit distinct regional characteristics. However, examining only the 500 hPa level may overlook important vertical variations in the circulation structure. In this section, therefore, the full vertical profiles of the regional Hadley and Walker circulations, as derived from the averaging intervals outlined by the black boxes in Figure 4.1, are analyzed and compared with observed precipitation. For all regional circulation, the main wet seasons will be the focus; all other seasons can be found in the appendix (see Fig. A.2–A.6).

4.1.2.1. West Africa

The West African monsoon is among the most extensively studied circulation systems in Africa (Sultan et al., 2003; Sultan and Janicot, 2003; Nicholson, 2013; Biasutti, 2019). Its seasonal rainfall is vital to the region's population's socioeconomic well-being. To illustrate the main features of the regional circulation, Figure 4.2 shows the zonally averaged mean daily meridional mass flux (also called the regional Hadley circulation), the time-mean zonally averaged divergent circulation, and the zonally averaged mean daily JJA IMERG precipitation for West Africa (17.5°W–4.5°E). Areas below topography are blanked out.

Three main circulation features are evident: (1) A deep cross-equatorial circulation characterized by a narrow ascending branch between 0° and 15°N, upper-level southward flow leading to a broad subsidence region between 0° and 25°S, and a strong southward flow in the lower troposphere (900–750 hPa) with a very shallow return flow near the surface from 28°S to 0° (1000–900 hPa), closing the cell back toward the rising branch. (2) A shallow Atlantic-Guinean cell extending from approximately 3°S to 3°N, confined below about 550 hPa, with ascent near the Guinean coast and descent over the equatorial Atlantic. (3) A shallow Saharan cell spanning roughly 15°N–30°N, with pronounced ascent around 15°–25°N and strong descent farther north, from 25°N to 30°N, within the 900–550 hPa layer.

The large-scale circulation pattern identified here is broadly consistent with previous studies of the West African monsoon. The deep meridional overturning cell is a robust feature found across all studies covering this region (Nicholson, 2009; Meynadier et al., 2010; Thorncroft et al., 2011; Fink et al., 2017; Raj et al., 2019; Niang et al., 2020). However, unlike in some earlier analyses (Nicholson, 2009; Thorncroft et al., 2011; Fink et al., 2017), the present

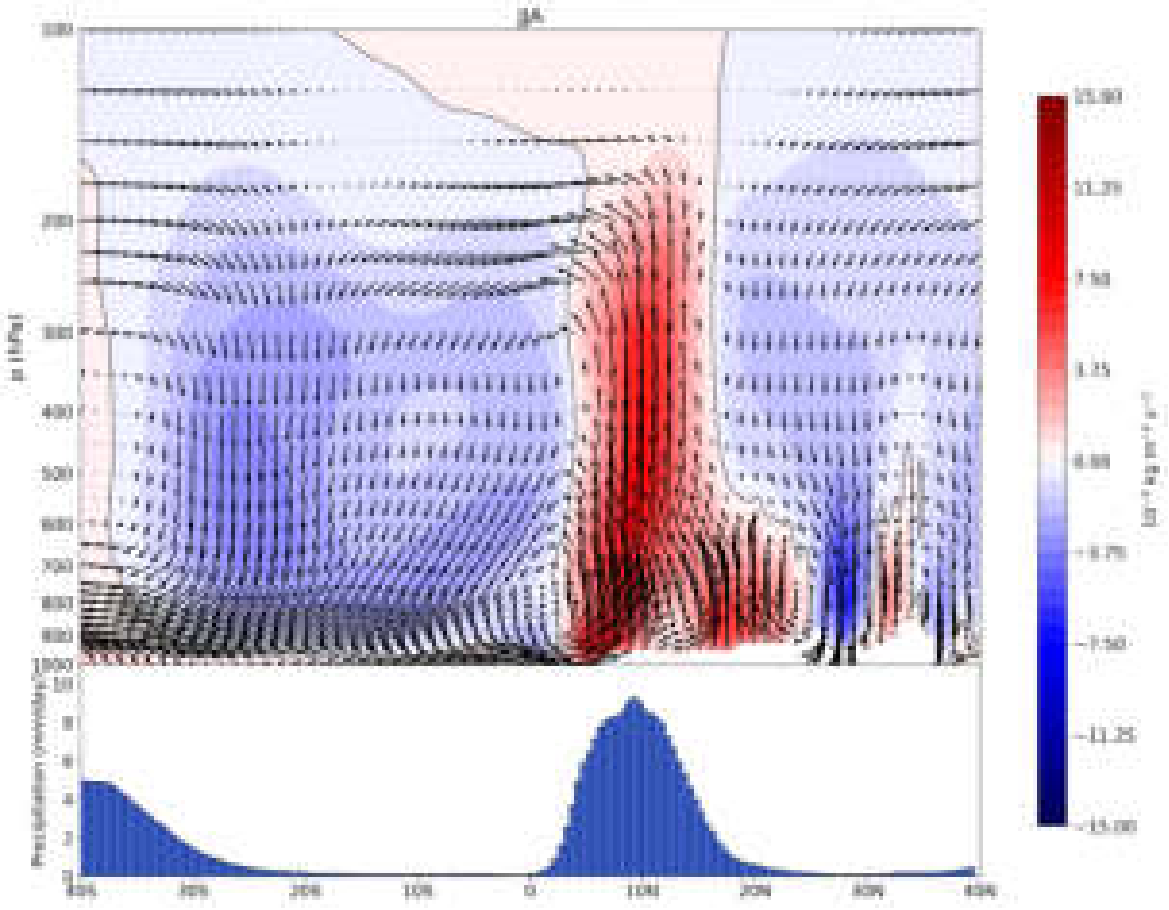

Figure 4.2.: The regional Hadley circulation over West Africa (leftmost box in Figure 1, second column) calculated from ERA5 (1960–2022) for JJA, averaged over the longitudes 17.5° W–4.5° E. The mean meridional mass flux (kg m^{-2} s^{-1}) is shown as shaded colors. Mean IMERG precipitation, averaged over the same longitudes, is shown as bars spaced every 0.5°. Vectors represent the divergent circulation components (u_ϕ, ω_ϕ). The solid black line marks the zero contour. Fields below the maximum orography are omitted.

results do not show a clear poleward flow to the north from the main ascending branch. The shallow Saharan circulation, associated with the Saharan Heat Low, is also a recurrent feature in the literature (Nicholson, 2009; Meynadier et al., 2010; Thorncroft et al., 2011; Fink et al., 2017; Raj et al., 2019; Niang et al., 2020) and is well captured here. In contrast, a shallow monsoon circulation connecting the Saharan Heat Low to the Guinean coast, characterized by a southward return flow (Nicholson, 2009; Thorncroft et al., 2011; Fink et al., 2017), is not evident in our results. Instead, a southward flow into the main ascending core and a shallow circulation cell with descent to the north of the heat low are found, consistent with Raj et al. (2019). A further shallow circulation cell is found between the Guinea Coast and the Atlantic. This Guinean Coast cell is identified in some studies (Raj et al., 2019; Niang et al., 2020) but absent or weakly represented in others. As stated by Nicholson (2009), the maximum in precipitation is not collocated with the surface trade-wind convergence

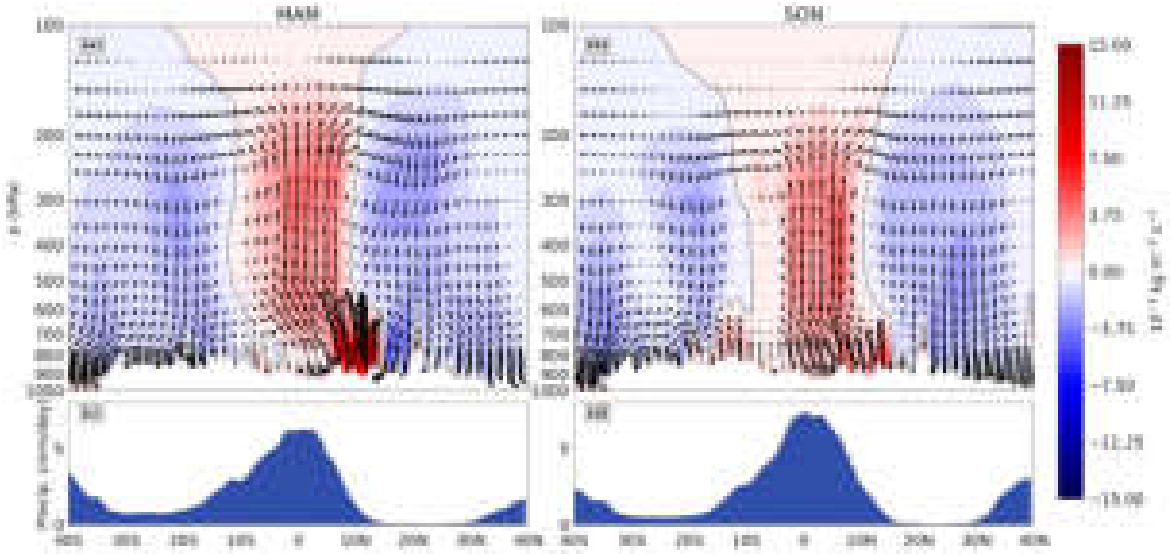

Figure 4.3.: Same as Figure 4.2, but for Central Africa (8° E–28° E) and the seasons MAM and SON.

(around 20°N). Instead, as was shown in Figure 4.1, it coincides with the region of strongest ascent at 500 hPa.

4.1.2.2. Central Africa

Compared with West Africa, the central African climate has generally received less attention (Pokam et al., 2022). Its main circulation characteristics are illustrated in Figure 4.3, which shows the regional Hadley circulation, the time-mean zonally averaged divergent circulation, and the zonally averaged mean daily IMERG precipitation for MAM and SON over Central Africa (8°E–28°E).

Two main features stand out. First, both seasons exhibit a classical Hadley-like structure, with a deep and narrow ascending branch near the equator and broad descent to the north and south. The flow diverges aloft and flows poleward in both hemispheres, however no low-level return flow is observed. Unlike Longandjo and Rouault (2024), a shallow circulation cell embedded within the main ascending branch is not evident here. Instead, a pronounced shallow ascent occurs around 10°N in both seasons, particularly strong during SON. In SON, this shallow feature closely resembles the Saharan Heat Low observed during JJA over West Africa, with low-level convergence centered in the Northern Hemisphere. Thus, rather than representing a distinct shallow circulation cell, this feature may be better interpreted as a heat low. The core deep ascent remains centered near the equator at mid- to upper levels, giving the circulation a slightly tilted vertical structure. As in West Africa, the maximum precipitation is collocated with the maximum meridional mass flux at 500 hPa. Similarly to what was found by Nicholson (2018) and Longandjo and Rouault (2020, 2024), this region does not coincide with the surface wind convergence, suggesting that precipitation formation here is largely decoupled from the “classical ITCZ” and is likely influenced moisture transport and the resulting mid-tropospheric moisture convergence

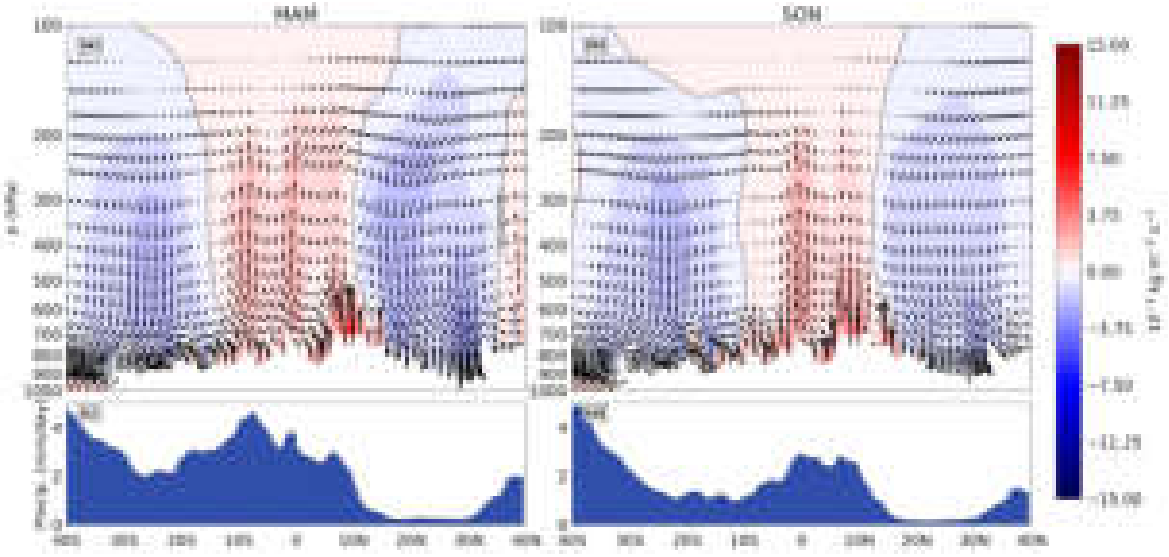

Figure 4.4.: Same as Figure 4.2, but for East Africa (28°E–50°E) and the seasons MAM and SON.

(Longandjo and Rouault, 2024). The highest precipitation amounts occur in SON, coinciding with stronger and more confined ascent.

4.1.2.3. East Africa

The regional Hadley circulation weakens considerably over East Africa (28°E–50°E), which, like Central Africa, experiences two main rainy seasons. These are typically the long rains (MAM) and the short rains (October–December (OND)), but for consistency with the rest of this study, SON is used here (results for OND and SON are similar, but everything is shifted more southwards).

Over East Africa, only a broad region of deep ascent is observed, with no evidence of a shallow circulation. The upper-level poleward flow is relatively weak, and no low-level return flow or associated low-level convergence can be identified. Unlike in the other regions, ascent does not occur in a single homogeneous core: three distinct centers of deep ascent are present during MAM, and two during SON. These ascent regions are centered over areas of high topography, and precipitation peaks are collocated with these zones of relatively strong ascent. In general, as in the other regions, precipitation coincides with upward motion. However, an exception is found between 20°S and 40°S, where relatively high precipitation occurs in a region of descent. This area is mostly oceanic, and the precipitation there is likely associated with the rotational circulation, such as passing cyclones. Another cause for the observed high precipitation could be shallow orographic precipitation associated with the southeasterly trade winds. Overall, the contrast between the strong, deep ascent over West and Central Africa and the weaker, topographically fragmented ascent over East Africa again highlights the Hadley circulation's strong regional structure across the continent.

In general, when the regional Hadley circulations of all three regions defined in the present work are compared to the regional Hadley circulation shown in de Oliveira et al. (2018), the

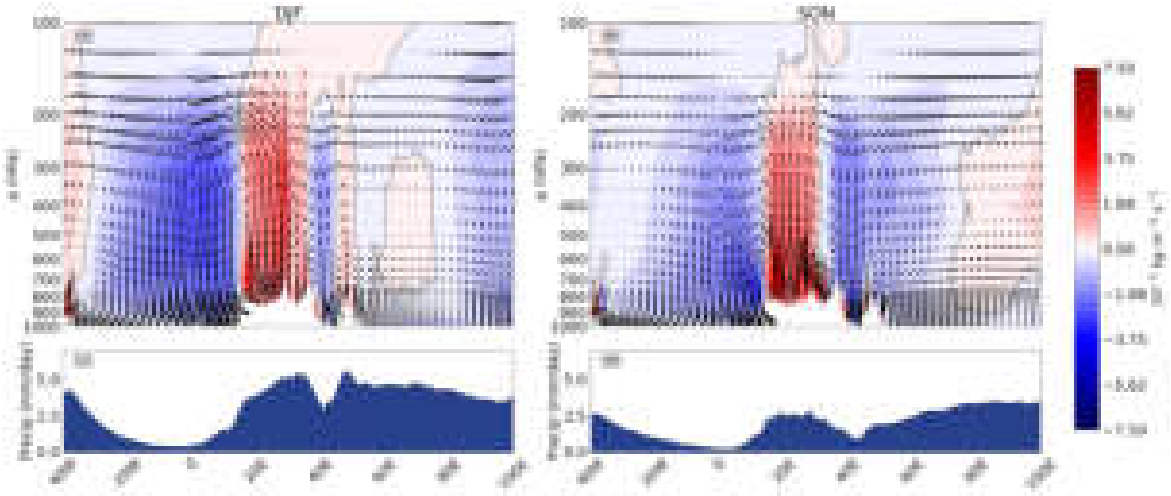

Figure 4.5.: The regional Walker circulation over Africa south of the equator (box in Figure 1, third column) from ERA5 (1960–2022) for DJF and SON, averaged over the latitudes 0°S–34.5°S. The mean zonal mass flux (kg m^{-2} s^{-1}) is shown as shaded colors. Mean IMERG precipitation, averaged over the same latitudes, is shown as bars spaced every 0.5°. Vectors represent the divergent circulation components (u_λ, ω_λ). The solid black line marks the zero contour. Fields below the maximum orography are omitted.

added benefit of choosing smaller sub-regions becomes apparent. The circulations in WA, CA, and EA all have their own distinct spatial and seasonal characteristics, which are lost when averaging over a broader longitude band.

4.1.3. Regional Walker Circulations

The focus now moves from the zonally averaged circulation to the meridionally averaged circulation. Previous studies have primarily focused on Equatorial Central Africa and have identified a deep zonal overturning circulation as an important feature (Pokam et al., 2014; Cook and Vizy, 2016; Longandjo and Rouault, 2020; Zhao and Cook, 2021). Pokam et al. (2014) and Longandjo and Rouault (2020), furthermore identify a co-occurring shallow zonal circulation cell, termed the Congo Basin cell. However, as shown in Figure 4.1, the circulation extends beyond the equatorial region: a broad zone of ascent spans from the equator to the Cape, characterized by rising motion over the continent and subsidence over the adjacent oceans. To better understand this broader zonal structure, therefore, the regional Walker circulation over Africa south of the Equator is discussed here.

Figure 4.5 presents the meridionally averaged zonal mass flux, the associated divergent circulation, and the meridionally averaged daily mean precipitation over Africa south of the Equator (0–34.5°S) for DJF and SON.

Four distinct zonal circulation cells can be seen: (1) An anticlockwise circulation with ascent over continental Africa and descent over the subtropical Atlantic is present in all seasons. (2) A clockwise circulation with ascent over continental Africa and descent over the Indian

Ocean is present in SON. (3) An anticlockwise circulation with ascent over Madagascar and descent over the adjacent Mozambique-Channel is present in DJF. (4) Another anticlockwise circulation, featuring descent over the western Indian Ocean and ascent toward its eastern side, occurs in MAM, JJA, and SON.

Cell (4) corresponds to the well-known Indian Ocean Walker cell identified in previous studies. It is very weak in DJF, largely masked in the meridional mean by the strong ascent over Madagascar, and relatively weak in SON because its climatological position lies north of the averaging regions. Cell (1), the Africa–Atlantic circulation, appears distinct from the deep Congo Basin Walker cell described by Cook and Vizy (2016), as it reaches peak intensity in DJF and SON rather than in June–September (JJAS). Consistent with Longandjo and Rouault (2020), a shallow (below 550 hPa) zonal cell extending from the African continent toward the Atlantic (20°E–8°E) is also identified, present in SON and JJA but not year-round as previously suggested for the shallow Congo Basin cell. In DJF, only a deep circulation over the African continent and Madagascar is present. In particular, zonal ascent over Madagascar is found consistently in many reanalysis products (see Fig. 7 in Schwendike et al., 2015), but is known to be missing in many climate models (Munday and Washington, 2018). This inaccuracy results in a misrepresentation of the water balance between Madagascar and subtropical southern Africa in these models. However, Munday and Washington (2018) find that ascent over Madagascar is part of the larger Indian Ocean Walker cell, whereas the present work identifies a distinct Madagascar-Mozambique Channel cell.

As with the regional Hadley circulation, regions of ascent generally coincide with enhanced precipitation. In some areas, however, elevated precipitation occurs alongside zonal descent; this apparent mismatch arises because precipitation is primarily controlled by the total mass flux, not the zonal component alone. Within the averaging region defining the regional Walker circulation, strong meridional ascent persists. The relatively high precipitation thus indicates that in these areas, the local Hadley circulation mainly drives it.

4.2. Correlation Between Mass Flux and Precipitation

The previous section has shown that the mean mass flux patterns closely match the observed precipitation patterns. However, it remains to be determined whether total mass flux and precipitation also exhibit similar variability. To address this question, the Spearman correlation between total mass flux and precipitation was computed using multiple rainfall products from the FROGS dataset. To ensure spatial consistency with the FROGS data, the mass flux fields were regridded to a $1^\circ \times 1^\circ$ grid spacing using conservative remapping as implemented in the Climate Data Operators (Schulzweida, 2023). The resulting Pearson correlations between total mass flux and precipitation from various sources for the period 2000–2021 are shown in Figure 4.6. Gridpoints with mean precipitation below 1 mm day^{-1} are blanked out.

Among the different rainfall products, ERA5 shows by far the strongest correlation with the total mass flux in all seasons, as expected given that ERA5 precipitation and vertical

velocity are both derived from the same assimilation and forecasting system. However, the Spearman correlation is not one at every gridpoint; notable areas with lower correlation are regions with low positive or negative mass flux (see Fig. 4.1) and over the Congo Basin. The lower correlation suggests that deep ascent is not the primary driver of precipitation variability in these areas. Instead, variability is likely influenced by the rotational circulation features, shallow orographic precipitation, shallow circulations, and more.

Overall, the solely station-based GPCC shows the weakest correlation with the total mass flux across all seasons. In contrast, all precipitation products that use satellite observations exhibit similar spatial patterns of semi-strong correlation, but with lower magnitudes than ERA5. These weaker correlations are expected, as the comparison involves modeled mass flux versus observed precipitation. Two notable exceptions are observed: (1) all products show particularly low correlations in JJA, and (2) correlations are low to near zero over the Congo Basin for all seasons.

Previous studies have reported relatively good agreement between ERA5 precipitation and the Climatic Research Unit (CRU) gauge dataset during JJA/JJAS over the Sahel-Guinea coast area (Quagraine et al., 2020; Steinkopf and Engelbrecht, 2022). They furthermore showed that CRU in the same season has a high correlation with other datasets such as GPCC and CHIRPS, suggesting that these datasets should also be reasonably well correlated with ERA5. However, both studies used monthly data and periods spanning roughly 1980–2016/2017. The low correlations observed here during JJA may therefore reflect the shorter analysis period or the higher temporal resolution (daily) used in this study. When focusing on a shorter and more recent period (1998–2018), Hersbach et al. (2020), like the present work, report relatively weak correlations over the Sahel-Guinea Coast region, even though their analysis is based on monthly data. This supports the interpretation that the reduced agreement arises at least partly from the shorter evaluation period. Another possible explanation for the lack of correlation could be that mesoscale convective systems (MCSs) dominate precipitation in this region (Feng et al., 2021), and the spatial pattern of MCS contribution to total precipitation closely matches the areas where ERA5 performs poorly. This could also explain why ERA5 precipitation exhibits weak correlations with observed rainfall over the Congo Basin, as was also found by Hersbach et al. (2020). Like over the Sahel, MCSs dominate rainfall over the Congo basins. In general, the finding that correlation is reduced due to MCSs would align with previous work showing that ERA5 misrepresents MCS-related precipitation and is known to underestimate it (Chen et al., 2022; Torsah et al., 2025). For the Congo Basin, part of the low correlation between mass flux and observed precipitation comes from the fact that ERA5 itself shows a weaker mass-flux–precipitation relationship in this region. Because observational datasets generally correlate even less strongly with mass flux than ERA5 precipitation does, this already-weak baseline further reduces the mass-flux–observed-rainfall correlation. Despite these areas of lower correlation, the reasonably strong correlation in other regions indicates that ERA5 mass flux can provide insights into observed precipitation variability.

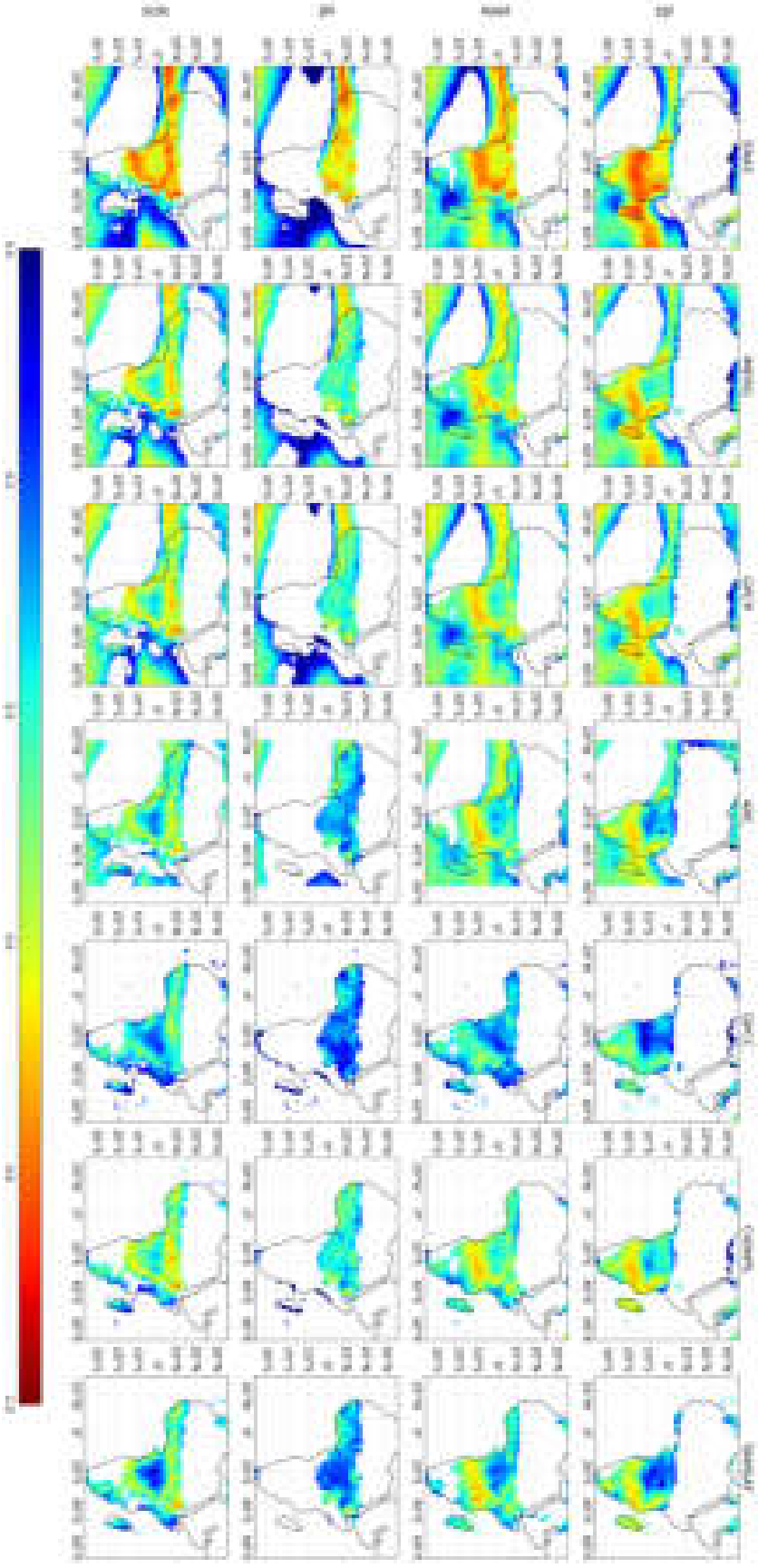

Figure 4.6.: Spearman rank correlation between total mass flux (kg m^{-2} s^{-1}) and precipitation from multiple precipitation products (mm day^{-1}) for the seasons DJF (first row), MAM (second row), JJA (third row) and SON (fourth row) for the period 2000–2020.

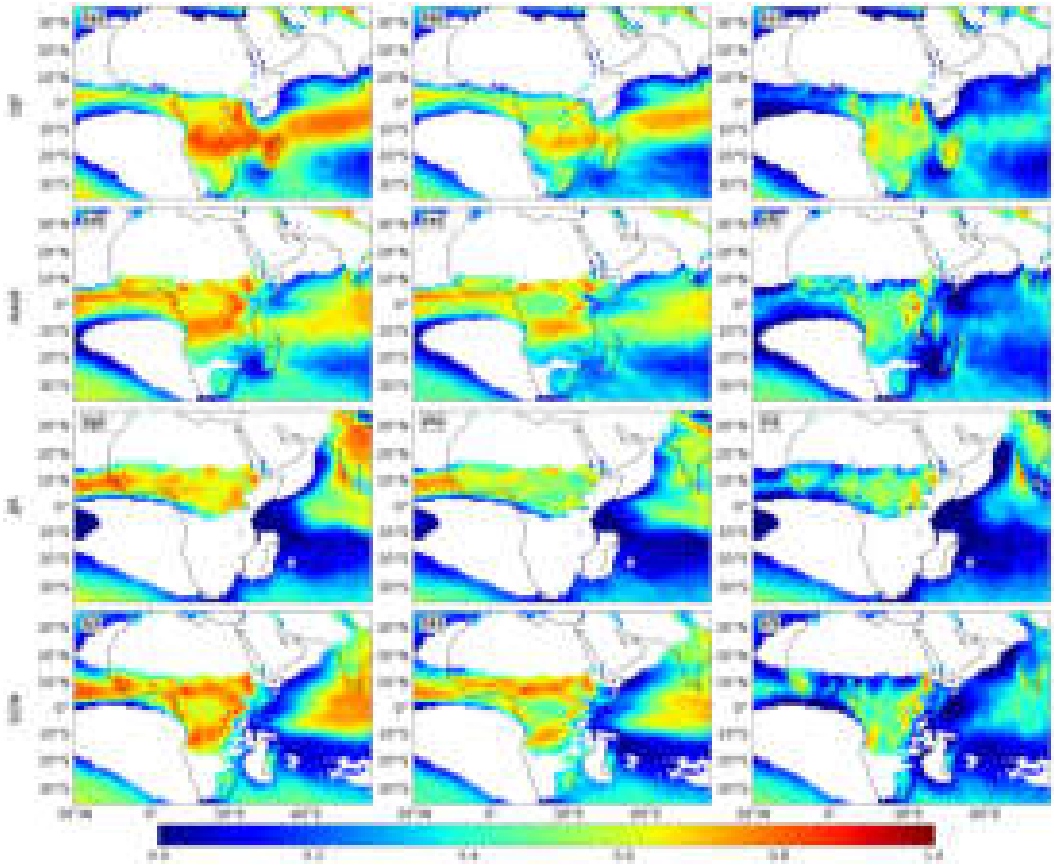

Figure 4.7.: Spearman rank correlation between ERA5 precipitation (mm day^{-1}) and total (first column), meridional (second column) and zonal mass flux (third column) (kg m^{-2} s^{-1}) for the seasons DJF (first row), MAM (second row), JJA (third row) and SON (fourth row) for the period 2000–2020.

4.2.1. Correlation Between Local Circulation Components and Precipitation

By examining correlations between ERA5 precipitation and not only the total mass flux but also its meridional and zonal components, we can assess whether the local Hadley or Walker circulation contributes more to rainfall variability. Figure 4.7 shows the Spearman correlation coefficient between the daily ERA5 precipitation and total mass flux (first column), the meridional mass flux at 500 hPa (second column), and the zonal mass flux at 500 hPa (third column). Areas with a mean precipitation rate of below 1 mm day^{-1} have been omitted. The correlation pattern between meridional mass flux and ERA5 precipitation closely resembles that between total mass flux and precipitation, suggesting that the local Hadley circulation accounts for most of the rainfall variability. The meridional mass flux is especially weakly correlated over the Congo Basin, which explains the lack of correlation between total mass flux and precipitation. The areas with the highest correlation in the zonal mass flux are generally high-elevation regions, such as the East African and Angolan Highlands. Both these mountain ranges are North-South orientated, and the high correlation between zonal mass flux and precipitation might indicate the importance of deep orographic precipitation. Outside these concentrated areas, the local Walker circulation shows relatively

low correlations, even in seasons when its mass flux is equal to or greater than the meridional mass flux. Interestingly, the zonal mass flux exhibits similar correlation levels in JJA, when zonal ascent is largely absent, as in DJF and SON, the seasons with the strongest ascent.

4.3. Trends in Mass Flux and Associated Trends in Precipitation

In previous work, Schwendike et al. (2015) applied the ψ-vector method to multiple reanalysis datasets to examine global trends (1979–2009) in the local Hadley and Walker circulations, demonstrating its advantages for regional trend analysis and its usefulness in studying precipitation changes. This section aims to apply the same method to investigate recent changes in the local Hadley and Walker circulations over Africa and to compare these trends with modeled and observed precipitation trends, ultimately providing insight into the drivers behind the precipitation changes.

Figure 4.8 shows the linear trends from 2000 to 2020 in total mass flux at 500 hPa and daily precipitation from various gridded rainfall products derived from the FROGS data. As with the correlation, the mass flux fields were regridded to a grid spacing of $1° \times 1°$ to ensure consistency. As shown in Figure 4.1, the mean total mass flux and mean daily precipitation share similar spatial patterns. Figure 4.8 further reveals that their linear trends over time are also highly consistent (in regions where precipitation occurs). Overall, there is reasonable agreement among the rainfall products, particularly between ERA5, IMERG, GPCP, CHIRPS, and TAMSAT. CHIRPS and TAMSAT show similar spatial patterns but generally exhibit lower-magnitude trends than the other datasets. The ARC data especially stands out, when all other data shows a patchwork of increasing/decreasing trends, the ARC data shows a big homogeneous area of strongly increasing precipitation. When looking at the time series averaged over the area with a strong trend (not shown), it shows that in all seasons the positive trend is due to a rapid increase from 2019 to 2020, reaching a 70% per year increase in JJA.

Several coherent precipitation trends emerge across the majority of the datasets analyzed. In Madagascar, there is a notable decrease in rainfall during DJF and MAM. This decline is consistent with station-based analyses by Randriamarolaza et al. (2022), who report a pronounced decline in annual precipitation indices and an increase in drought indices during these seasons since the 2000s. Supporting this, Rigden et al. (2024) show that soil moisture and the Normalized Difference Vegetation Index (NDVI) in Madagascar have sharply declined since the start of the 20th century, further indicating a long-term drying trend.

In contrast, rainfall in East Africa has increased during MAM and SON. The positive trend in MAM precipitation has been previously observed by Wainwright et al. (2019) and Palmer et al. (2023), who used CHIRPS, ARC, GPCP, and TAMSAT data. This increase represents a reversal of the long-term drying trend previously observed in the region (Funk et al., 2005, 2008; Williams and Funk, 2011; Funk et al., 2015a) and reflects a recent rainfall recovery, likely associated with a lengthening of the rainy season (Wainwright et al., 2019).

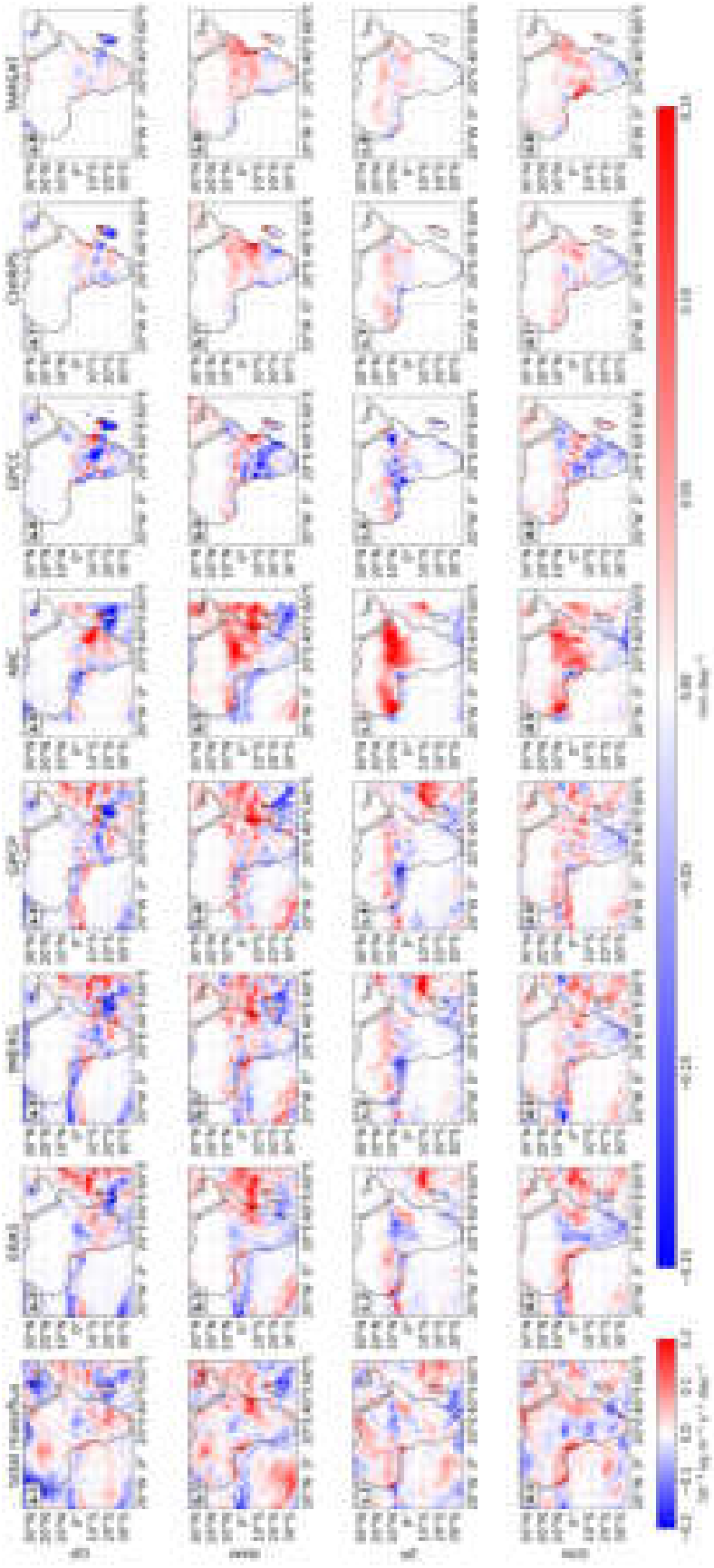

Figure 4.8.: Trends in total mass flux at 500 hPa (first column) (kg m^{-2} s^{-1} day^{-1}) and in precipitation from multiple precipitation products (mm day^{-2}) for the seasons DJF (first row), MAM (second row), JJA (third row) and SON (fourth row) for the period 2000–2020.

The increase in SON precipitation over East Africa has also been reported previously by Manatsa and Behera (2013) and Nicholson (2015), and is attributed to recent, more pIOD like conditions.

Over the Sahel, an increase in JJA precipitation is evident in all products, although it is mostly confined to the western Sahel in ERA5 and GPCC. This finding aligns well with multiple studies documenting the post-1980s recovery of Sahel rainfall (Sanogo et al., 2015; Biasutti, 2019; Nicholson et al., 2018a). ERA5 actually shows a negative trend over the eastern Sahel and fails to capture the drying over the eastern Guinea Coast that appears in the other products and was previously reported by Efon et al. (2023). Furthermore, the Sahel rainfall recovery is mostly absent from the 1983–2020 ERA5 trend (Fig. A.7). This is surprising, given that the 80s were a historical rainfall minimum in the Sahel, from which a distinct recovery is evident in the other datasets. Together, these inconsistencies further highlight the mismatch between observed and modeled JJA rainfall in the region.

The last trend that shows broad consistency across datasets is the decline in SON precipitation over Southern Africa. This drying has been partially reported by Mahlalela et al. (2020), who analyzed both station and CHIRPS data and found a declining trend in the Eastern Cape region between 1981 and 2018. The trend in southwestern Africa appears to continue the generally drier conditions observed during the ON season for the 1980–1999 period (Nicholson et al., 2018b).

A prominent trend, visible across all seasons in the ERA5 data but not clearly present in the other products, is a decrease in precipitation and, consequently, in total mass flux over Central Africa and the Congo Basin. The GPCC data also shows some areas of decreasing precipitation over Central Africa, whereas the satellite products exhibit noisier, less coherent trends in this region. The drying trend over Central Africa appears to be a robust, long-term feature in ERA5. As shown in Appendix A.7, ERA5 is the only dataset to show a substantial decrease in precipitation over Central Africa across all seasons since 1983. As with the low correlation found for JJA mass flux, the mismatch between modelled and observed trends over the Congo Basin is consistent with previously reported weak correlations in this region. The negative trend in precipitation over the Congo Basin in reanalysis datasets has been the subject of numerous studies (see Kenfack et al., 2024), and its discrepancy with observed precipitation trends has also been noted before by Gleixner et al. (2020).

4.3.1. Trends in the Local Circulation Components

Areas showing coherent rainfall trends across different observational and reanalysis products offer greater confidence that the detected changes are physically meaningful rather than artifacts of individual datasets. Investigating the corresponding trends in the local Hadley and local Walker circulation mass fluxes can thus shed light on possible mechanisms responsible for these rainfall variations. Figure 4.9 shows the decomposition of the total mass flux trend shown previously in Figure 4.8.

Firstly, the decrease in DJF and MAM precipitation over Madagascar is primarily associated with a reduction in meridional mass flux over the southern part of the island and a decrease

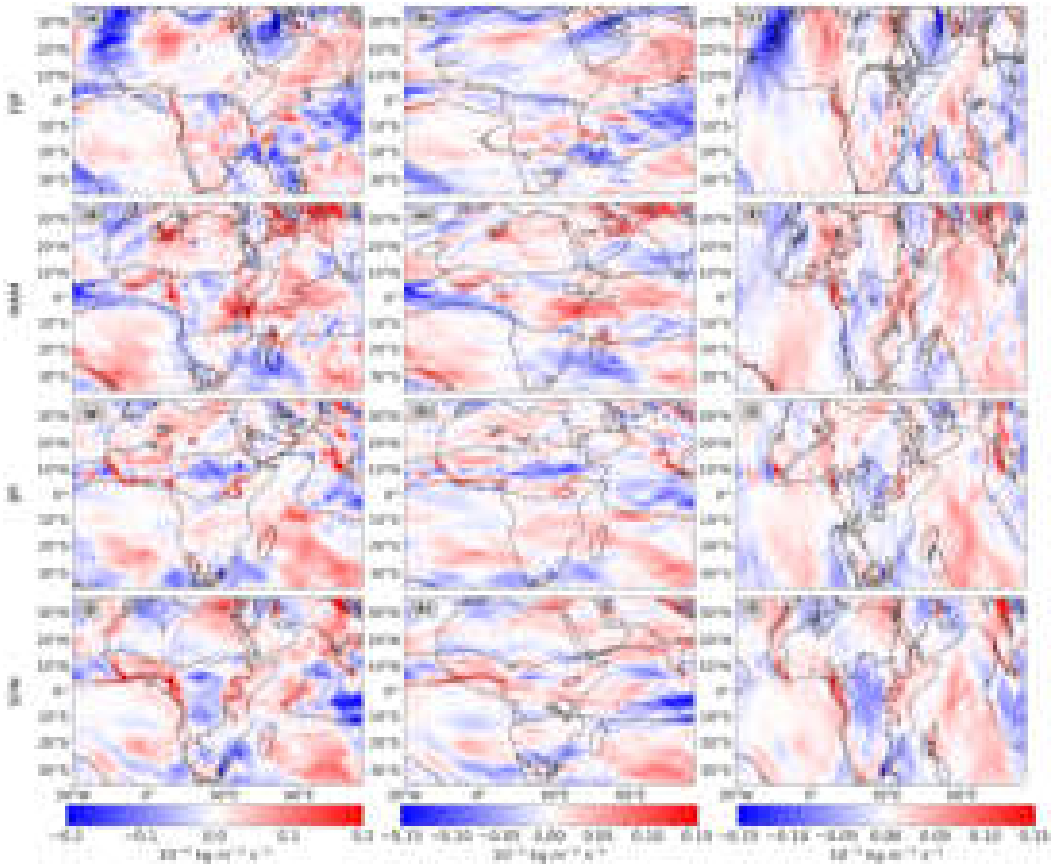

Figure 4.9.: Trends in total (first column), meridional (second column) and zonal mass flux (third column) (kg m^{-2} s^{-1}) for the seasons DJF (first row), MAM (second row), JJA (third row) and SON (fourth row) for the period 2000–2020.

in zonal mass flux mainly along the eastern and western coasts. The reduction in zonal mass flux along the coasts is accompanied by an increase over central Madagascar, suggesting a strengthening and contraction of the Madagascar-Mozambique Channel Walker cell. This strengthening also contributes to the observed increase in precipitation over the northern part of the island. Projected drying trends over southern Madagascar are ascribed to an expansion of the Hadley circulation by Rigden et al. (2024). However, this explanation does not entirely match the observed changes in meridional mass flux, which indicate a decrease in the strength of both the ascending and descending branches of the local Hadley circulation in DJF and a northward shift of the ascending branch in MAM.

Moving from the southwestern Indian Ocean to East Africa, the increase in MAM precipitation over East Africa appears to be driven primarily by an increase in zonal mass flux, complemented by a strengthening of the meridional mass flux near Kenya and Somalia. Wainwright et al. (2019) identified the cooling of March SSTs south of Madagascar as a potential driver of this recent rainfall recovery, as it promotes the northward progression of the seasonal rainband. The increase in meridional mass flux during MAM is concentrated mainly around the northern part of the mean ascending branch of the local Hadley circulation (Fig. 4.9), indicating a more northward-focused rainband, consistent

with the mechanism proposed by Wainwright et al. (2019). For SON, the observed increase in precipitation has been proposed to be linked to pIOD conditions (Manatsa and Behera, 2013; Nicholson, 2015). Indeed, the trend in zonal mass flux (Fig. 4.9i) during SON closely resembles the zonal mass flux anomaly associated with a typical pIOD event (Fig. 4.10e), supporting this explanation.

Further to the west over the Sahel, the increase in JJA precipitation results from roughly equal contributions of enhanced meridional and zonal mass fluxes. The dry conditions in the Sahel during the 1980s are often attributed to an anomalously southward position of the ITCZ, and consequently, a southward displacement of the ascending branch of the local Hadley circulation. However, there is no strong signal in the meridional mass flux trends indicating a recent northward migration. This may partly reflect the comparatively weak recovery of Sahel rainfall in the ERA5 data and should be interpreted with caution given the generally low correlation with observed precipitation in this area.

Moving from the Sahel to Southern Africa, the decrease in SON rainfall is associated with a decrease in meridional mass flux in the southern part of the region and a decrease in zonal mass flux further north. Mahlalela et al. (2020) suggest that changes in the South Atlantic and South Indian Ocean semi-permanent anticyclones could be among the drivers of reduced SON precipitation over the Eastern Cape region, and they find no clear link to large-scale climate modes. However, as shown later and also noted by Mahlalela et al. (2020), pIOD events generally lead to drier conditions over Southern Africa. Furthermore, there has been an observed and projected increase in consecutive pIOD events (Wang et al., 2024b) as well as a projected increase in extreme pIOD events (Cai et al., 2014). Thus, as with the increase in SON precipitation over Eastern Africa, part of the observed drying trend may be explained by changes in the IOD, which could become even more influential in the future.

Finally, the drying trend over Central Africa, which is unique to ERA5, is mainly driven by a decrease in zonal mass flux. This is accompanied by an increase in zonal mass flux near the western and eastern coasts, indicating an overall weakening of the Africa-Atlantic and Africa-Indian Ocean Walker cells. This link between the drying trend and the Walker circulation was already proposed in earlier work by Malhi and Wright (2004), who noted that the African tropical rain forest zone is sensitive to small fluctuations in the Walker circulation. Consistent with this large-scale dynamical perspective, Kenfack et al. (2024) attribute the decrease in precipitation to a decline in the atmospheric heating source, accompanied by reduced vertical moisture advection, vertical velocity, and horizontal MSE advection. These findings are consistent with a weakening of the African Walker cells. Consequently, the observed zonal mass flux trends and the discrepancy between observed and ERA5 rainfall trends may stem from an inaccurate representation of atmospheric heating trends in ERA5.

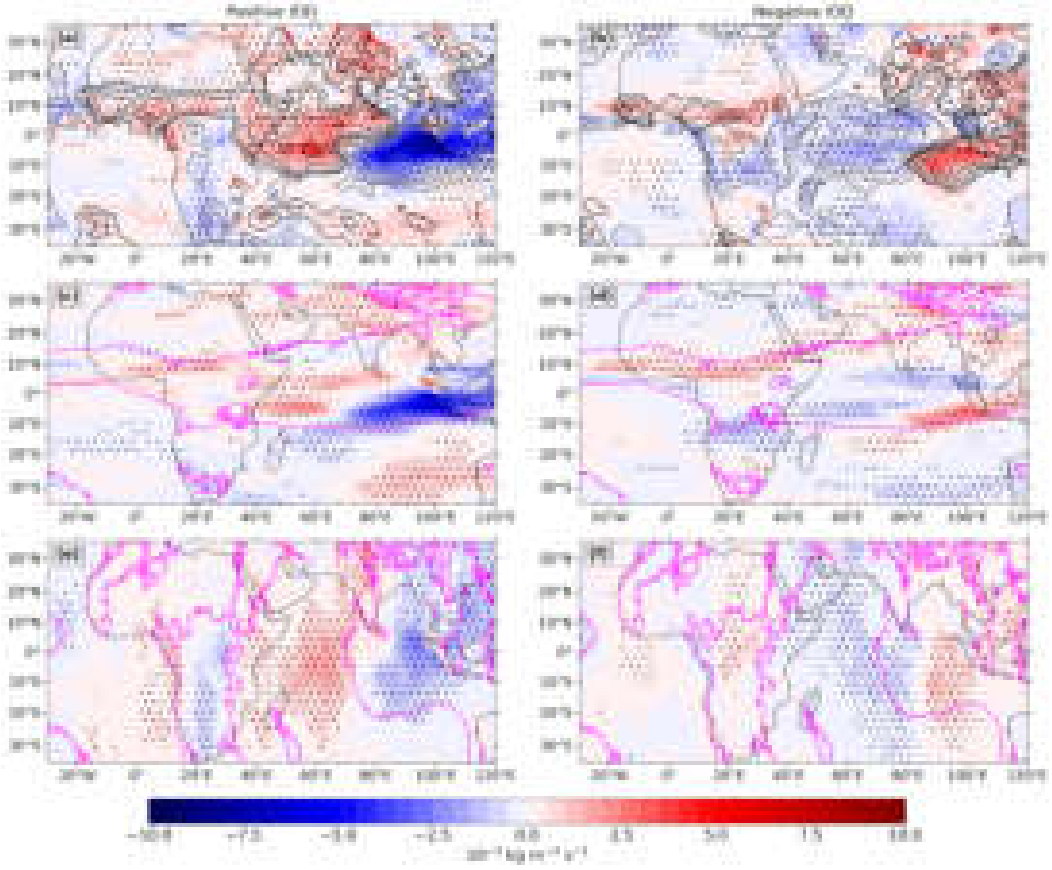

Figure 4.10.: Indian Ocean Dipole (IOD) phase anomalies of the local Hadley and Walker circulations and their combined anomaly at 500 hPa with respect to the 1960–2022 mean. The total (top row), meridional (middle row), and zonal mass flux (bottom row) (kg m^{-2} s^{-1}) for positive IOD phase (left column) and negative IOD phase (right column). The total mass flux anomaly (first column) is overlaid with the corresponding GPCP precipitation anomaly (black contours) at levels of -5, -2, -1, -0.5, -0.25, 0.25, 0.5, 1, 2, and 5 mm day^{-1}. Areas with statistically significant anomalies at the 95% confidence level are dotted. The solid magenta contours denote the zero line of the annual mean local Hadley and Walker circulations.

4.4. The Indian Ocean Dipole

Interannual changes in Indian Ocean SSTs, expressed through the IOD, are well known to be closely linked to variations in the Indian Ocean Walker cell. Associated changes and interactions with the Asian summer monsoon and thus with the local Hadley circulation have also received considerable attention, but have not been fully quantified. This section, therefore, examines how the IOD modifies the local Hadley and Walker circulations and how these circulation changes translate into rainfall anomalies over Africa and the Indian Ocean.

Figure 4.10 shows total, meridional, and zonal mass flux anomalies at 500 hPa for the positive (pIOD; first column) and negative (nIOD; second column) phases of the IOD in SON (the season with matured IOD). Note that years with ENSO-IOD concurrence, and

thus the influence of ENSO, have not been filtered out. The first row shows the total mass flux anomaly (shading) together with the associated GPCP precipitation anomaly (black contours). The second row shows the meridional mass flux anomaly (shading) with the mean zero contour of the meridional mass flux (magenta line), while the third row shows the zonal mass flux anomaly (shading) with the mean zero contour of the zonal mass flux (magenta contour). Shading in the first row is restricted to significant total mass flux anomalies, stippling in the first row indicates significant precipitation anomalies, and stippling in the second and third row indicates significant mass flux anomalies.

The IOD is characterized by changes in the zonal SST gradient between the western and eastern tropical Indian Ocean (Saji et al., 1999). Because of this predominantly zonal pattern of SST anomalies, it is straightforward to infer that IOD events involve changes in the Walker circulation, with enhanced convection over the warmer western Indian Ocean (WIO) and suppressed convection over the cooler EIO during the positive phase. This zonal signal is also evident from the results of the decomposition shown in Figure 4.10e-f, where, during a pIOD event, a positive zonal mass flux anomaly is observed over the WIO and a corresponding negative anomaly over the EIO, separated by the mean zero contour (magenta contour Fig. 4.10e), thus signaling a weakening of the Indian Ocean Walker cell. The influence extends past the Indian Ocean; a pIOD event is accompanied by a decrease in strength of the Africa-Atlantic and Africa-Indian Ocean Walker cells, with a negative zonal mass flux anomaly over the continent and positive anomalies over the bordering oceans. This could be explained by a reduction in the zonal temperature gradient between the continent and the Indian Ocean, which weakens the Central Africa-Indian Ocean Walker cell. Since transport from the east is essential for supplying moisture to Central Africa in SON (Kenfack et al., 2024), this could make ascent less favorable and thus help explain the weakening of the Africa-Atlantic Walker cell.

Less obvious, is the response of the Hadley circulation to an IOD event. Previous studies have argued that changes in monsoon winds or a northward-shifted ITCZ may link the IOD to meridional overturning anomalies, but these mechanisms have not been well quantified. The observed IOD-related meridional SST anomaly in the EIO, which is as strongly correlated with rainfall anomalies as the zonal SST anomaly (Weller and Cai, 2014), suggests that perhaps a response in the meridional circulation should be expected. The actual response of the local Hadley circulation becomes evident from Figure 4.10 c-d; its magnitude is comparable to or even larger than that of the local Walker circulation, particularly during a pIOD event. During a pIOD event, there is a strong negative meridional mass flux anomaly over the EIO, especially near Sumatra, and a positive anomaly over the WIO. The negative meridional mass flux anomaly is collocated with the negative SST anomaly (Saji et al., 1999) and lies exactly at the location of the mean southern edge of the ascending branch of the local Hadley circulation (see Fig. 4.10c). Furthermore, near the northern edge of the ascending branch, there is increased meridional mass flux. Combined, this suggests a northward shift of the ascending branch, and consequently, of the ITCZ. These results provide strong support for previous hypotheses linking positive pIOD events to a northward displacement of the local Hadley circulation. The associated northward shift represents the dominant anomaly during pIOD events, extending westwards across much of the Indian Ocean basin to approximately 70°E.

The positive pIOD-related SST anomalies in the WIO are distributed meridionally homogeneously (Saji et al., 1999); however, a response of the local Hadley circulation is still observed. The positive meridional mass flux anomaly appears as two regions straddling the equator, similar to the mean ascending branch of the local Hadley circulation over the WIO in SON, which is also split about the equator (see Fig. 4.1k). This suggests that the meridional response represents a local intensification of the mean pattern, likely associated with increased moisture availability. Although the absolute change in meridional mass flux highlights two localized regions of strengthening, the percentage change (not shown) is relatively homogeneous across most of the WIO, indicating that the apparent spatial structure primarily reflects an amplification of the existing mean circulation rather than a distinct localized response. For a nIOD event (Fig. 4.10 second column), the signal over the Indian Ocean is reversed, but with an overall weaker amplitude, particularly near Sumatra. This is in line with previous literature (Ogata et al., 2013) and is attributed to the reduced efficiency of coastal downwelling near Java-Sumatra, given the already deep thermocline. Over Africa, the signal is less reversed: during nIOD events, Central Africa experiences anomalously low meridional mass flux (with no anomaly observed during pIOD events), the zonal mass flux shows no significant change, and the Sahel exhibits anomalously high meridional mass flux, a pattern also seen during pIOD events.

The net effect of the changes in the local Walker and Hadley circulation closely matches the changes in observed precipitation. Changes in East African rainfall associated with IOD events are well documented (Latif et al., 1999; Birkett et al., 1999; Black et al., 2003; Behera et al., 2005) and as can be seen from Figure 4.10, these rainfall anomalies can be primarily attributed to modifications in the local Walker circulation, with an additional contribution from the local Hadley circulation during pIOD events. Confirming the findings of Weller and Cai (2014), and perhaps extending them further, changes in precipitation near Sumatra appear to result as much from changes in the meridional circulation as from zonal circulation, if not more so. Both pIOD and nIOD events enhance precipitation over the central Sahel by strengthening the meridional mass flux. Although exactly how the same pattern can occur in both pIOD and nIOD events remains unclear. During pIOD events, rainfall decreases over southern Africa. This is caused by a reduction in zonal mass flux in the northern part of the region, along with a decrease in meridional mass flux in the southern part. Another drying signal is also evident over Central Africa: consistent with (Moihamette et al., 2022), nIOD events seem to suppress precipitation in the region, mainly due to weakened meridional mass flux over South Central Africa.

4.5. Kelvin Waves

Figures 4.11–4.13 show the annual mean total, meridional, and zonal mass flux anomalies at 500 hPa associated with the dry, first neutral, wet, and second neutral phases of a Kelvin wave detected at 6.5°W (Fig. 4.11), 17°E (Fig. 4.12), and 39°E (Fig. 4.13). Although seasonal differences occur, mainly in the location of the meridional mass-flux anomalies, the overall pattern is similar. To keep the number of figures manageable, the annual mean

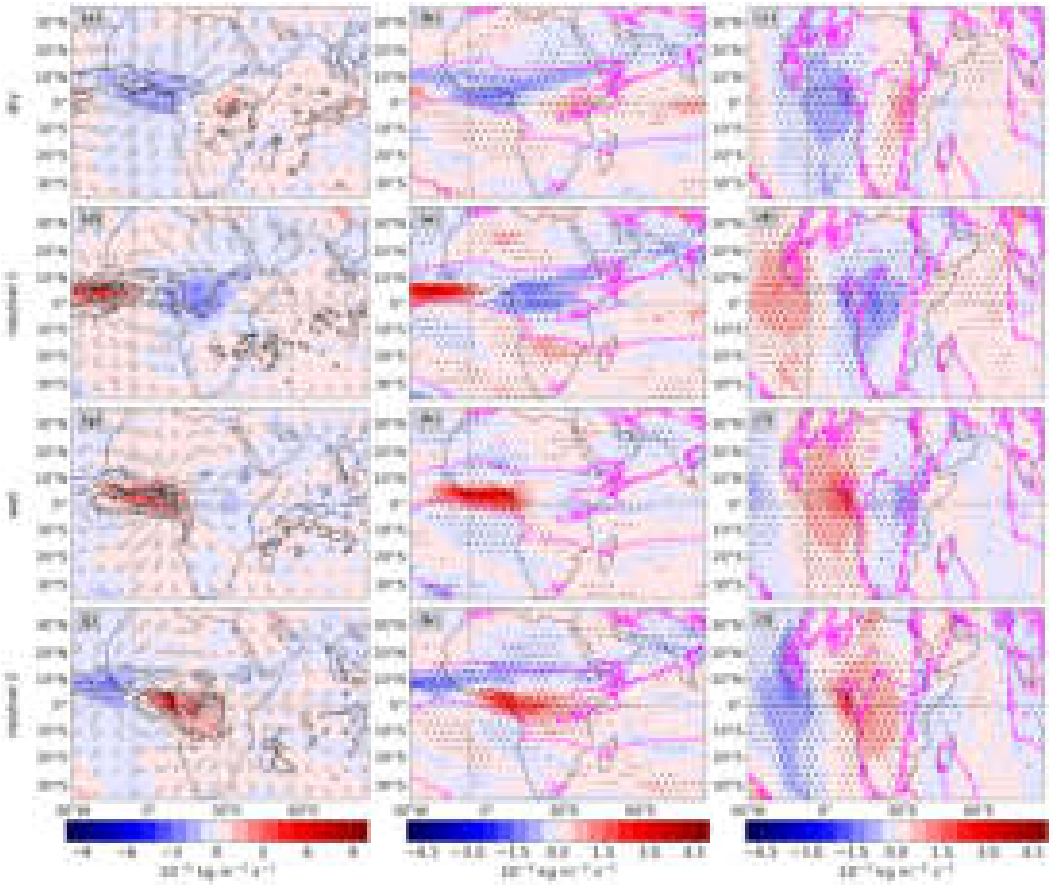

Figure 4.11.: Total (first column), meridional (second column), and zonal mass flux (third column) anomalies at 500 hPa associated with the dry, transition 1, wet, and transition 2 phases of a Kelvin wave detected at 6.5°W. The intersection of the dotted black lines indicates the latitude-longitude point used for wave identification. The total mass flux anomalies are overlaid with corresponding GPCP precipitation anomalies (black contours; -5, -3, -1, 1, 3, and 5 mm day^{-1}). The vectors show anomalies in the 850 hPa divergent flow (u_ϕ, u_λ) (m s^{-1}), vectors below topography are omitted. Areas with statistically significant mass flux anomalies at the 95 % confidence level are dotted. Solid magenta contours denote the zero line of the annual mean local Hadley and Walker circulations.

was chosen. The latitude-longitude point used for identification is indicated on each plot by the intersection of the two dotted black lines. The total mass flux anomaly (first column) is overlaid with the corresponding GPCP precipitation anomaly (black contours) at levels of -5, -3, -1, 1, 3, and 5 mm day $^{-1}$. The vectors indicate anomalies in the divergent circulation (u_ϕ and u_λ), revealing areas of convergence and divergence. Areas with statistically significant mass flux anomalies at the 95% confidence level are dotted. The solid magenta contours denote the zero contour of the annual mean local Hadley and Walker circulations.

Looking from one row of the Figures to the next, the wave's movement across the continent can be seen. Precipitation anomalies follow a pattern of alternating dry and wet areas (consistent with previous works, e.g., Schlueter et al., 2019; Ayesiga et al., 2022; Phadtare and Fernando, 2025) collocated with the areas of divergence/convergence as well as decreased/increased total mass flux. Furthermore, consistent with Ayesiga et al. (2022), near

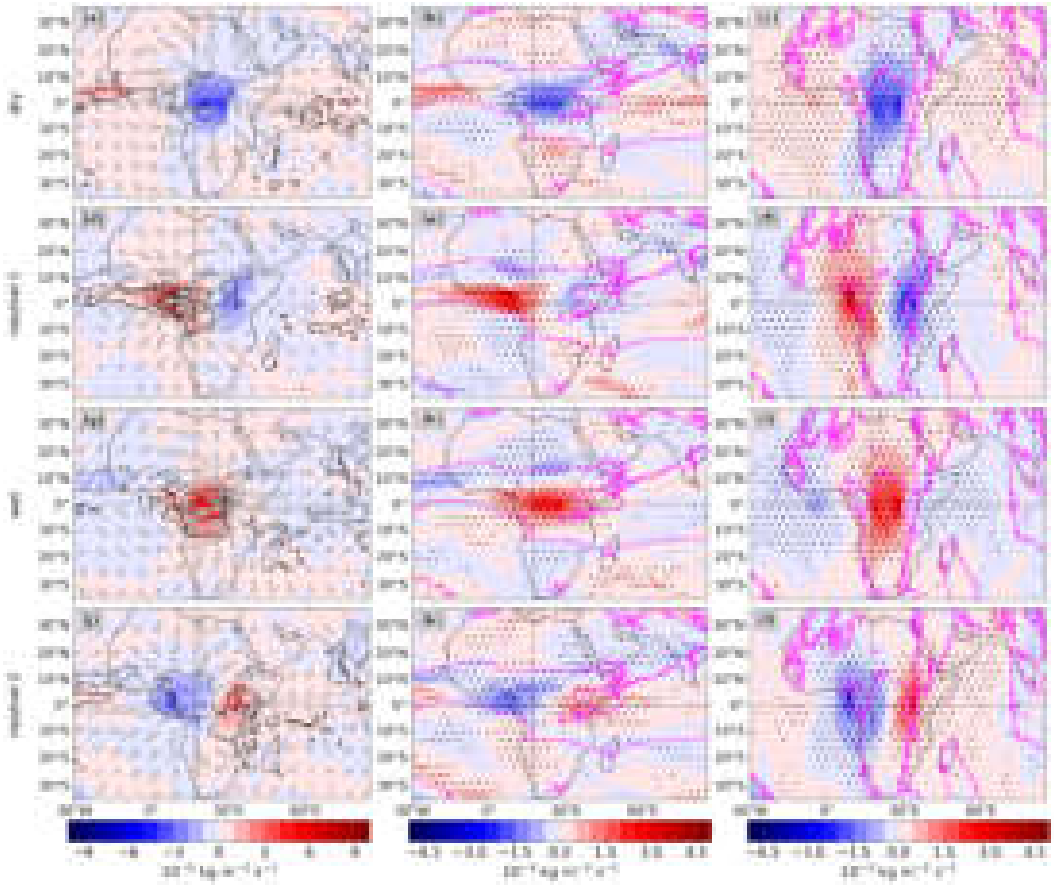

Figure 4.12.: Same as Figure 4.11 but for Kelvin waves detected at 17°E.

the West African Coast, strong anomalous westerlies collocated with the mass flux anomalies are observed (Figs. 4.11g,j; 4.12d,g), which likely play an essential role in strengthening the mass flux by increasing moisture flux convergence. While theoretical dry Kelvin waves are characterized solely by a zonal wind component, the presence of strong meridional wind anomalies (first column in Figs. 4.2, 4.3, 4.4) indicates that convective coupling, enhanced by moisture flux convergence, further modulates the total Kelvin wave response.

The observed zonal mass flux anomalies closely resemble the theoretical Kelvin wave structure (see Kiladis et al., 2009), exhibiting equatorially symmetric, horizontally aligned bands of enhanced and reduced zonal mass flux corresponding to the regions of convergence and divergence. The anomalies are strongest on the equator and decrease in magnitude poleward. The zonal mass flux anomalies are often of comparable or even greater magnitude than their meridional counterparts. This implies a relatively larger fractional change, since the mean zonal mass flux is generally smaller than the mean meridional mass flux. This may reflect that the local Walker circulation, with its zonally-driven flow, is sensitive to both zonal wind perturbations and to the convergence-divergence patterns associated with a passing Kelvin wave, whereas the meridionally oriented local Hadley circulation responds only to the latter. The relative amplitude of these anomalies can reach up to 50% for the local Hadley circulation and up to 100% for the local Walker circulation (i.e., a doubling

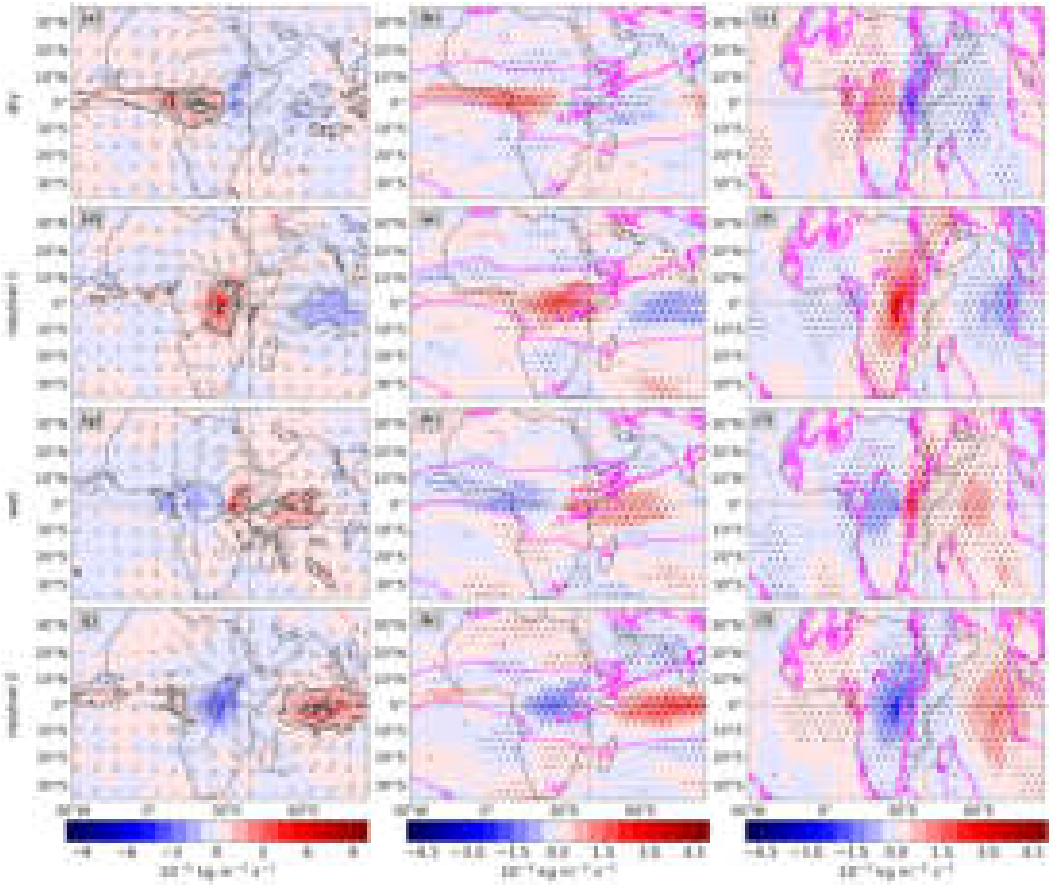

Figure 4.13.: Same as Figure 4.11 but for Kelvin waves detected at 39°E.

or near-complete suppression of its strength), similar to the results found for the MJO by Schwendike et al. (2021). This further highlights the significant influence of these transient phenomena on the variability of the large-scale tropical circulation. The strongest anomalies in both total mass flux are observed over Central Africa, where then the largest precipitation anomalies also occur. This is mainly due to the anomalies in zonal mass fluxes strengthening sharply over Central Africa. The second-strongest modulations appear near West Africa, but as they are mostly over the ocean, the anomalies over Central African are most relevant for livelihoods.

The local Hadley circulation response is characterized by meridionally elongated bands of enhanced and reduced mass flux, centered around regions of low-level convergence and divergence. These regions are primarily located straddling the equator, except over West Africa, where they are slightly shifted into the Northern Hemisphere, following the mean position of the ascending branch of the local Hadley circulation (consistent with: Straub and Kiladis, 2002). This indicates that the Kelvin waves tend to change meridional mass flux in areas of preexisting ascent. In contrast, the change in zonal mass flux is evident in both the mean ascent and descent regions. This can be explained by the fact that Kelvin waves have no meridional wind component, so they affect only the meridional mass flux through their convective coupling, and thus only in the area of mean ascent.

The meridional mass flux anomalies have a larger zonal extent than the zonal mass flux anomalies (particularly over the ocean) and a much narrower meridional extent. A Kelvin wave moves relatively fast, thus leaving little time for the atmosphere to respond and possibly re-balance; therefore, only very localized responses are seen (e.g., no strengthening of the Hadley downwards branch when ascent in the upward branch increases). There is likely some local ascent/descent that cancels out the increased descent/ascent at the margins, thus thinning out the anomaly patterns.

Multiple regional differences in the Kelvin wave response have already been discussed. Perhaps the most apparent difference is the change in the wave signal when approaching 30°E. At this longitude, the wave signal decreases in both area and strength, as illustrated by the transition from Figure 4.12a,g to 4.12d,j and from Figure 4.13d to 4.13e. This weakening of the wave as it passes the East African highlands is a known behavior (Mounier et al., 2007; Baranowski et al., 2016). Ayesiga et al. (2022) ascribe it to a reduction in moisture supply, due to the highlands disrupting the anomalous westerlies. Phadtare and Fernando (2025) corroborate that the highlands disrupt low-level convergence but adds that the upper-level signal and precipitation still propagate eastwards.

Examining the decomposed signal during this transition, both the meridional and zonal mass-flux anomalies weaken after crossing the highlands. Before the highlands are fully cleared, the zonal anomalies remain relatively strong but contract in spatial extent (Fig. 4.12c,i to 4.12f,l), whereas the meridional anomalies are already substantially reduced (Fig. 4.12b,h to 4.12e,k). For waves in the wet phase detected at 39°E (Fig. 4.13, third row), which have passed the highlands, the zonal mass-flux signal has almost entirely degraded, while the meridional signal weakens only slightly. If the highlands block low-level zonal wind convergence, the zonal mass flux signal is expected to degrade strongly, and the reduced moisture supply would also weaken the meridional mass flux. The fact that the Hadley circulation passes the highlands aligns with the findings of Phadtare and Fernando (2025), as the meridional signal is strongest in the upper levels (not shown) and can therefore pass the highlands and later reinvigorate over the moist ocean (Fig. 4.13.k).

5. Conclusions and Outlook

5.1. Main Findings

Using data from ERA5, the ψ-vector method, and multiple rainfall datasets for the periods 1960–2022 and 2000–2020, the present work analyzed the climatology, variability, and trends of local Hadley and Walker circulations over Africa, as well as their relationships with precipitation, the IOD, and equatorial Kelvin waves.

The two main methodological advantages of the present study are: (i) the use of the ψ-vector, which enables an unambiguous separation of the three-dimensional divergent flow into meridional and zonal components, and (ii) the comparison of many independent rainfall products, which helps to understand uncertainties.

The main findings are:

1. **Rainfall and mass flux relationship:**
    - ERA5-derived total ascending mass flux reproduces observed mean precipitation patterns well, both in latitude-pressure cross-sections and in latitude-longitude maps.
    - Total ascending mass flux has reasonably high correlations with most observational rainfall products, except during JJA and over the Congo Basin.
    - The meridional mass flux exhibits higher correlations with rainfall than the zonal mass flux, indicating that the local Hadley circulation plays a dominant role in rainfall variability in Africa.
    - **Recent precipitation trends (2000–2020):** Consistent precipitation trends across multiple datasets include: (i) decreasing DJF and MAM rainfall over Madagascar; (ii) increasing MAM and SON rainfall over East Africa (iii) increasing JJA rainfall in parts of the Sahel; (iv) decreasing SON rainfall in Southern Africa
    - **Circulation trends driving these changes:**
        - Madagascar drying: weakened meridional mass flux over southern Madagascar and decreased zonal mass flux along the coasts, consistent with weaker local Hadley circulation and stronger Madagascar-Mozambique Channel Walker cell.

  - East Africa rainfall recovery: increased meridional mass flux near the northern edge of the local Hadley circulation in MAM and increased zonal mass flux in SON.
  - Western Sahel rainfall recovery: roughly equal contributions from changes in zonal and meridional mass flux.
  - Southern Africa drying: reduced zonal mass flux in the northern part and reduced meridional mass flux in the southern part.

2. **Response to IOD events:**
   - Local Hadley circulation responds as strongly or more strongly than the local Walker circulation.
   - A pIOD is characterized by a northward displacement of the local Hadley circulation over the EIO, a strengthening over the WIO, and a weakening of the Africa–Atlantic and Africa–Indian Ocean Walker cells.
   - During nIOD events, a strengthening of the circulation is observed near the Java–Sumatra region, accompanied by a weakening across much of the Indian Ocean and a decrease in meridional mass flux over southern Central Africa.
3. **Equatorial Kelvin waves:**
   - Kelvin waves substantially modulate the large-scale circulations over Africa, altering the intensity of the local Hadley circulation by ∼50% and the local Walker circulation by ∼100%.
   - Strong meridional mass flux anomalies emerge despite theoretically purely zonal wind perturbations. These anomalies are confined to regions of mean ascent, causing the total wave signal to travel along the mean ascending branch of the local Hadley circulation.
   - East of 30°E, the Kelvin wave signal weakens sharply, primarily due to a reduction in the zonal mass flux perturbation. In contrast, the meridional response persists at upper levels and passes over the highlands.

5.2. Place in the Broader Context

5.2.1. Precipitation and Mass Flux

The ERA5-derived total ascending mass flux shows a high correlation with ERA5 precipitation, and, consistent with previous literature, also a good correlation with observed precipitation (Hersbach et al., 2020). As also noted in Hersbach et al. (2020), there is a distinct lack of correlation with precipitation over the Sahel–Guinea Coast and Congo Basin regions. For the former, the low correlation may be due to the recent time period (2000–2020) used in this study. For both, another possible explanation is the misrepresentation of MCSs

in ERA5, as the areas of low correlation coincide with regions where MCS precipitation contributes a high percentage of total observed rainfall (Feng et al., 2021). Precipitation associated with MCSs is known to have inaccuracies and to be underestimated in ERA5 (Chen et al., 2022; Torsah et al., 2025).

The coherent rainfall trends identified here are broadly consistent with previous work, and the associated changes in meridional and zonal mass fluxes help to confirm or nuance previously proposed processes behind these trends. The finding that Madagascar's drying is related to a weakened meridional mass flux and reduced coastal zonal mass flux aligns with earlier evidence of a long-term decline in rainfall and general drying (Randriamarolaza et al., 2022; Rigden et al., 2024), but it nuances prior explanations by showing that the local Hadley circulation has not simply expanded; instead, both its ascending and descending branches have weakened, while the Madagascar Walker cell has strengthened and contracted.

The recent rainfall recovery in East Africa is also in line with previous work (Wainwright et al., 2019; Palmer et al., 2023). In MAM, strengthened meridional mass flux occurs precisely along the northern edge of the mean ascending branch of the local Hadley circulation, supporting the idea that cooler SSTs south of Madagascar promote a more northward position of the rain belt (Wainwright et al., 2019). In SON, the zonal mass flux trends closely mirror the canonical pIOD-related circulation anomalies, consistent with the findings of Manatsa and Behera (2013) and Nicholson (2015). For the Sahel, most rainfall products support the well-established narrative of a recent rainfall recovery (Sanogo et al., 2015; Biasutti, 2019; Nicholson et al., 2018a), while ERA5 shows a more mixed picture, with a recovery in the western Sahel but a negative trend in the east. This again highlights the mismatch between observed and modeled JJA rainfall in the region. Finally, the identification of Southern African drying as a combined reduction in northern zonal and southern meridional mass flux partly aligns with regional evidence of declining SON rainfall (Mahlalela et al., 2020), as with the changes in East Africa, trends could be explained by increasingly frequent pIOD-like conditions.

5.2.2. The Indian Ocean Dipole: Meridional Response

The zonal response to an IOD event has long been recognized (Saji et al., 1999; Webster et al., 1999; Hameed and Yamagata, 2003; Cai et al., 2013; Mohtadi et al., 2017; Lu et al., 2018), and significant zonal mass flux anomalies have also been observed. However, the present work is the first to explicitly quantify the strength and spatial pattern of the local Hadley circulation response, showing that it can be comparable to or even exceed the local Walker circulation changes, particularly during pIOD phases. Furthermore, this suggests that changes in the meridional circulation are a key driver of observed precipitation anomalies, consistent with the findings of Weller and Cai (2014). The anomalously northern position of the local Hadley circulation is not merely a response to a pIOD event, but has been suggested to help trigger (Kajikawa et al., 2003; Fischer et al., 2005; Rao et al., 2009) and further intensify them (Swapna and Krishnan, 2008). The present results support these hypothesizes and one can speculate on a mechanism for this feedback: the IOD-related SST anomaly near Sumatra is primarily located in the Southern Hemisphere (Saji et al., 1999).

During a pIOD event, increased ocean heat uptake (as a result of the SST decrease) locally cools the Southern Hemisphere, enhancing the inter-hemispheric temperature gradient and promoting a northward migration of the ITCZ (Schneider et al., 2014). A northward-shifted ITCZ tends to strengthen the Southern Hemisphere trade winds (Green and Marshall, 2017), locally intensifying low-level southerlies along the Java–Sumatra coast. Increased southerlies along a western coast in the Southern Hemisphere (such as the Java-Sumatra coast) increase upwelling of cold water south of about 5°S, and thus further cooling SSTs near Sumatra and completing the loop. This feedback would be most effective during JJA-SON, when the ascending branch of the local Hadley circulation and the ITCZ is closest to Sumatra (Schwendike et al., 2014). Therfore, this mechanism helps explain the seasonal locking of the IOD. It furthermore provides a pathway through which monsoon variability influences IOD development: a stronger JJA monsoon shifts the ascending branch northward, favoring pIOD conditions. Conversely, a weaker monsoon would reduce this tendency.

In addition, the proposed feedback may interact constructively with the Bjerknes effect, further intensifying SST anomalies in the EIO and providing an additional pathway for pIOD growth. The seasonal progression of pIOD development also supports these potential mechanisms (see Fig. 2 in Saji et al., 1999). Southerly wind anomalies first emerge in May–June along with a negative SST anomaly near Java. These signals then strengthen and spread from July to August, with both the southerlies and the cooling intensifying across the eastern basin. Only after this east-side development is well established do the easterly wind anomalies and warm SST anomaly in the WIO appear and grow. However, migrations of the ITCZ are known to be dampened by changes in trade winds and the resulting atmosphere-ocean interactions (Schneider et al., 2014; Green and Marshall, 2017), potentially limiting this ITCZ– IOD linkage.

5.2.3. Kelvin Wave Impacts on the Local Hadley and Walker Circulations

Recent work has highlighted the central role of moist convection in driving variability of the Hadley circulation. It suggests that zonal asymmetries and fluctuations on time scales from days to months are crucial to its behavior (Horinouchi, 2012; Hoskins et al., 2020; Hoskins and Yang, 2021; Schwendike et al., 2021; Tomassini and Yang, 2022; Thakur et al., 2024). The present results reinforce this view: Kelvin waves induce large meridional and zonal mass flux anomalies that are comparable in magnitude to the mean circulation itself. The zonal response resembles the theoretical Kelvin wave structure (Kiladis et al., 2009), while the meridional anomalies reveal how convective coupling and moisture-flux convergence generate a meridional response from a wave with a theoretically purely zonal wind perturbation. This supports the view proposed by Tomassini and Yang (2022) that both the wind perturbations associated with equatorial waves and their coupling to convection can shape the large-scale tropical circulation. Notably, as was observed for the MJO (Schwendike et al., 2021), the local Walker circulation exhibits the largest relative anomalies, suggesting that the superposition of direct wind perturbations and convectively driven mass flux changes produces the strongest fractional response.

As the wave moves over the continent, the net total mass flux and precipitation signal propagate near the equator, following the main ascending branch of the local Hadley circulation. The total mass flux anomalies are shifted north of the equator and exhibit their broadest meridional extent near the Guinea Coast. Over Central Africa, these anomalies reach their maximum intensity, particularly for the local Walker circulation, likely due to strong westerly wind anomalies, in agreement with Ayesiga et al. (2022). Consistent with Mounier et al. (2007) and Baranowski et al. (2016), the Kelvin wave signal significantly weakens as it crosses the East African highlands. In particular, the zonal mass flux perturbations diminish, probably due to reduced zonal moisture supply and lower-level convergence (Ayesiga et al., 2022; Phadtare and Fernando, 2025). The meridional component also weakens but remains sufficiently strong at higher levels to traverse the highlands, consistent with Phadtare and Fernando (2025).

Research has now addressed mixed Rossby–gravity (MRG) waves (Tomassini and Yang, 2022; Baruah et al., 2025), the MJO (Schwendike et al., 2021), and Kelvin waves, providing an initial understanding of how these features influence large-scale circulation. Tomassini and Yang (2022) show that upper-level Hadley circulation variability often exhibits structures associated with equatorial waves, which drive variability both directly via meridional winds and indirectly by exciting convection through low-level convergence. Baruah et al. (2025) find that strong east Pacific Hadley circulation seasons coincide with pronounced MRG activity, with wave-induced low-level convergence triggering deep convection and influencing circulation strength. Schwendike et al. (2021) demonstrate that both local Hadley and Walker circulations are enhanced when overlapping with convectively active MJO phases, causing shifts in subtropical jets toward regions of enhanced convection. These findings align with the present results, which show that Kelvin waves enhance local Hadley and Walker circulation when overlapping with the region, both by inducing low-level convergence that triggers convective coupling and through their zonal wind component.

5.3. Future Work

5.3.1. Precipitation and Mass Flux

To deepen the understanding of both the observed correlation between mass flux and precipitation and the drivers behind the detected trends, it would be valuable to extend this analysis to additional reanalysis products. Agreement across multiple reanalyses would increase confidence in the results, while regions of disagreement could help identify sources of uncertainty.

Regarding the trends themselves, much of the current reasoning is based on a qualitative comparison with previous studies and visual pattern matching. A more rigorous approach would involve directly analyzing the time series with quantitative methods. For example, instead of inferring an IOD influence from spatial similarity, one could examine the correlation between the trends and an IOD index, or apply other statistical tests to evaluate the strength and significance of the relationship.

5.3.2. Towards a Deeper Understanding of the IOD

Not every IOD event is the same: some authors distinguish between three types of pIOD events (Jiang et al., 2022), and some events are particularly strong relative to others (Lu et al., 2018; Ratna et al., 2021). A natural next step would be to analyze not only the mean response, but also individual events. Moreover, it would be valuable to examine not only the mature phase (SON) but also the periods preceding and following an event. This approach would allow for a better understanding of in which years, and in what types of IOD events, significant changes occur in the local Hadley circulation, as well as when during the development (initiation or decay) these changes are most pronounced. It would also enable analysis of differences in behavior during years with and without ENSO co-occurrence. More broadly, further investigation into the ENSO connection would be valuable, given that ENSO and the IOD are linked, the IOD and the monsoon are linked, and ENSO also influences the monsoon. Focusing on more variables in addition to mass flux and precipitation would then also allow for a test of the ITCZ- IOD feedback hypothesis.

A further area worth exploring is the role of the southern Indian Ocean in shaping IOD events. Previous studies propose that variations in this region, linked to phases of the Southern Annular Mode (SAM), influence the position and strength of subtropical highs and may induce southerly wind anomalies that trigger pIOD events (Zhang et al., 2020). On the other hand, research suggests that during the 2019 extreme pIOD event, IOD-related Rossby wave trains may have interacted with the observed stratospheric vortex weakening (Lim et al., 2020), implying that changes in the SAM might not only contribute to triggering a pIOD event, but that a pIOD could also influence the SAM. This interaction is particularly important because both the IOD and changes in the stratospheric vortex, together with the SAM, have been associated with the hot, dry conditions in eastern Australia that fueled the severe wildfire season (Lim et al., 2021). The zonal mass flux patterns at the bottom of Figure 5.1c, which resemble Rossby waves extending far north, depict conditions during the extreme pIOD event and suggest a negative phase of the SAM. This indicates that both processes were present at the same time, yet their interaction and mutual influence remain unclear, underscoring the need for targeted research to clarify the underlying mechanisms and assess their broader climate implications.

The findings of the present work, combined with potential future work, deepen our current understanding of the IOD and may lead to better forecasting of events or provide potential pathways in which a process such as climate change could alter the behavior of these events. For example, one could ask: if the Northern Hemisphere warms relatively faster than the Southern Hemisphere, does the ITCZ shift northward, and does the likelihood of pIOD events increase as a result?

5.3.3. Incorporating the Full Range of Equatorial Wave Types

Future work could extend the growing literature on interactions between equatorial waves and large-scale circulations to additional wave types, helping to build a more complete picture of their combined influences. Such work could also shed light on how the individual

effects of different wave types, along with their superposed interactions, collectively shape the mean large-scale circulation. As mentioned in Section 3.5, employing multiple identification methods, particularly for wave types beyond Kelvin waves, would be ideal. Expanding the analysis to other regions would allow investigation of how local conditions influence the wave-circulation interaction. In addition, using a wider range of reanalysis products and model datasets would help assess how different models capture the wave-circulation interaction, to see how robust the split of the total wave signal into meridional and zonal components found for the ERA5 data is.

5.3.4. How Does the Large-Scale Circulation Emerge?

The present work shows that the local Hadley and Walker Circulations are strongly localized in both their mean structure and their variability across long-term, interannual, and synoptic time scales. Although dividing the circulation into a Hadley circulation and a Walker circulation is conceptually useful, the atmosphere rarely behaves as a set of symmetric, steady-state cells. Figure 5.1 illustrates this point: alongside the satellite image from the introduction, which shows reality as semi-random, noisy cloud structures rather than a neat steady state, the decomposed mass-flux components reveal similarly irregular and strongly asymmetric patterns of ascent and descent. These snapshots remind us that the atmosphere does not separate neatly into distinct branches and that there is no clear boundary between small-scale convection and large-scale circulation. Coherent structures emerge only through temporal averaging; on shorter time scales, the system is continuous, transient, and far less orderly. These conceptual distinctions remain valuable, but they should be treated as idealizations of an inherently dynamic system. Taken together, this underscores a key ambition for future research: to bridge the gap between the rapidly evolving day-to-day circulation and the coherent, time-averaged structures that define the large-scale circulation.

5.4. Concluding Remarks

Large-scale circulation and its associated rainfall are vital for livelihoods across Africa and beyond. The present work contributes to current understanding in several ways. It confirms or refines proposed mechanisms behind recent rainfall trends over Africa. It quantifies the response of the local Hadley circulation to IOD events, showing a northward-shifted ascending branch over the EIO and a strengthening over the WIO during positive events. During negative events, the circulation strengthens near the Java-Sumatra region, while across much of the Indian Ocean, it weakens. Furthermore, the present work contributes to emerging evidence showing that synoptic-scale variability is crucial in shaping large-scale circulation. Convectively coupled Kelvin waves can amplify the local Walker circulation by up to a factor of two and modulate the local Hadley circulation through their convective coupling.

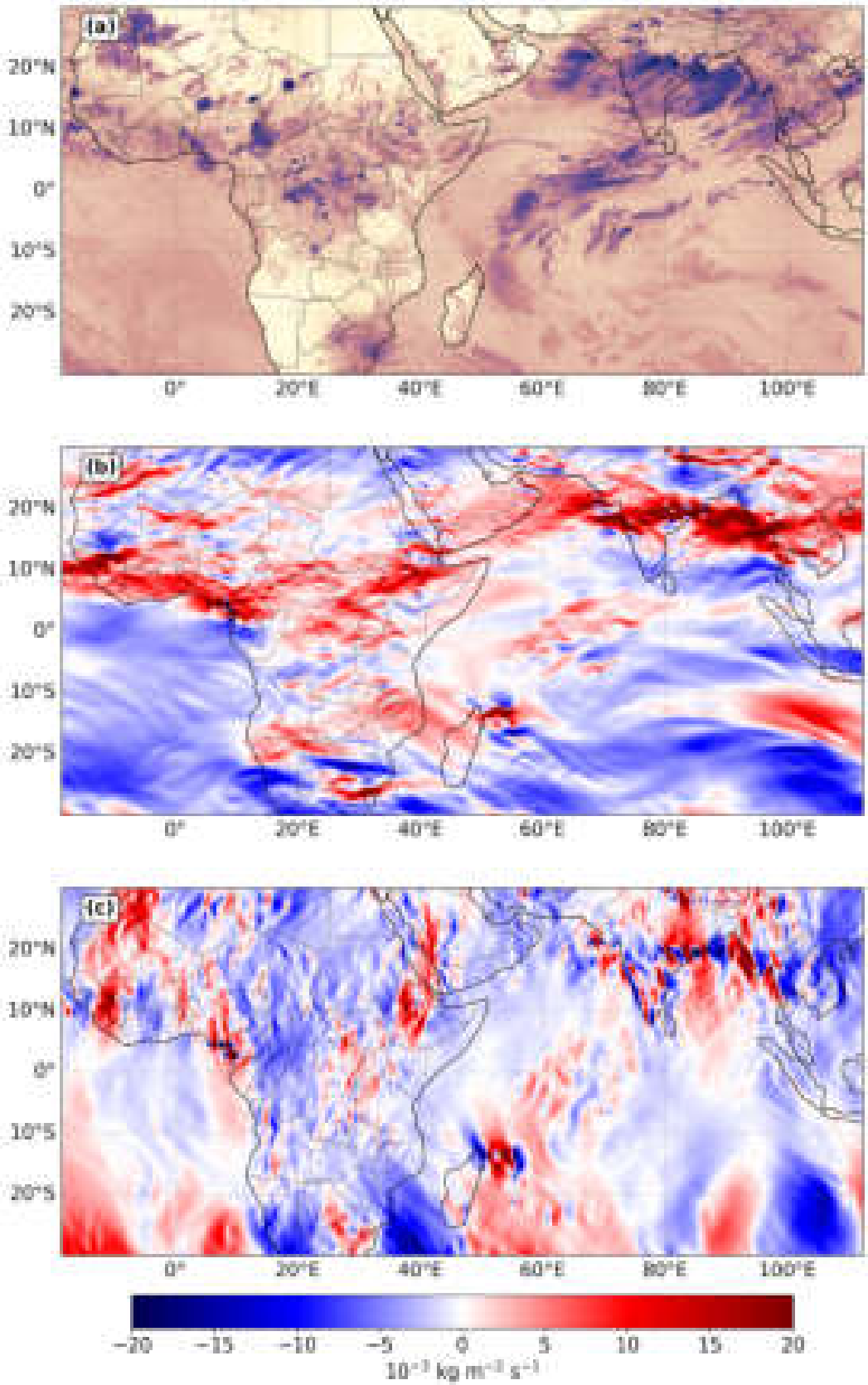

Figure 5.1.: Panels show data for 6 September 2019: (a) Brightness temperature (Band I5, Day) from VIIRS onboard NOAA-20, obtained via NASA Worldview (`https://go.nasa.gov/48JD2ps`); (b) meridional mass flux and (c) zonal mass flux, both derived from ERA5 .

Bibliography

Adler, R. F., and Coauthors, 2018: The Global Precipitation Climatology Project (GPCP) Monthly Analysis (New Version 2.3) and a Review of 2017 Global Precipitation. *Atmosphere*, **9 (4)**, 138, DOI: https://doi.org/10.3390/atmos9040138.

Ahmed, S. A., M. Guerrero Flórez, and P. Karanis, 2018: The impact of water crises and climate changes on the transmission of protozoan parasites in Africa. *Pathogens and Global Health*, **112 (6)**, 281–293, DOI: https://doi.org/10.1080/20477724.2018.1523778.

Ayesiga, G., C. E. Holloway, C. J. R. Williams, G.-Y. Yang, R. Stratton, and M. Roberts, 2022: Linking Equatorial African Precipitation to Kelvin Wave Processes in the CP4-Africa Convection-Permitting Regional Climate Simulation. *Journal of the Atmospheric Sciences*, **79 (5)**, 1271–1289, DOI: https://doi.org/10.1175/JAS-D-21-0039.1.

Bahaga, T. K., A. H. Fink, and P. Knippertz, 2019: Revisiting interannual to decadal teleconnections influencing seasonal rainfall in the Greater Horn of Africa during the 20th century. *International Journal of Climatology*, **39 (5)**, 2765–2785, DOI: https://doi.org/10.1002/joc.5986.

Baranowski, D. B., M. K. Flatau, P. J. Flatau, and A. J. Matthews, 2016: Impact of atmospheric convectively coupled equatorial Kelvin waves on upper ocean variability. *Journal of Geophysical Research: Atmospheres*, **121 (5)**, 2045–2059, DOI: https://doi.org/10.1002/2015JD024150.

Barichivich, J., E. Gloor, P. Peylin, R. J. W. Brienen, J. Schöngart, J. C. Espinoza, and K. C. Pattnayak, 2018: Recent intensification of Amazon flooding extremes driven by strengthened Walker circulation. *Science Advances*, **4 (9)**, eaat8785, DOI: https://doi.org/10.1126/sciadv.aat8785.

Baruah, P. P., J. M. Neena, and E. Suhas, 2025: The Role of Tropical Synoptic-Scale Disturbances in Modulating the Strength of East Pacific Hadley Circulation. *Journal of Geophysical Research: Atmospheres*, **130 (9)**, e2024JD042 980, DOI: https://doi.org/10.1029/2024JD042980.

Bauer, P., A. Thorpe, and G. Brunet, 2015: The quiet revolution of numerical weather prediction. *Nature*, **525 (7567)**, 47–55, DOI: https://doi.org/10.1038/nature14956.

Bayr, T., D. Dommenget, T. Martin, and S. B. Power, 2014: The eastward shift of the Walker Circulation in response to global warming and its relationship to ENSO variability. *Climate Dynamics*, **43 (9)**, 2747–2763, DOI: https://doi.org/10.1007/s00382-014-2091-y.

Behera, S. K., J.-J. Luo, S. Masson, P. Delecluse, S. Gualdi, A. Navarra, and T. Yamagata, 2005: Paramount Impact of the Indian Ocean Dipole on the East African Short Rains: A CGCM Study. *Journal of Climate*, **18 (21)**, 4514–4530, DOI: https://doi.org/10.1175/JCLI3541.1.

Bellomo, K., and A. C. Clement, 2015: Evidence for weakening of the Walker circulation from cloud observations. *Geophysical Research Letters*, **42 (18)**, 7758–7766, DOI: https://doi.org/10.1002/2015GL065463.

Biasutti, M., 2019: Rainfall trends in the African Sahel: Characteristics, processes, and causes. *WIREs Climate Change*, **10 (4)**, e591, DOI: https://doi.org/10.1002/wcc.591.

Birkett, C., R. Murtugudde, and T. Allan, 1999: Indian Ocean Climate event brings floods to East Africa's lakes and the Sudd Marsh. *Geophysical Research Letters*, **26 (8)**, 1031–1034, DOI: https://doi.org/10.1029/1999GL900165.

Bjerknes, J., 1969: ATMOSPHERIC TELECONNECTIONS FROM THE EQUATORIAL PACIFIC. *Monthly Weather Review*, **97 (3)**, 163–172, DOI: https://doi.org/10.1175/1520-0493(1969)097<0163:ATFTEP>2.3.CO;2.

Black, E., J. Slingo, and K. R. Sperber, 2003: An Observational Study of the Relationship between Excessively Strong Short Rains in Coastal East Africa and Indian Ocean SST. *Monthly Weather Review*, **131 (1)**, 74–94, DOI: https://doi.org/10.1175/1520-0493(2003)131<0074:AOSOTR>2.0.CO;2.

Burls, N. J., R. C. Blamey, B. A. Cash, E. T. Swenson, A. a. Fahad, M.-J. M. Bopape, D. M. Straus, and C. J. C. Reason, 2019: The Cape Town "Day Zero" drought and Hadley cell expansion. *npj Climate and Atmospheric Science*, **2 (1)**, 27, DOI: https://doi.org/10.1038/s41612-019-0084-6.

Cai, W., A. Santoso, G. Wang, E. Weller, L. Wu, K. Ashok, Y. Masumoto, and T. Yamagata, 2014: Increased frequency of extreme Indian Ocean Dipole events due to greenhouse warming. *Nature*, **510 (7504)**, 254–258, DOI: https://doi.org/10.1038/nature13327.

Cai, W., X.-T. Zheng, E. Weller, M. Collins, T. Cowan, M. Lengaigne, W. Yu, and T. Yamagata, 2013: Projected response of the Indian Ocean Dipole to greenhouse warming. *Nature Geoscience*, **6 (12)**, 999–1007, DOI: https://doi.org/10.1038/ngeo2009.

Chemke, R., 2021: Future Changes in the Hadley Circulation: The Role of Ocean Heat Transport. *Geophysical Research Letters*, **48 (4)**, e2020GL091 372, DOI: https://doi.org/10.1029/2020GL091372.

Chen, X., L. R. Leung, Z. Feng, and F. Song, 2022: Crucial Role of Mesoscale Convective Systems in the Vertical Mass, Water, and Energy Transports of the South Asian Summer Monsoon. *Journal of Climate*, **35 (1)**, 91–108, DOI: https://doi.org/10.1175/JCLI-D-21-0124.1.

Cliff, M., S. Jahn, A. B. Fouda, A. Latt, C. Lingani, and C. Trotter, 2025: Re-examining the meningitis belt: associations between environmental factors and epidemic meningitis

risk across Africa. medRxiv, DOI: https://doi.org/10.1101/2025.02.25.25322867.

Cook, K. H., and E. K. Vizy, 2016: The Congo Basin Walker circulation: dynamics and connections to precipitation. *Climate Dynamics*, **47 (3)**, 697–717, DOI: https://doi.org/10.1007/s00382-015-2864-y.

de Oliveira, C. P., L. Aímola, T. Ambrizzi, and A. C. V. Freitas, 2018: The Influence of the Regional Hadley and Walker Circulations on Precipitation Patterns over Africa in El Niño, La Niña, and Neutral Years. *Pure and Applied Geophysics*, **175 (6)**, 2293–2306, DOI: https://doi.org/10.1007/s00024-018-1782-4.

Defant, A., 1921: Die Zirkulation der Atmosphäre in den gemässigten Breiten der Erde Grundzüge einer Theorie der Klimaschwankungen. *Geografiska Annaler*, **3 (3)**, 209–266, URL: https://www.jstor.org/stable/pdf/519434.pdf.

Deser, C., A. S. Phillips, and M. A. Alexander, 2010: Twentieth century tropical sea surface temperature trends revisited. *Geophysical Research Letters*, **37 (10)**, DOI: https://doi.org/10.1029/2010GL043321.

Diaz, H. F., R. S. Bradley, and M. Beniston, Eds., 2004: *The Hadley Circulation: Present, Past and Future*, Advances in Global Change Research, Vol. 21. Springer Netherlands, Dordrecht, DOI: https://doi.org/10.1007/978-1-4020-2944-8.

Dimet, F.-X. L., and O. Talagrand, 1986: Variational algorithms for analysis and assimilation of meteorological observations: theoretical aspects. *Tellus A*, **38A (2)**, 97–110, DOI: https://doi.org/10.1111/j.1600-0870.1986.tb00459.x.

Efon, E., R. D. Ngongang, C. Meukaleuni, B. B. S. Wandjie, S. Zebaze, A. Lenouo, and M. Valipour, 2023: Monthly, Seasonal, and Annual Variations of Precipitation and Runoff Over West and Central Africa Using Remote Sensing and Climate Reanalysis. *Earth Systems and Environment*, **7 (1)**, 67–82, DOI: https://doi.org/10.1007/s41748-022-00326-w.

Fasullo, J. T., and K. E. Trenberth, 2008: The Annual Cycle of the Energy Budget. Part II: Meridional Structures and Poleward Transports. *Journal of Climate*, **21 (10)**, 2313–2325, DOI: https://doi.org/10.1175/2007JCLI1936.1.

Feng, Z., and Coauthors, 2021: A Global High-Resolution Mesoscale Convective System Database Using Satellite-Derived Cloud Tops, Surface Precipitation, and Tracking. *Journal of Geophysical Research: Atmospheres*, **126 (8)**, e2020JD034 202, DOI: https://doi.org/10.1029/2020JD034202.

Ferrel, W., 1860: *The Motions of Fluids and Solids Relative to the Earth's Surface: Comprising Applications to the Winds and the Currents of the Ocean*. Ivison, Phinney, and Company, URL: https://play.google.com/books/reader?id=N8ErAQAAMAAJ&pg=GBS.PP4&hl=nl.

Fink, A. H., and Coauthors, 2017: Mean Climate and Seasonal Cycle. *Meteorology of Tropical West Africa*, John Wiley & Sons, Ltd, 1–39, DOI: https://doi.org/10.1002/9781118391297.ch1.

Fischer, A. S., P. Terray, E. Guilyardi, S. Gualdi, and P. Delecluse, 2005: Two Independent Triggers for the Indian Ocean Dipole/Zonal Mode in a Coupled GCM. *Journal of Climate*, **18 (17)**, 3428–3449, DOI: https://doi.org/10.1175/JCLI3478.1.

Funk, C., M. D. Dettinger, J. C. Michaelsen, J. P. Verdin, M. E. Brown, M. Barlow, and A. Hoell, 2008: Warming of the Indian Ocean threatens eastern and southern African food security but could be mitigated by agricultural development. *Proceedings of the National Academy of Sciences*, **105 (32)**, 11 081–11 086, DOI: https://doi.org/10.1073/pnas.0708196105.

Funk, C., A. H. Fink, L. Harrison, Z. Segele, H. S. Endris, G. Galu, D. Korecha, and S. Nicholson, 2023: Frequent but Predictable Droughts in East Africa Driven by a Walker Circulation Intensification. *Earth's Future*, **11 (11)**, e2022EF003 454, DOI: https://doi.org/10.1029/2022EF003454.

Funk, C., S. E. Nicholson, M. Landsfeld, D. Klotter, P. Peterson, and L. Harrison, 2015a: The Centennial Trends Greater Horn of Africa precipitation dataset. *Scientific Data*, **2 (1)**, 150 050, DOI: https://doi.org/10.1038/sdata.2015.50.

Funk, C., and Coauthors, 2005: Recent drought tendencies in Ethiopia and equatorial-subtropical eastern Africa. Tech. rep., USAID. URL: https://pubs.usgs.gov/publication/70259484.

Funk, C., and Coauthors, 2015b: The climate hazards infrared precipitation with stations—a new environmental record for monitoring extremes. *Scientific Data*, **2 (1)**, 150 066, DOI: https://doi.org/10.1038/sdata.2015.66.

Gleixner, S., T. Demissie, and G. T. Diro, 2020: Did ERA5 Improve Temperature and Precipitation Reanalysis over East Africa? *Atmosphere*, **11 (9)**, 996, DOI: https://doi.org/10.3390/atmos11090996.

Green, B., and J. Marshall, 2017: Coupling of Trade Winds with Ocean Circulation Damps ITCZ Shifts. *Journal of Climate*, **30 (12)**, 4395–4411, DOI: https://doi.org/10.1175/JCLI-D-16-0818.1.

Griffiths, M. L., and Coauthors, 2010: Evidence for Holocene changes in Australian–Indonesian monsoon rainfall from stalagmite trace element and stable isotope ratios. *Earth and Planetary Science Letters*, **292 (1)**, 27–38, DOI: https://doi.org/10.1016/j.epsl.2010.01.002.

Hadley, G., 1735: VI. Concerning the cause of the general trade-winds. *Philosophical Transactions of the Royal Society of London*, **39 (437)**, 58–62, DOI: https://doi.org/10.1098/rstl.1735.0014.

Halley, E., 1686: An historical account of the trade winds, and monsoons, observable in the seas between and near the Tropicks, with an attempt to assign the physical cause of the said winds. *Philosophical Transactions of the Royal Society of London*, **16 (183)**, 153–168, DOI: https://doi.org/10.1098/rstl.1686.0026.

Hameed, S., and T. Yamagata, 2003: Possible impacts of Indian Ocean Dipole Mode events on global climate. *Climate Research - CLIMATE RES*, **25**, 151–169, DOI: https://doi.org/10.3354/cr025151.

Hartmann, D. L., 1994: *Global Physical Climatology*. Academic Press, San Diego, New York, Boston, London, Sydney, Tokyo, and Toronto.

Held, I. M., and A. Y. Hou, 1980: Nonlinear Axially Symmetric Circulations in a Nearly Inviscid Atmosphere. *Journal of the Atmospheric Sciences*, **37 (3)**, 515–533, DOI: https://doi.org/10.1175/1520-0469(1980)037<0515:NASCIA>2.0.CO;2.

Hersbach, H., and Coauthors, 2020: The ERA5 global reanalysis. *Quarterly Journal of the Royal Meteorological Society*, **146 (730)**, 1999–2049, DOI: https://doi.org/10.1002/qj.3803.

Hesterberg, T., 2011: Bootstrap. *WIREs Computational Statistics*, **3 (6)**, 497–526, DOI: https://doi.org/10.1002/wics.182.

Horinouchi, T., 2012: Moist Hadley Circulation: Possible Role of Wave–Convection Coupling in Aquaplanet Experiments. *Journal of the Atmospheric Sciences*, **69 (3)**, 891–907, DOI: https://doi.org/10.1175/JAS-D-11-0149.1.

Hoskins, B. J., and G.-Y. Yang, 2021: The Detailed Dynamics of the Hadley Cell. Part II: December–February. *Journal of Climate*, **34 (2)**, 805–823, DOI: https://doi.org/10.1175/JCLI-D-20-0504.1.

Hoskins, B. J., G.-Y. Yang, and R. M. Fonseca, 2020: The detailed dynamics of the June–August Hadley Cell. *Quarterly Journal of the Royal Meteorological Society*, **146 (727)**, 557–575, DOI: https://doi.org/10.1002/qj.3702.

Hu, S., J. Cheng, and J. Chou, 2017: Novel three-pattern decomposition of global atmospheric circulation: generalization of traditional two-dimensional decomposition. *Climate Dynamics*, **49 (9)**, 3573–3586, DOI: https://doi.org/10.1007/s00382-017-3530-3.

Hua, W., L. Zhou, H. Chen, S. E. Nicholson, A. Raghavendra, and Y. Jiang, 2016: Possible causes of the Central Equatorial African long-term drought. *Environmental Research Letters*, **11 (12)**, 124 002, DOI: https://doi.org/10.1088/1748-9326/11/12/124002.

Huffman, G. J., D. T. Bolvin, R. Joyce, O. A. Kelley, E. J. Nelkin, J. Tan, D. C. Watters, and B. J. West, 2023: Integrated Multi-satellitE Retrievals for GPM (IMERG) Technical Documentation. NASA Tech. Doc.

IEA, 2020: Climate Impacts on African Hydropower. Tech. rep., The International Energy Agency. URL: https://www.iea.org/reports/climate-impacts-on-african-hydropower,.

Intergovernmental Panel On Climate Change (IPCC), 2023: *Climate Change 2021 – The Physical Science Basis: Working Group I Contribution to the Sixth Assessment Report of the Intergovernmental Panel on Climate Change*. 1st ed., Cambridge University Press, DOI: https://doi.org/10.1017/9781009157896.

Jain, S., T. Turkington, W. L. Tan, C. Schwartz, A. A. Scaife, and T. G. Shepherd, 2025: Towards developing an operational Indian ocean dipole warning system for Southeast Asia. *Scientific Reports*, **15 (1)**, 14 728, DOI: https://doi.org/10.1038/s41598-025-99261-9.

Jiang, J., Y. Liu, J. Mao, J. Li, S. Zhao, and Y. Yu, 2022: Three Types of Positive Indian Ocean Dipoles and Their Relationships with the South Asian Summer Monsoon. *Journal of Climate*, **35 (1)**, 405–424, DOI: https://doi.org/10.1175/JCLI-D-21-0089.1.

Joseph, L., N. Skliris, D. Dey, R. Marsh, and J. Hirschi, 2024: Increased Summer Monsoon Rainfall Over Northwest India Caused by Hadley Cell Expansion and Indian Ocean Warming. *Geophysical Research Letters*, **51 (16)**, e2024GL108 829, DOI: https://doi.org/10.1029/2024GL108829.

Kajikawa, Y., T. Yasunari, and R. Kawamura, 2003: The Role of the Local Hadley Circulation over the Western Pacificon the Zonally Asymmetric Anomalies over the Indian Ocean. *Journal of the Meteorological Society of Japan*, **81 (2)**, 259–276, DOI: https://doi.org/10.2151/jmsj.81.259.

Kang, S. M., D. M. W. Frierson, and I. M. Held, 2009: The Tropical Response to Extratropical Thermal Forcing in an Idealized GCM: The Importance of Radiative Feedbacks and Convective Parameterization. *Journal of the Atmospheric Sciences*, **66 (9)**, 2812–2827, DOI: https://doi.org/10.1175/2009JAS2924.1.

Kenfack, K., A. T. Tamoffo, L. A. D. Tchotchou, F. Marra, S. Kaissassou, H. N. Nana, and D. A. Vondou, 2024: Processes behind the decrease in Congo Basin precipitation during the rainy seasons inferred from ERA-5 reanalysis. *International Journal of Climatology*, **44 (5)**, 1778–1799, DOI: https://doi.org/10.1002/joc.8410.

Keyser, D., B. D. Schmidt, and D. G. Duffy, 1989: A Technique for Representing Three-Dimensional Vertical Circulations in Baroclinic Disturbances. *Monthly Weather Review*, **117 (11)**, 2463–2494, DOI: https://doi.org/10.1175/1520-0493(1989)117<2463:ATFRTD>2.0.CO;2.

Kiladis, G. N., M. C. Wheeler, P. T. Haertel, K. H. Straub, and P. E. Roundy, 2009: Convectively coupled equatorial waves. *Reviews of Geophysics*, **47 (2)**, DOI: https://doi.org/10.1029/2008RG000266.

King, J. A., R. Washington, and S. Engelstaedter, 2021: Representation of the Indian Ocean Walker circulation in climate models and links to Kenyan rainfall. *International Journal of Climatology*, **41 (S1)**, E616–E643, DOI: https://doi.org/10.1002/joc.6714.

Knippertz, P., and Coauthors, 2022: The intricacies of identifying equatorial waves. *Quarterly Journal of the Royal Meteorological Society*, **148 (747)**, 2814–2852, DOI: https://doi.org/10.1002/qj.4338.

Kurane, I., 2010: The Effect of Global Warming on Infectious Diseases. *Osong Public Health and Research Perspectives*, **1 (1)**, 4–9, DOI: https://doi.org/10.1016/j.phrp.2010.12.004.

Lamptey, B., and Coauthors, 2024: Challenges and ways forward for sustainable weather and climate services in Africa. *Nature Communications*, **15**, 2664, DOI: https://doi.org/10.1038/s41467-024-46742-6.

Latif, M., D. Dommenget, M. Dima, and A. Grötzner, 1999: The Role of Indian Ocean Sea Surface Temperature in Forcing East African Rainfall Anomalies during December–January 1997/98. *Journal of Climate*, **12 (12)**, 3497–3504, DOI: https://doi.org/10.1175/1520-0442(1999)012<3497:TROIOS>2.0.CO;2.

Lau, K.-M., and S. Yang, 2003: Walker Circulation. *Encyclopedia of Atmospheric Sciences*, J. R. Holton, Ed., Academic Press, Oxford, 2505–2510, DOI: https://doi.org/10.1016/B0-12-227090-8/00450-4.

Lau, W. K. M., and K.-M. Kim, 2015: Robust Hadley Circulation changes and increasing global dryness due to CO2 warming from CMIP5 model projections. *Proceedings of the National Academy of Sciences*, **112 (12)**, 3630–3635, DOI: https://doi.org/10.1073/pnas.1418682112.

Levine, X. J., and T. Schneider, 2015: Baroclinic Eddies and the Extent of the Hadley Circulation: An Idealized GCM Study. *Journal of the Atmospheric Sciences*, **72 (7)**, 2744–2761, DOI: https://doi.org/10.1175/JAS-D-14-0152.1.

Lim, E.-P., and Coauthors, 2020: The 2019 Antarctic sudden stratospheric warming. *SPARC International Project Office*, **54**, 10–13, URL: https://www.researchgate.net/publication/348993899_The_2019_Antarctic_sudden_stratospheric_warming.

Lim, E.-P., and Coauthors, 2021: The 2019 Southern Hemisphere Stratospheric Polar Vortex Weakening and Its Impacts. *Bulletin of the American Meteorological Society*, **102 (6)**, E1150–E1171, DOI: https://doi.org/10.1175/BAMS-D-20-0112.1.

Lim Kam Sian, K. T. C., A. Dosio, B. O. Ayugi, D. F. T. Hagan, L. L. Kebacho, and V. Ongoma, 2023: Dominant modes of precipitation over Africa, and their associated atmospheric circulations from observations. *International Journal of Climatology*, **43 (10)**, 4603–4618, DOI: https://doi.org/10.1002/joc.8105.

Lionello, P., R. D'Agostino, D. Ferreira, H. Nguyen, and M. S. Singh, 2024: The Hadley circulation in a changing climate. *Annals of the New York Academy of Sciences*, **1534 (1)**, 69–93, DOI: https://doi.org/10.1111/nyas.15114.

Longandjo, G.-N. T., and M. Rouault, 2020: On the Structure of the Regional-Scale Circulation over Central Africa: Seasonal Evolution, Variability, and Mechanisms. *Journal of Climate*, **33 (1)**, 145–162, DOI: https://doi.org/10.1175/JCLI-D-19-0176.1.

Longandjo, G.-N. T., and M. Rouault, 2024: Revisiting the Seasonal Cycle of Rainfall over Central Africa. *Journal of Climate*, **37 (3)**, 1015–1032, DOI: https://doi.org/10.1175/JCLI-D-23-0281.1.

Lorenz, E. N., 1983: A History of Prevailing Ideas about the General Circulation of the Atmosphere. *Bulletin of the American Meteorological Society*, **64 (7)**, 730–734, URL: https:

//www.jstor.org/stable/26223119.

Lu, B., and Coauthors, 2018: An extreme negative Indian Ocean Dipole event in 2016: dynamics and predictability. *Climate Dynamics*, **51 (1)**, 89–100, DOI: https://doi.org/10.1007/s00382-017-3908-2.

Lubis, S. W., and C. Jacobi, 2015: The modulating influence of convectively coupled equatorial waves (CCEWs) on the variability of tropical precipitation. *International Journal of Climatology*, **35 (7)**, 1465–1483, DOI: https://doi.org/10.1002/joc.4069.

Ma, J., R. Chadwick, K.-H. Seo, C. Dong, G. Huang, G. R. Foltz, and J. H. Jiang, 2018: Responses of the Tropical Atmospheric Circulation to Climate Change and Connection to the Hydrological Cycle. *Annual Review of Earth and Planetary Sciences*, **46**, 549–580, DOI: https://doi.org/10.1146/annurev-earth-082517-010102.

Mafwele, B. J., and J. W. Lee, 2022: Relationships between transmission of malaria in Africa and climate factors. *Scientific Reports*, **12 (1)**, 14 392, DOI: https://doi.org/10.1038/s41598-022-18782-9.

Mahlalela, P. T., R. C. Blamey, N. C. G. Hart, and C. J. C. Reason, 2020: Drought in the Eastern Cape region of South Africa and trends in rainfall characteristics. *Climate Dynamics*, **55 (9)**, 2743–2759, DOI: https://doi.org/10.1007/s00382-020-05413-0.

Mahlobo, D., F. Engelbrecht, T. Ndarana, H. B. Abubakar, M. F. Olabanji, and K. Ncongwane, 2024: Analysis of the Hadley cell, subtropical anticyclones and their effect on South African rainfall. *Theoretical and Applied Climatology*, **155 (2)**, 1035–1054, DOI: https://doi.org/10.1007/s00704-023-04674-z.

Mahlobo, D. D., T. Ndarana, S. Grab, and F. Engelbrecht, 2019: Integrated climatology and trends in the subtropical Hadley cell, sunshine duration and cloud cover over South Africa. *International Journal of Climatology*, **39 (4)**, 1805–1821, DOI: https://doi.org/10.1002/joc.5917.

Maidment, R. I., and Coauthors, 2017: A new, long-term daily satellite-based rainfall dataset for operational monitoring in Africa. *Scientific Data*, **4 (1)**, 170 063, DOI: https://doi.org/10.1038/sdata.2017.63.

Malhi, Y., and J. Wright, 2004: Spatial patterns and recent trends in the climate of tropical rainforest regions. *Philosophical Transactions of the Royal Society of London. Series B: Biological Sciences*, **359 (1443)**, DOI: https://doi.org/10.1098/rstb.2003.1433.

Manatsa, D., and S. K. Behera, 2013: On the Epochal Strengthening in the Relationship between Rainfall of East Africa and IOD. *Journal of Climate*, **26 (15)**, 5655–5673, DOI: https://doi.org/10.1175/JCLI-D-12-00568.1.

Mathew, S. S., and K. K. Kumar, 2019: Characterization of the long-term changes in moisture, clouds and precipitation in the ascending and descending branches of the Hadley Circulation. *Journal of Hydrology*, **570**, 366–377, DOI: https://doi.org/10.1016/j.jhydrol.

2018.12.047.

Meynadier, R., O. Bock, S. Gervois, F. Guichard, J.-L. Redelsperger, A. Agustí-Panareda, and A. Beljaars, 2010: West African Monsoon water cycle: 2. Assessment of numerical weather prediction water budgets. *Journal of Geophysical Research: Atmospheres*, **115 (D19)**, DOI: https://doi.org/10.1029/2010JD013919.

Mohtadi, M., M. Prange, E. Schefuß, and T. C. Jennerjahn, 2017: Late Holocene slowdown of the Indian Ocean Walker circulation. *Nature Communications*, **8**, 1015, DOI: https://doi.org/10.1038/s41467-017-00855-3.

Moihamette, F., W. M. Pokam, I. Diallo, and R. Washington, 2022: Extreme Indian Ocean dipole and rainfall variability over Central Africa. *International Journal of Climatology*, **42 (10)**, 5255–5272, DOI: https://doi.org/10.1002/joc.7531.

Mounier, F., G. N. Kiladis, and S. Janicot, 2007: Analysis of the Dominant Mode of Convectively Coupled Kelvin Waves in the West African Monsoon. *Journal of Climate*, **20 (8)**, 1487–1503, DOI: https://doi.org/10.1175/JCLI4059.1.

Munday, C., and R. Washington, 2018: Systematic Climate Model Rainfall Biases over Southern Africa: Links to Moisture Circulation and Topography. *Journal of Climate*, **31 (18)**, 7533–7548, DOI: https://doi.org/10.1175/JCLI-D-18-0008.1.

Niang, C., A. M. Mancho, V. J. García-Garrido, E. Mohino, B. Rodriguez-Fonseca, and J. Curbelo, 2020: Transport pathways across the West African Monsoon as revealed by Lagrangian Coherent Structures. *Scientific Reports*, **10 (1)**, 12 543, DOI: https://doi.org/10.1038/s41598-020-69159-9.

Nicholson, S. E., 2009: A revised picture of the structure of the "monsoon" and land ITCZ over West Africa. *Climate Dynamics*, **32 (7)**, 1155–1171, DOI: https://doi.org/10.1007/s00382-008-0514-3.

Nicholson, S. E., 2013: The West African Sahel: A Review of Recent Studies on the Rainfall Regime and Its Interannual Variability. *International Scholarly Research Notices*, **2013 (1)**, 453 521, DOI: https://doi.org/10.1155/2013/453521.

Nicholson, S. E., 2015: Long-term variability of the East African 'short rains' and its links to large-scale factors. *International Journal of Climatology*, **35 (13)**, 3979–3990, DOI: https://doi.org/10.1002/joc.4259.

Nicholson, S. E., 2018: The ITCZ and the Seasonal Cycle over Equatorial Africa. *Bulletin of the American Meteorological Society*, **99 (2)**, 337–348, DOI: https://doi.org/10.1175/BAMS-D-16-0287.1.

Nicholson, S. E., A. H. Fink, and C. Funk, 2018a: Assessing recovery and change in West Africa's rainfall regime from a 161-year record. *International Journal of Climatology*, **38 (10)**, 3770–3786, DOI: https://doi.org/10.1002/joc.5530.

Nicholson, S. E., C. Funk, and A. H. Fink, 2018b: Rainfall over the African continent from the 19th through the 21st century. *Global and Planetary Change*, **165**, 114–127, DOI: https://doi.org/10.1016/j.gloplacha.2017.12.014.

Novella, N. S., and W. M. Thiaw, 2013: African Rainfall Climatology Version 2 for Famine Early Warning Systems. *Journal of Applied Meteorology and Climatology*, **52 (3)**, 588–606, DOI: https://doi.org/10.1175/JAMC-D-11-0238.1.

Ogata, T., S.-P. Xie, J. Lan, and X. Zheng, 2013: Importance of Ocean Dynamics for the Skewness of the Indian Ocean Dipole Mode. *Journal of Climate*, **26 (7)**, 2145–2159, DOI: https://doi.org/10.1175/JCLI-D-11-00615.1.

Oort, A. H., and J. J. Yienger, 1996: Observed Interannual Variability in the Hadley Circulation and Its Connection to ENSO. *Journal of Climate*, **9 (11)**, 2751–2767, DOI: https://doi.org/10.1175/1520-0442(1996)009<2751:OIVITH>2.0.CO;2.

Palmer, P. I., and Coauthors, 2023: Drivers and impacts of Eastern African rainfall variability. *Nature Reviews Earth & Environment*, **4 (4)**, 254–270, DOI: https://doi.org/10.1038/s43017-023-00397-x.

Phadtare, J., and H. J. S. Fernando, 2025: On the Propagation of Convectively Coupled Kelvin Waves From Africa to the Indian Ocean. *Geophysical Research Letters*, **52 (12)**, e2024GL114 419, DOI: https://doi.org/10.1029/2024GL114419.

Pokam, W., D. A. Vondou, and P. H. Kamsu-Tamo, 2022: Central African Climate. *Congo Basin Hydrology, Climate, and Biogeochemistry*, American Geophysical Union (AGU), 13–23, DOI: https://doi.org/10.1002/9781119657002.ch2.

Pokam, W. M., C. L. Bain, R. S. Chadwick, R. Graham, D. J. Sonwa, and F. M. Kamga, 2014: Identification of Processes Driving Low-Level Westerlies in West Equatorial Africa. *Journal of Climate*, **27 (11)**, 4245–4262, DOI: https://doi.org/10.1175/JCLI-D-13-00490.1.

Quagraine, K. A., F. Nkrumah, C. Klein, N. A. B. Klutse, and K. T. Quagraine, 2020: West African Summer Monsoon Precipitation Variability as Represented by Reanalysis Datasets. *Climate*, **8 (10)**, 111, DOI: https://doi.org/10.3390/cli8100111.

Raj, J., H. K. Bangalath, and G. Stenchikov, 2019: West African Monsoon: current state and future projections in a high-resolution AGCM. *Climate Dynamics*, **52 (11)**, 6441–6461, DOI: https://doi.org/10.1007/s00382-018-4522-7.

Ramotubei, T. S., W. A. Landman, M. J. Mateyisi, S. S. Nangombe, and A. F. Beraki, 2025: Simulation of the African ITCZ during austral summer seasons and ENSO phases: application of an RCM derived from stretched grid ESM. *Frontiers in Climate*, **7**, DOI: https://doi.org/10.3389/fclim.2025.1504756.

Randriamarolaza, L. Y. A., E. Aguilar, O. Skrynyk, S. M. Vicente-Serrano, and F. Domínguez-Castro, 2022: Indices for daily temperature and precipitation in Madagascar, based on quality-controlled and homogenized data, 1950–2018. *International Journal of Climatology*,

42 (1), 265–288, DOI: https://doi.org/10.1002/joc.7243.

Rao, S. A., J.-J. Luo, S. K. Behera, and T. Yamagata, 2009: Generation and termination of Indian Ocean dipole events in 2003, 2006 and 2007. *Climate Dynamics*, **33 (6)**, 751–767, DOI: https://doi.org/10.1007/s00382-008-0498-z.

Rasp, S., and Coauthors, 2024: WeatherBench 2: A Benchmark for the Next Generation of Data-Driven Global Weather Models. *Journal of Advances in Modeling Earth Systems*, **16 (6)**, e2023MS004 019, DOI: https://doi.org/10.1029/2023MS004019.

Ratna, S. B., A. Cherchi, T. J. Osborn, M. Joshi, and U. Uppara, 2021: The Extreme Positive Indian Ocean Dipole of 2019 and Associated Indian Summer Monsoon Rainfall Response. *Geophysical Research Letters*, **48 (2)**, e2020GL091 497, DOI: https://doi.org/10.1029/2020GL091497.

Rayner, N. A., D. E. Parker, E. B. Horton, C. K. Folland, L. V. Alexander, D. P. Rowell, E. C. Kent, and A. Kaplan, 2003: Global analyses of sea surface temperature, sea ice, and night marine air temperature since the late nineteenth century. *Journal of Geophysical Research: Atmospheres*, **108 (D14)**, DOI: https://doi.org/10.1029/2002JD002670.

Rigden, A., C. Golden, D. Chan, and P. Huybers, 2024: Climate change linked to drought in Southern Madagascar. *npj Climate and Atmospheric Science*, **7 (1)**, 41, DOI: https://doi.org/10.1038/s41612-024-00583-8.

Riley, E. M., B. E. Mapes, and S. N. Tulich, 2011: Clouds Associated with the Madden–Julian Oscillation: A New Perspective from CloudSat. *Journal of the Atmospheric Sciences*, **68 (12)**, 3032–3051, DOI: https://doi.org/10.1175/JAS-D-11-030.1.

Roca, R., L. V. Alexander, G. Potter, M. Bador, R. Jucá, S. Contractor, M. G. Bosilovich, and S. Cloché, 2019: FROGS: a daily 1° × 1° gridded precipitation database of rain gauge, satellite and reanalysis products. *Earth System Science Data*, **11 (3)**, 1017–1035, DOI: https://doi.org/10.5194/essd-11-1017-2019.

Saji, N. H., B. N. Goswami, P. N. Vinayachandran, and T. Yamagata, 1999: A dipole mode in the tropical Indian Ocean. *Nature*, **401 (6751)**, 360–363, DOI: https://doi.org/10.1038/43854.

Sanogo, S., A. H. Fink, J. A. Omotosho, A. Ba, R. Redl, and V. Ermert, 2015: Spatio-temporal characteristics of the recent rainfall recovery in West Africa. *International Journal of Climatology*, **35 (15)**, 4589–4605, DOI: https://doi.org/10.1002/joc.4309.

Schlueter, A., A. H. Fink, P. Knippertz, and P. Vogel, 2019: A Systematic Comparison of Tropical Waves over Northern Africa. Part I: Influence on Rainfall. *Journal of Climate*, **32 (5)**, 1501–1523, DOI: https://doi.org/10.1175/JCLI-D-18-0173.1.

Schneider, E. K., 1977: Axially Symmetric Steady-State Models of the Basic State for Instability and Climate Studies. Part II. Nonlinear Calculations. *Journal of the Atmospheric Sciences*, **34 (2)**, 280–296, DOI: https://doi.org/10.1175/1520-0469(1977)034<0280:

ASSSMO>2.0.CO;2.

Schneider, T., T. Bischoff, and G. H. Haug, 2014: Migrations and dynamics of the intertropical convergence zone. *Nature*, **513 (7516)**, 45–53, DOI: https://doi.org/10.1038/nature13636.

Schneider, U., S. Hänsel, E. Rustemeier, P. Finger, A. Becker, A. Rauthe-Schöch, and M. Ziese, 2022: GPCC Full Data Daily Version 2022 at 1.0°: Daily Land-Surface Precipitation from Rain-Gauges built on GTS-based and Historic Data. DOI: https://doi.org/10.5676/DWD_GPCC/FD_D_V2022_100.

Schulzweida, U., 2023: CDO User Guide. URL: https://doi.org/10.5281/zenodo.10020800.

Schwendike, J., G. J. Berry, K. Fodor, and M. J. Reeder, 2021: On the Relationship Between the Madden-Julian Oscillation and the Hadley and Walker Circulations. *Journal of Geophysical Research: Atmospheres*, **126 (4)**, e2019JD032 117, DOI: https://doi.org/10.1029/2019JD032117.

Schwendike, J., G. J. Berry, M. J. Reeder, C. Jakob, P. Govekar, and R. Wardle, 2015: Trends in the local Hadley and local Walker circulations. *Journal of Geophysical Research: Atmospheres*, **120 (15)**, 7599–7618, DOI: https://doi.org/10.1002/2014JD022652.

Schwendike, J., P. Govekar, M. J. Reeder, R. Wardle, G. J. Berry, and C. Jakob, 2014: Local partitioning of the overturning circulation in the tropics and the connection to the Hadley and Walker circulations. *Journal of Geophysical Research: Atmospheres*, **119 (3)**, 1322–1339, DOI: https://doi.org/10.1002/2013JD020742.

Sharma, S., K.-J. Ha, W. Cai, E.-S. Chung, and T. Bódai, 2022: Local meridional circulation changes contribute to a projected slowdown of the Indian Ocean Walker circulation. *npj Climate and Atmospheric Science*, **5 (1)**, 15, DOI: https://doi.org/10.1038/s41612-022-00242-w.

Simane, B., T. Kapwata, N. Naidoo, G. Cissé, C. Y. Wright, and K. Berhane, 2025: Ensuring Africa's Food Security by 2050: The Role of Population Growth, Climate-Resilient Strategies, and Putative Pathways to Resilience. *Foods*, **14 (2)**, 262, DOI: https://doi.org/10.3390/foods14020262.

Spencer, H., R. T. Sutton, J. M. Slingo, M. Roberts, and E. Black, 2005: Indian Ocean Climate and Dipole Variability in Hadley Centre Coupled GCMs. *Journal of Climate*, **18 (13)**, 2286–2307, DOI: https://doi.org/10.1175/JCLI3410.1.

Stachnik, J. P., and C. Schumacher, 2011: A comparison of the Hadley circulation in modern reanalyses. *Journal of Geophysical Research: Atmospheres*, **116 (D22)**, DOI: https://doi.org/10.1029/2011JD016677.

Stechmann, S. N., and H. R. Ogrosky, 2014: The Walker circulation, diabatic heating, and outgoing longwave radiation. *Geophysical Research Letters*, **41 (24)**, 9097–9105, DOI: https://doi.org/10.1002/2014GL062257.

Steinkopf, J., and F. Engelbrecht, 2022: Verification of ERA5 and ERA-Interim precipitation over Africa at intra-annual and interannual timescales. *Atmospheric Research*, **280**, 106 427, DOI: https://doi.org/10.1016/j.atmosres.2022.106427.

Straub, K. H., and G. N. Kiladis, 2002: Observations of a Convectively Coupled Kelvin Wave in the Eastern Pacific ITCZ. *Journal of the Atmospheric Sciences*, **59 (1)**, 30–53, DOI: https://doi.org/10.1175/1520-0469(2002)059<0030:OOACCK>2.0.CO;2.

Sultan, B., and S. Janicot, 2003: The West African Monsoon Dynamics. Part II: The "Preonset" and "Onset" of the Summer Monsoon. *Journal of Climate*, **16 (21)**, 3407–3427, DOI: https://doi.org/10.1175/1520-0442(2003)016<3407:TWAMDP>2.0.CO;2.

Sultan, B., S. Janicot, and A. Diedhiou, 2003: The West African Monsoon Dynamics. Part I: Documentation of Intraseasonal Variability. *Journal of Climate*, **16 (21)**, 3389–3406, DOI: https://doi.org/10.1175/1520-0442(2003)016<3389:TWAMDP>2.0.CO;2.

Swapna, P., and R. Krishnan, 2008: Equatorial undercurrents associated with Indian Ocean Dipole events during contrasting summer monsoons. *Geophysical Research Letters*, **35 (14)**, DOI: https://doi.org/10.1029/2008GL033430.

Thakur, A., J. Sukhatme, and N. Harnik, 2024: Investigating the role of tropical and extratropical waves in the Hadley circulation via present-day Earth-like to globally uniform sea-surface temperature forcing. *Quarterly Journal of the Royal Meteorological Society*, **150 (763)**, 3578–3600, DOI: https://doi.org/10.1002/qj.4784.

Thomson, J., 1892: XVII. Bakerian lecture.-On the grand currents of atmospheric circulation. *Philosophical Transactions of the Royal Society of London. (A.)*, **183**, 653–684, DOI: https://doi.org/10.1098/rsta.1892.0017.

Thorncroft, C. D., H. Nguyen, C. Zhang, and P. Peyrillé, 2011: Annual cycle of the West African monsoon: regional circulations and associated water vapour transport. *Quarterly Journal of the Royal Meteorological Society*, **137 (654)**, 129–147, DOI: https://doi.org/10.1002/qj.728.

Tokinaga, H., S.-P. Xie, A. Timmermann, S. McGregor, T. Ogata, H. Kubota, and Y. M. Okumura, 2012: Regional Patterns of Tropical Indo-Pacific Climate Change: Evidence of the Walker Circulation Weakening. *Journal of Climate*, **25 (5)**, 1689–1710, DOI: https://doi.org/10.1175/JCLI-D-11-00263.1.

Tomassini, L., 2020: The Interaction between Moist Convection and the Atmospheric Circulation in the Tropics. *Bulletin of the American Meteorological Society*, **101 (8)**, E1378–E1396, DOI: https://doi.org/10.1175/BAMS-D-19-0180.1.

Tomassini, L., and G.-Y. Yang, 2022: Tropical moist convection as an important driver of Atlantic Hadley circulation variability. *Quarterly Journal of the Royal Meteorological Society*, **148 (748)**, 3287–3302, DOI: https://doi.org/10.1002/qj.4359.

Torsah, G. A., M. A. Osei, J. N. A. Aryee, J. A. A. Oti, and L. K. Amekudzi, 2025: Triggers of inland heavy rainfall inducing convective storms in West Africa : Case study of June, 2021. *Weather and Climate Extremes*, **47**, 100 740, DOI: https://doi.org/10.1016/j.wace.2024.100740.

UNDPAfrica, 2012: Africa Human Development Report 2012 Towards a Food Secure Future. Tech. rep., United Nations. DOI: https://doi.org/10.22004/ag.econ.267636, URL: https://ageconsearch.umn.edu/record/267636.

Vinayachandran, P. N., N. H. Saji, and T. Yamagata, 1999: Response of the equatorial Indian Ocean to an unusual wind event during 1994. *Geophysical Research Letters*, **26 (11)**, 1613–1616, DOI: https://doi.org/10.1029/1999GL900179.

Wainwright, C. M., J. H. Marsham, R. J. Keane, D. P. Rowell, D. L. Finney, E. Black, and R. P. Allan, 2019: 'Eastern African Paradox' rainfall decline due to shorter not less intense Long Rains. *npj Climate and Atmospheric Science*, **2 (1)**, 34, DOI: https://doi.org/10.1038/s41612-019-0091-7.

Walker, C. C., and T. Schneider, 2006: Eddy Influences on Hadley Circulations: Simulations with an Idealized GCM. *Journal of the Atmospheric Sciences*, **63 (12)**, 3333–3350, DOI: https://doi.org/10.1175/JAS3821.1.

Walker, G. T., 1925: CORRELATION IN SEASONAL VARIATIONS OF WEATHER—A FURTHER STUDY OF WORLD WEATHER. *Monthly Weather Review*, **53 (6)**, 252–254, DOI: https://doi.org/10.1175/1520-0493(1925)53<252:CISVOW>2.0.CO;2.

Wang, G., W. Cai, K. Yang, A. Santoso, and T. Yamagata, 2020: A Unique Feature of the 2019 Extreme Positive Indian Ocean Dipole Event. *Geophysical Research Letters*, **47 (18)**, e2020GL088 615, DOI: https://doi.org/10.1029/2020GL088615.

Wang, G., and Coauthors, 2024a: The Indian Ocean Dipole in a warming world. *Nature Reviews Earth & Environment*, **5 (8)**, 588–604, DOI: https://doi.org/10.1038/s43017-024-00573-7.

Wang, J., S. Sun, Y. Zu, and Y. Fang, 2024b: Increased Frequency of Consecutive Positive IOD Events Under Global Warming. *Geophysical Research Letters*, **51 (20)**, e2024GL111 182, DOI: https://doi.org/10.1029/2024GL111182.

Wang, X.-Y., and Coauthors, 2021: Underestimated responses of Walker circulation to ENSO-related SST anomaly in atmospheric and coupled models. *Geoscience Letters*, **8 (1)**, 17, DOI: https://doi.org/10.1186/s40562-021-00186-8.

Watanabe, M., T. Iwakiri, Y. Dong, and S. M. Kang, 2023: Two Competing Drivers of the Recent Walker Circulation Trend. *Geophysical Research Letters*, **50 (23)**, e2023GL105 332, DOI: https://doi.org/10.1029/2023GL105332.

Webster, P. J., A. M. Moore, J. P. Loschnigg, and R. R. Leben, 1999: Coupled ocean–atmosphere dynamics in the Indian Ocean during 1997–98. *Nature*, **401 (6751)**, 356–360, DOI: https:

//doi.org/10.1038/43848.

Weller, E., and W. Cai, 2014: Meridional variability of atmospheric convection associated with the Indian Ocean Dipole Mode. *Scientific Reports*, **4 (1)**, 3590, DOI: https://doi.org/10.1038/srep03590.

Wheeler, M., and G. N. Kiladis, 1999: Convectively Coupled Equatorial Waves: Analysis of Clouds and Temperature in the Wavenumber–Frequency Domain. *Journal of the Atmospheric Sciences*, **56 (3)**, 374–399, DOI: https://doi.org/10.1175/1520-0469(1999)056<0374:CCEWAO>2.0.CO;2.

Williams, A. P., and C. Funk, 2011: A westward extension of the warm pool leads to a westward extension of the Walker circulation, drying eastern Africa. *Climate Dynamics*, **37 (11)**, 2417–2435, DOI: https://doi.org/10.1007/s00382-010-0984-y.

Yang, G.-Y., B. Hoskins, and J. Slingo, 2003: Convectively Coupled Equatorial Waves: A New Methodology for Identifying Wave Structures in Observational Data. *Journal of the Atmospheric Sciences*, **60 (12)**, 1637–1654, DOI: https://doi.org/10.1175/1520-0469(2003)060<1637:CCEWAN>2.0.CO;2.

Yano, J.-I., M. W. Moncrieff, and W. W. Grabowski, 2002: Walker-Type Mean Circulations and Convectively Coupled Tropical Waves as an Interacting System. *Journal of the Atmospheric Sciences*, **59 (9)**, 1566–1577, DOI: https://doi.org/10.1175/1520-0469(2002)059<1566:WTMCAC>2.0.CO;2.

Yu, B., and F. W. Zwiers, 2010: Changes in equatorial atmospheric zonal circulations in recent decades. *Geophysical Research Letters*, **37 (5)**, DOI: https://doi.org/10.1029/2009GL042071.

Yu, B., F. W. Zwiers, G. J. Boer, and M. F. Ting, 2012: Structure and variances of equatorial zonal circulation in a multimodel ensemble. *Climate Dynamics*, **39 (9)**, 2403–2419, DOI: https://doi.org/10.1007/s00382-012-1372-6.

Zaplotnik, Z., M. Pikovnik, and L. Boljka, 2022: Recent Hadley Circulation Strengthening: A Trend or Multidecadal Variability? *Journal of Climate*, **35 (13)**, 4157–4176, DOI: https://doi.org/10.1175/JCLI-D-21-0204.1.

Zhang, L.-Y., Y. Du, W. Cai, Z. Chen, T. Tozuka, and J.-Y. Yu, 2020: Triggering the Indian Ocean Dipole From the Southern Hemisphere. *Geophysical Research Letters*, **47 (15)**, e2020GL088 648, DOI: https://doi.org/10.1029/2020GL088648.

Zhao, S., and K. H. Cook, 2021: Influence of Walker circulations on East African rainfall. *Climate Dynamics*, **56 (7)**, 2127–2147, DOI: https://doi.org/10.1007/s00382-020-05579-7.

A. Appendix

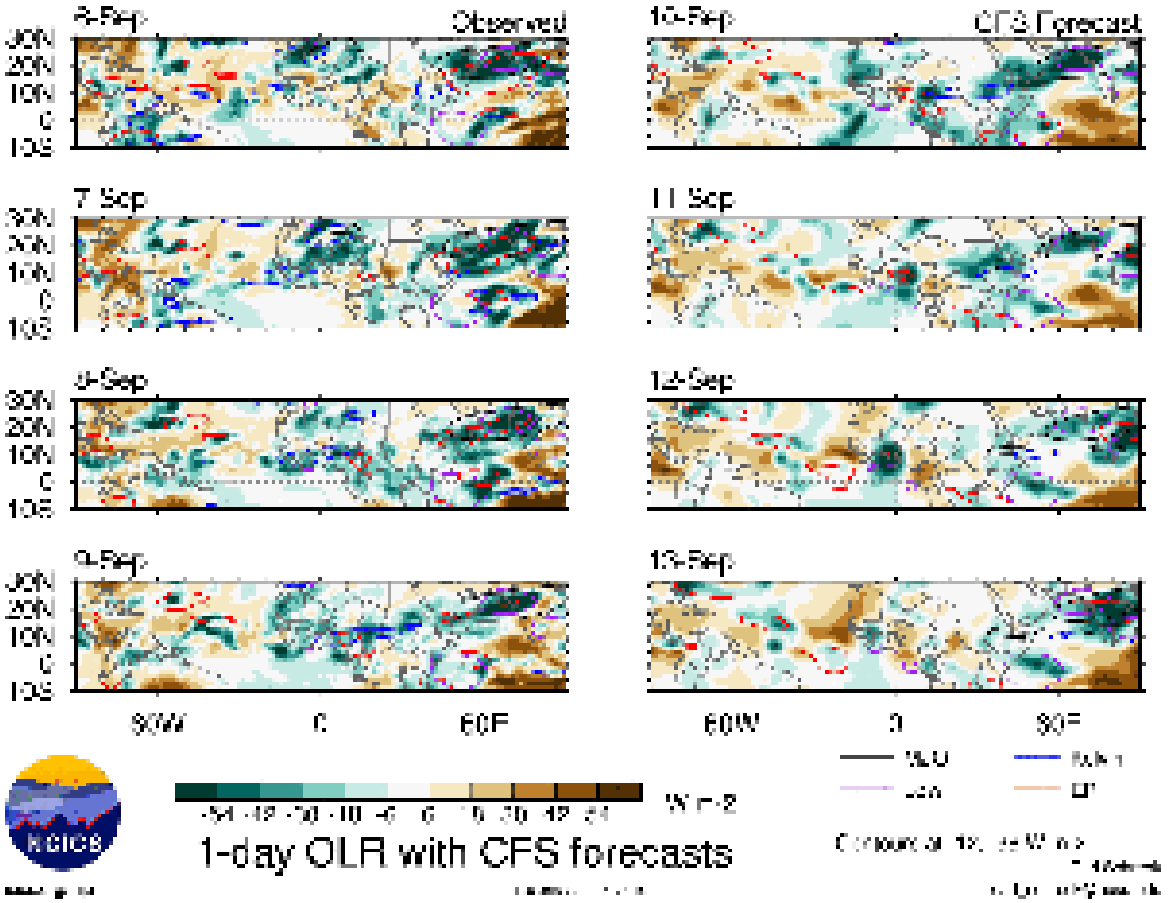

Figure A.1.: latitude-lognitude OLR map produced on 10-09-2019 by the North Carolina Institute for Climate Studies. Shading shows anomalies from climatology in the past. In the future, shading is either the sum of all modes or the NCEP coupled forecast system model forecast and its departure from its own climatology. Contours identify the MJO, equatorial Rossby waves, Kelvin waves, and the low-frequency background (> 120 days). Source: `https://ncics.org/pub/mjo/archive/2019/2019-09-10/v2/`

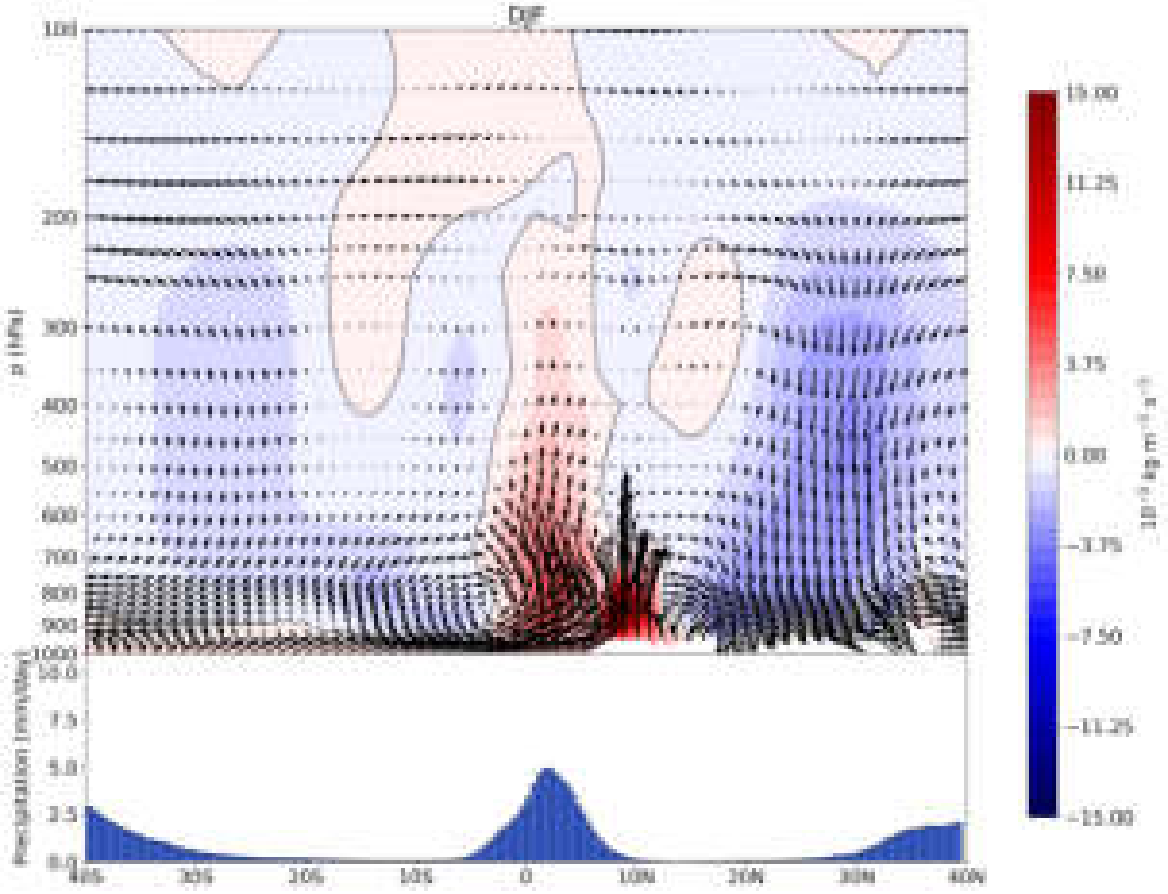

Figure A.2.: Same as Figure 4.2, but the season DJF

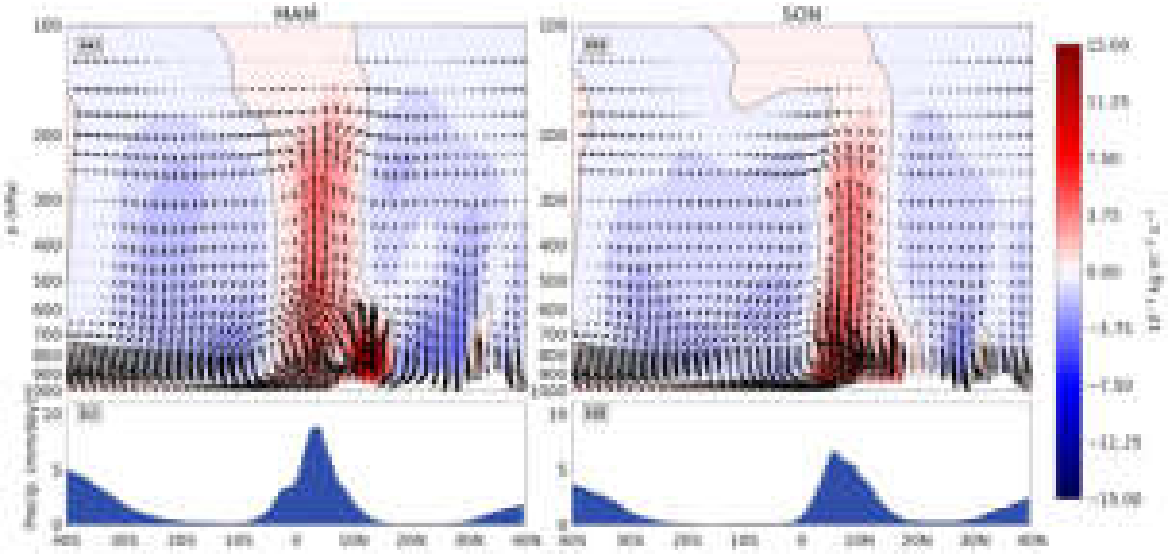

Figure A.3.: Same as Figure 4.2, but for the seasons MAM and SON.

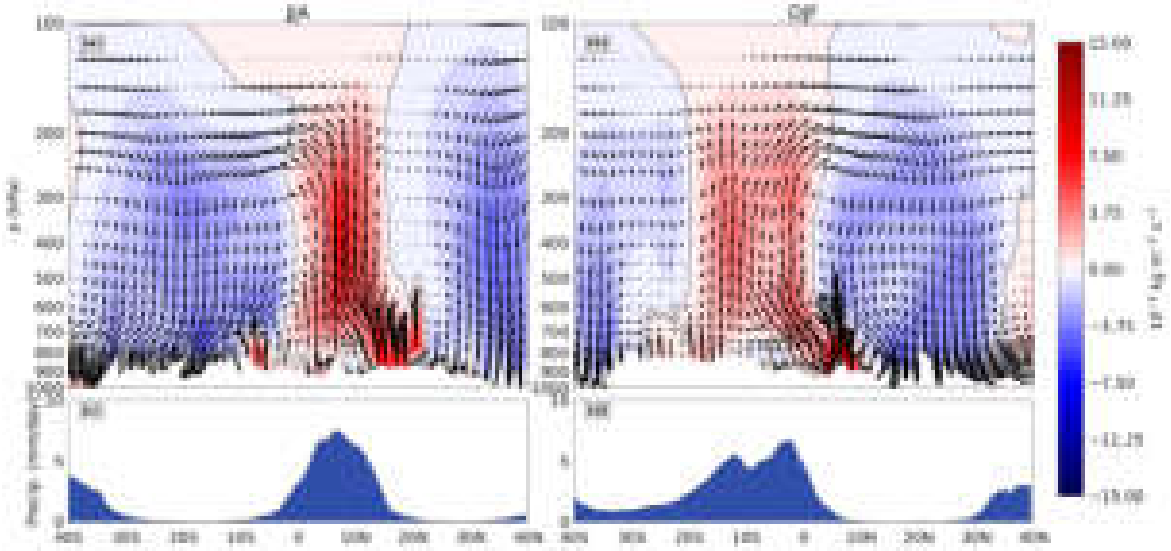

Figure A.4.: Same as Figure 4.2, but for Central Africa (8° E–28° E) and the seasons DJF and JJA.

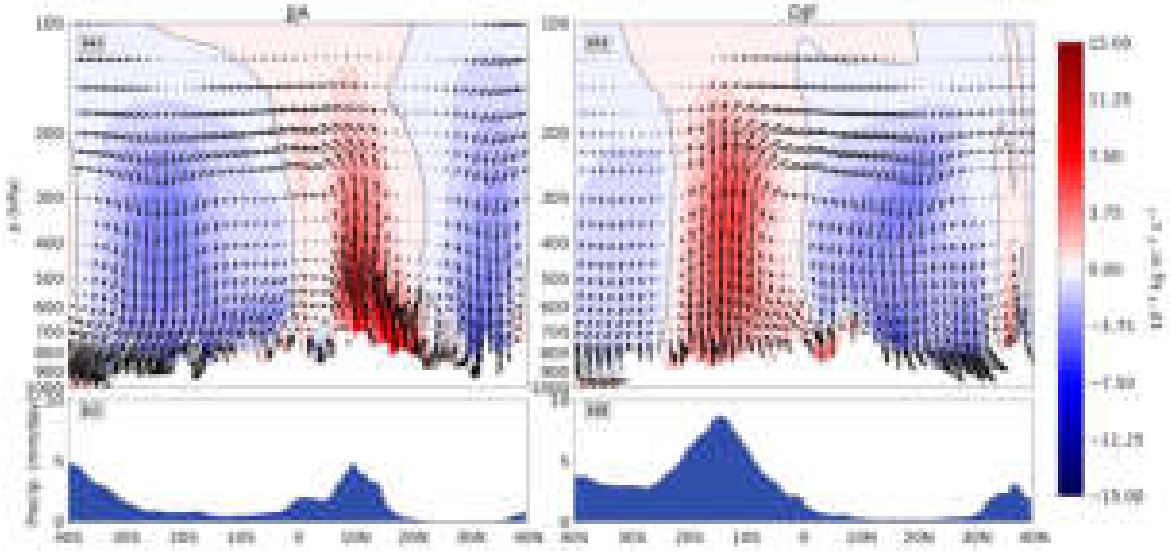

Figure A.5.: Same as Figure 4.2, but for East Africa (28°E–50°E) and the seasons DJF and MAM.

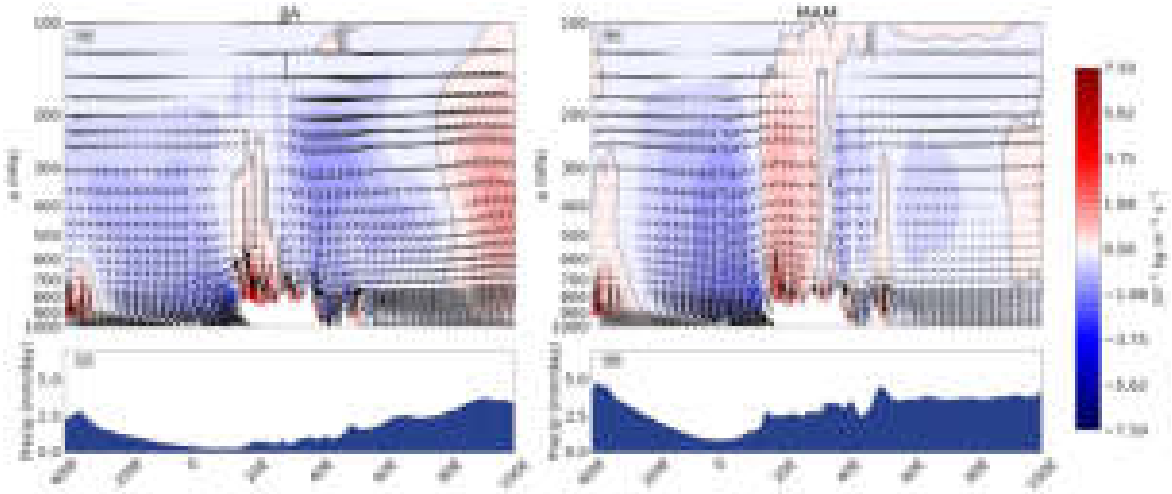

Figure A.6.: Same as Figure 4.5, but for the seasons MAM and JJA.

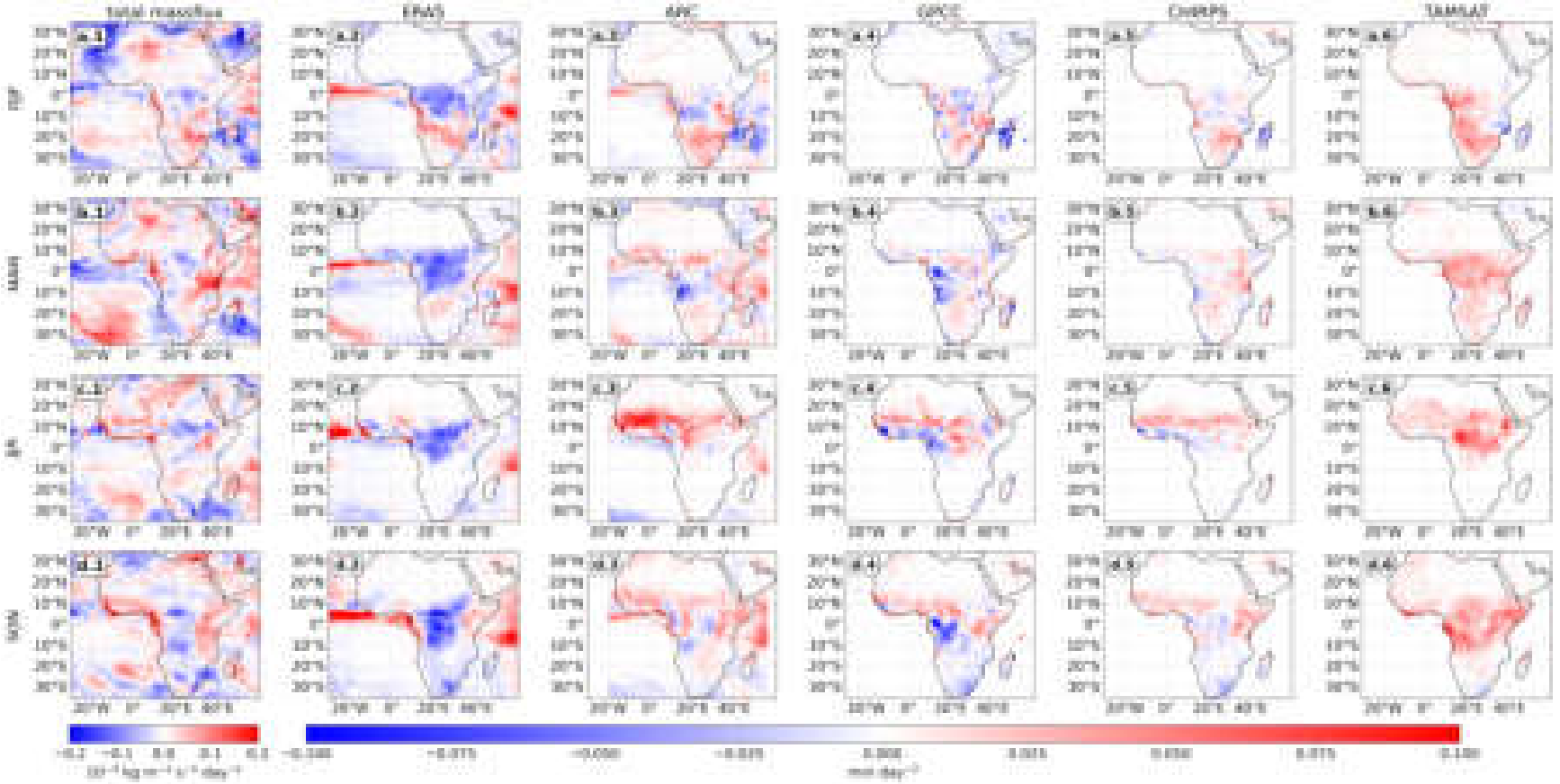

Figure A.7.: Trends in total mass flux at 500 hPa(first column) (kg m^{-2} s^{-1} day^{-1}) and in precipitation from multiple precipitation products (mm day^{-2}) for the seasons DJF (first row), MAM (second row), JJA (third row) and SON (fourth row) for the period 1983-2020.

Acknowledgments

I would like to extend a big thanks to my supervisors, Andreas Fink and Juliane Schwendike, for their steady guidance and encouragement throughout this project. Andreas has been a great supervisor both for my thesis and for my student assistant job. Thanks for the consistently good advice and humor. Thanks to Juliane, who, even through the virtual world, was still able to provide very helpful supervision and was always very kind. Further thanks go to Peter Knippertz for first getting me interested in tropical meteorology and for the always useful and motivating comments. I want to thank all three for helping organize my trip to Leeds. I really appreciated the opportunity, and thanks to Juliane and the colleagues in Leeds who made it a nice trip and who shared their time and expertise with me. Further thanks go out to the people from my working group and the fellow students from the office for making a nice daily working environment. Thank you also to Chris Funk and Appo Vondou, for their nice talks and useful comments. Thanks to Sugata Narsey for providing the script that was the basis of my work.

I acknowledge the support of the state of Baden-Württemberg through bwHPC, which facilitated access to high-performance computing resources. I acknowledge the use of imagery from the NASA Worldview application (https://worldview.earthdata.nasa.gov), part of the NASA Earth Science Data and Information System (ESDIS). I would like to thank the contributors to the Froggs dataset (https://frogs.ipsl.fr/download-data/), as well as the developers of essential Python packages, including Matplotlib, NumPy, Xarray, Dask, Cartopy, SciPy, and Windspharm.

I acknowledge the use of the generative AI assistant ChatGPT during the development of this thesis, which was used to assist with code improvement, Grammatical and stylistic enhancements, and translation. Further AI tools used for language improvements and translation were: DeepL (https://www.deepl.com) and Grammarly (https://app.grammarly.com/). I adapted and integrated the suggestions from the AI sources according to my own review, and take full responsibility for the final content

Finally, a special thanks goes out to Sarah for being herself and to my parents for their tireless 25-year-long support and funding. Could not have done it without you all.